DEVELOPMENT OF AN ANTI-CORROSION THERMALLY SPRAYED COATING

SYSTEM FOR OIL AND GAS TRANSMISSION PIPELINE

A Dissertation
Submitted to the Graduate Faculty
of the
North Dakota State University
of Agriculture and Applied Science

By

Sahar Abualigaledari

In Partial Fulfillment of the Requirements
for the Degree of
DOCTOR OF PHILOSOPHY

Major Department:
Mechanical Engineering

June 2018

Fargo, North Dakota

North Dakota State University
Graduate School

Title

DEVELOPMENT OF AN ANTI-CORROSION THERMALLY SPRAYED
COATING SYSTEM FOR OIL AND GAS TRANSMISSION PIPELINE

By

Sahar Abualigaledari

The Supervisory Committee certifies that this *disquisition* complies with North Dakota
State University's regulations and meets the accepted standards for the degree of

DOCTOR OF PHILOSOPHY

SUPERVISORY COMMITTEE:

Dr. Fardad Azarmi

Chair

Dr. Chad Ulven

Dr. Ying Huang

Dr. Yechun Wang

Dr. Andriy Voronov

Approved:

June 19th 2018	Alan Kallmeyer
Date	Department Chair

ABSTRACT

Corrosion, a leading cause of failure in metallic transmission pipelines, significantly impacts the reliability and safety of metallic pipelines. To prevent and mitigate pipeline corrosion, various non-metallic coatings and assessment methods have been implemented with different coating techniques. However, reliable, cost-effective, and environmental friendly corrosion mitigation approaches are yet needed to be achieved. Thermal metallic sprayed coatings have shown to be an effective means for pipeline corrosion prevention in marine environments with low cost, but it is not yet studied for on-shore buried and cased crossing pipelines. In this project, innovative composite self-sensing thermal sprayed coatings are proposed to prevent, monitor, mitigate, and manage pipeline corrosion for on-shore buried metallic transmission pipelines. This project focuses on developing the metallic corrosion resistant coating with thermal spray techniques. The compositions, mechanical properties, corrosion resistance, and effectiveness of composite thermal sprayed coatings have been investigated theoretically, numerically, and experimentally.

ACKNOWLEDGEMENTS

TABLE OF CONTENTS

LIST OF TABLES

LIST OF FIGURES

CHAPTER 1. INTRODUCTION

1.1. Corrosion in Oil and Gas Transmission Pipeline

Corrosion is one of the major reasons for failure of onshore transmission pipelines [1]. This electrochemical reaction has also drawn to be one of the most common causes of explosion in the petroleum industry in the United States [2]. According to a survey by Pipeline and Hazardous Materials Safety Administration (PHMSA), the total of %18 of the significant incident in both onshore and offshore in the 20-years period from 1988 through 2008 has been mainly due to the corrosion. Figure 1.1 depicts the crucial causes of failure in the petroleum industry. However, it has been reported that, during the same period, 34.5 percent of all serious incident attributed to excavation damage while corrosion accounted for only %5.8 of both offshore and onshore's major incidents [2]. Furthermore, the costs invested for different types of corrosion, having been estimated by National Association of Corrosion Engineers (NACE), turned out to be $276 billion. $7 billion of this total is attributed to onshore gas and liquid transmission pipeline.
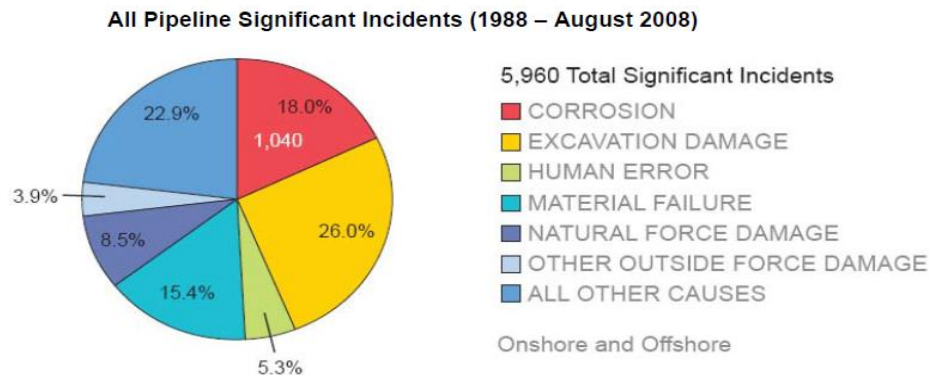
Figure 1.1. Causes of significant incidents in onshore and offshore pipelines [1].

Figure 1.2 has illustrated the cost of corrosion for transmission onshore pipelines in percentage of Gross Domestic Product (GDP) in the United States, having been issued by NACE in 2013. It is very important to indicate the location where most significant corrosion incident have occurred.
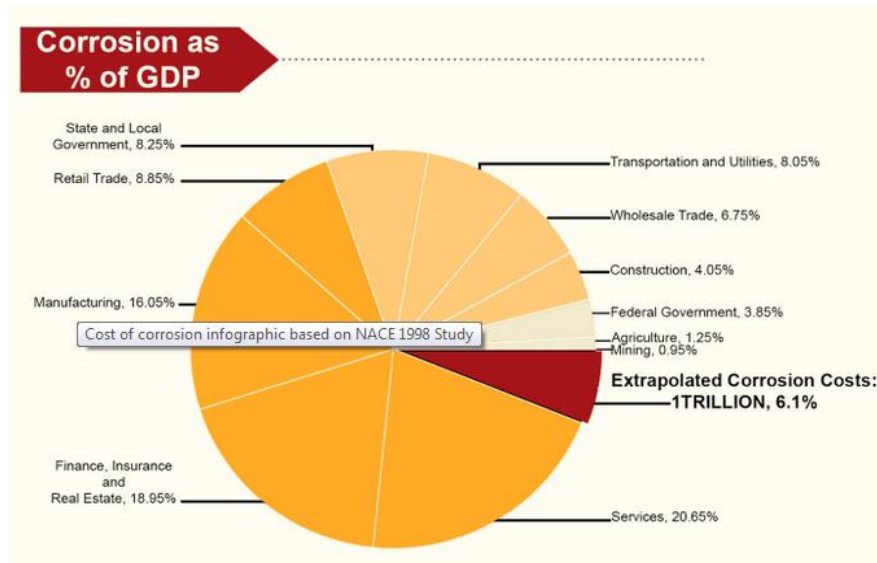
Figure 1.2. Cost of corrosion in U. S. Transmission onshore pipelines [3].

According to Figure 1.3 reported by PHMSA, there have been 40 to 65 notable incidents per year on pipeline during the past 20 years (averaged to 52 incidents per year). More than half of these failures were attributed to onshore liquid pipelines. Gas transmission pipeline turned out to have the second highest failure frequency.
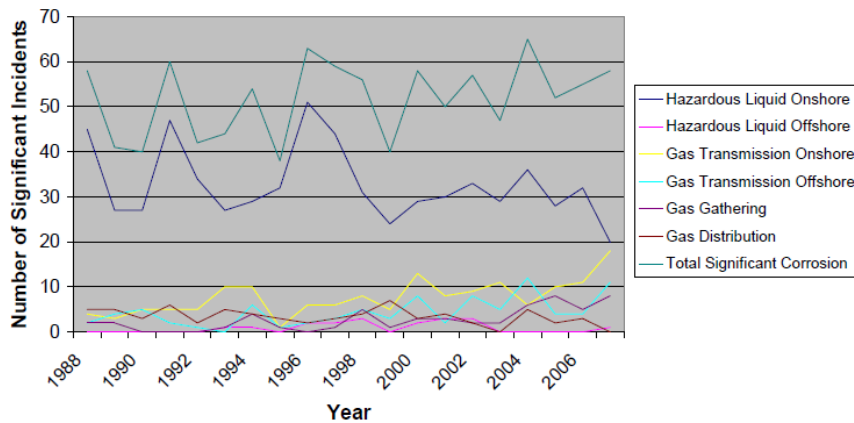
Figure 1.3. History of significant corrosion incidents in the US [2].

There are several ways to define corrosion. In general, corrosion is known as the most undesirable spontaneous electrochemical process. The definition used by primary support organization in corrosion industry (NACE) is "the deterioration of material, usually a metal, which

2

is resulted from a reaction with its environment". The most common example of these electrochemical phenomena is rusting of iron metal or iron alloys such as ordinary carbon steel. In the pipeline corrosion stand point, the metal is line-pipe steel, primarily comprised Fe with 1-2 percent alloying elements which usually are added to improve the strength and toughness [2]. The amount of cost imposed to the industry caused by corrosion for replacement and maintenance was estimated around billions of dollars each year. Therefore, from economic stand point, it is very crucial to understand the corrosion process to mitigate and inhibit this detrimental phenomenon.

It has been reported that most of the metals need a very short time to react with oxygen [4]. In the case of pipelines made from carbon-steel, the deterioration would be attributed to the dissolution of Fe into the corrosive environment, which reduces the strength of the pipeline. The Fe ions typically react with water and/or oxygen to form a corrosion deposited of rust and iron oxides. However, in some cases, they may react with carbon dioxide or hydrogen sulfide to form iron carbonate or iron sulfide. The anodic reaction during the corrosion of the pipeline can be illustrated by the equation (1) [4]:

$$Fe \longrightarrow Fe^{++} + 2e^- \qquad\qquad (Eq.\ 1.1)$$

As the equation shows, Fe dissolves during the anodic reaction and the produced electrons from the reaction move through the metal pipe to another location where they are consumed in a reaction that produces hydroxyl ion. The reduction half-reaction of oxygen in mist air has potential of +0.40 V. Here are the two most possible half-reaction equations during corrosion in Fe [4].

$$O_2 + 2H_2O + 4e^- \longrightarrow 4OH^- \qquad\qquad (Eq.\ 1.2)$$

$$2H_2O + 2e^- \longrightarrow H_2 + 2OH^- \qquad\qquad (Eq.\ 1.3)$$
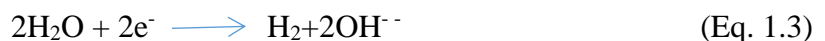
The simple schematic of the corrosion cell was shown in Figure 1.4.
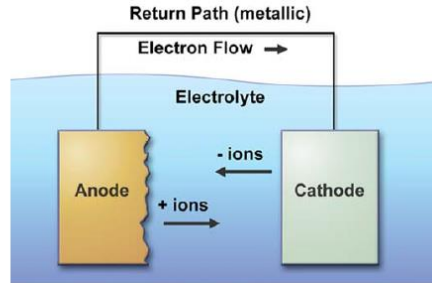
Figure 1.4. Schematic of a basic corrosion cell [4].

1.2. Corrosion Mechanism in Onshore Buried Pipeline

The science behind corrosion mechanism has been well-understood both in terms of mechanisms and methods of control. However, it has been reported that pipelines, either buried or on the ground, continue to experience a modest but notable number of failure attributed to corrosion mechanism more sophisticated than that of a piece of steel in a beaker of salt water. Common causes of corrosion on underground pipelines are indicated as: low-resistivity soils, anaerobic bacteria, dissimilar metals, differences in soil composition, differential aeration of the soil around the pipe, and stray direct current from external sources. These factors yield to different types of corrosion on the pipeline which the most important and common ones are pitting, selective seam corrosion, microbial corrosion, stray current corrosion, and galvanic corrosion. The different types of corrosion mechanisms are illustrated briefly in the following sections.

1.2.1. Pitting

The most common type of corrosion formation in pipelines is pitting which occurs more than uniform reduction of the wall thickness [4, 5]. This is explained due to the fact that during the corrosion the environment of anodic area tends to become more acidic. In fact, the Fe ions in solution react with the hydroxide ions of the water to generate an excess of hydrogen ion which makes the anodic environment more acidic which tends to localized corrosion [4, 5].

$$Fe^{++} + H_2O \longrightarrow FeOH + H^+ \qquad\qquad (Eq.\ 1.4)$$
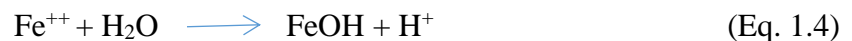
On the other hand, hydroxide ions produced at the cathodic area makes it less acidic and less likely to be corroded. Thus, by creating a pit on the surface, consecutive corrosive attack tends to be concentrated at that location. Therefore, pitting is most probably to occur on the surface rather than the uniform reduction in wall thickness. However, the pits may overlap and produce a general but irregular thinning of the pipe wall.

1.2.2. Selective Seam Corrosion

Most of the pipes installed in the industry are seamed or welded. Two typical welding methods have been used for pipelines are submerged-arc welding or upset-butt welding. The filler used for submerged-arc welding contains compositions slightly different from that of the body of the pipe. Furthermore, both welding methods provide heat affected zone next to the weld metal area which have different microstructure than the rest of the pipe due to the dissimilar cooling rates. The seamed region itself might contain cracks, flaws, or discontinuities as well. Taking all into the consideration, the seamed or welded areas of the pipe usually are more susceptible to corrosion [4, 5].

1.2.3. Microbial Corrosion

Microbiologically Influenced Corrosion (MIC) is usually caused by bacteria, molds, and fungi or their by-products and results in degradation of materials. There are two possible actions [5]:

-Acid by-products, such as sulphur, hydrogen sulfate, or ammonia attack the pipe or the protective layer. The main types are sulfate-reducing bacteria (SRB) and acid-producing bacteria (APB).

-Direct interaction between the microbes and the metal which are in contact with each other.

Mechanism of the MIC corrosion was illustrated in Figure 1.5.
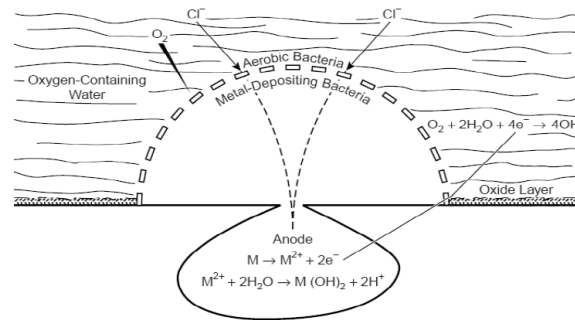
Figure 1.5. Possible reactions under tubercles created by metal deposition bacteria [5].

1.2.4. Stray Current Corrosion

Stray current corrosion usually occurs when a direct current flows through unintended path and the flow of electrons supports corrosion. This phenomenon can occur in soils and flowing or stationary fluids. There are several common methods to control the current and reduce the corresponding corrosion. Insulation, using earthing sources, cathodic protection, and sacrificial anode are the most common methods to mitigate and inhibit the stray current corrosion [4, 5].

1.2.5. Galvanic Corrosion

Galvanic corrosion occurs when two different metals with different electronegativities are in contact with each other. In this case, the metals with higher willingness of giving up valance electron will act as an anode and the one with the higher electronegativity will attract electron and act as cathode. In order to have galvanic corrosion taking place, an additional path for ion and electron movement (suitable electrolyte) is also necessary to complete the formation of an electrochemical cell. Using a proper insulator or coating to avoid the electrical contact between the metals is a common method to prohibit the galvanic corrosion. Another solution would be selection of metals close together in galvanic series [4, 5].

1.3. Corrosion in Cased Crossing Pipeline

The main reason for the use of cased crossing is to provide the capability to remove or replace carrier pipeline without disturbing the road or rail-crossing. In fact, casing pipe served as a duct that allowed the carrier to be installed through and under the obstruction, joint by joint, minimizing the possibility of connection damage [6]. Casing accommodates higher dead loads (overburden for deep pipe), live loads (traffic), and prevents third party damage to the pipeline. On the other hand, greater strength and/or pipeline wall thickness, concrete coatings and other methods could provide protection to the pipeline from mechanical damages and external loads [6, 7]. Figure 1.6 shows the simple configuration of cased pipe.
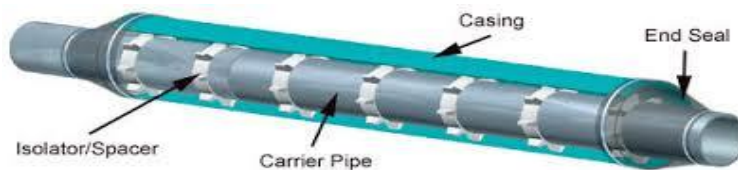
Figure 1.6. Schematic of cased pipe [1].

Some of disadvantages of using casings are: additional design and construction costs, additional maintenance and monitoring of electrical isolation and the problems associated with electrical shorts, including remediation, and increased load on cathodic protection systems. Sometimes the annular space between the pipe and casing is filled with an electrolyte, which triggers electrical shielding corrosion and crevice corrosion. In the case of cathodic protection (CP) it has also been reported that mud or debris deposited in the electrolyte in contact with the pipe may intupt a continuous electrical path to the casing. Another issue with casing is possibility of short circuit between pipelines and casing which follows by consuming the available CP current by casing and reducing CP effectiveness at other locations along the pipeline. However, several pipeline failures caused by external corrosion on cased pipes in the past have caused injuries to the

people and, damaged the property or the environment. It has been predicted that more failures are likely to occur in the future because of aging the cased pipes.

It is simply not practical to assess many cased pipes for external corrosion damage by using standard assessment methods for the following reasons [1]:

- Pipeline configuration prevents the possibility of the use of in-line non-destructive-tests methods for inspection.

- Service interruption and water consumption usage for pressure testing is unacceptable, exclusively for natural gas pipeline.

To conclude, there is a real demand for economic and effective External Corrosion Direct Assessment (ECDA) methodology that can be employed at the cased crossing since the conventional aboveground indirect inspection tools used in ECDA are not effective for cased pipe in that there is no electrical path in the annulus between the casing and the carrier pipes. Even if an electrolyte is introduced into the annulus, the casing may act as a shield such that the results from most indirect inspection tools regarding the CP level or coating condition may not be particularly meaningful.

1.4. Corrosion Protection Methods

1.4.1. Electrochemical Methods

Corrosion can be controlled by application of electrochemistry principles. This method could break down into two distinct areas which are (1) sacrificial anode and (b) cathodic protection [5].

1.4.1.1. Sacrificial Anode

In this method, corrosion can occur on a piece of metal with the lower electronegativity to protect the main metal against corrosion. Zinc and magnesium are the most common metals having

been used to this end. Some applications of this protection technique are: galvanized bolts, automobile steel and mail boxes, zincs placed outboard engines and steel boat hulls, aluminum blocks on oil rings, etc. Typical coatings used to protect steel with this principal are: zinc, aluminum, and cadmium [4].

1.4.1.2. Cathodic Protection by Impressed Current

The objective of the inducing current is to ensure the component requiring protection maintained in its cathodic region by the application of a voltage or cathodic current. The schematic of this system is shown in Figure 1.7.
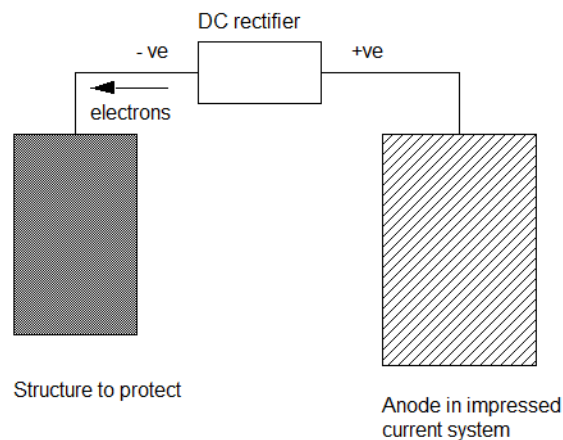
Figure 1.7. Schematic of impressed current system [8].

The main advantage of using this system is being cost-effective. However, the disadvantages include requirement of complicated control system due to interference of several factors, and unsafe operation of the system in the case of power failure, and loss of passiveness of the system with change of environment. These negative factors reduced the application of the anodic protection as a common technology for corrosion protection. Table 1.1 shows the required currents for cathodic protection.

Table 1.1. Required currents for cathodic protection [8].

Immersed in Seawater	Well Coated	Poor Coating	Uncoated Stationary
Stationary 1-2 (0.1-0.2)	2-20 (0.2-2)	20-30 (2-3)	--
Low Vel 1-3 f/s (0.3-1m/s)	2-5	5-20	50-100
Med Vel 3-7 f/s (1-2 m/s)	5-7	10-30	150-300
High Vel Turb flow	250-1000	250-1000	250-1000
Buried Underground	0.5-5	5-15	15-40
Soil resistivity Ω. M	1-2	0.5-1	0.1-0.05

1.4.2. Inhibitors

Inhibitors mostly are sort of chemicals used to reduce and mitigate corrosion. There are different types of inhibitor including: adsorption inhibitors, poisons, scavengers, filming inhibitors, and vapor phase. They sacrifices during chemical reaction and protect the main material against corrosion [5].

1.4.3. Coating

1.4.3.1. Soft Coating (Polymer-based)

There has been a noticeable improvement in the coating technology in the past two decades. The coatings which basically were designed for the corrosion protection, now, must be able to withstand high temperature service condition and be strong enough to resist against damages during handling and construction. In case of buried pipelines, the coating as the outer surface has also need to be strong enough to withstand applied stress by soil or soil movement. The most common types of soft coatings are used to protect pipeline against corrosion are: coal-tar based coatings, asphalt coatings, early grease coatings, early cold and hot applied tapes, and the first coal tar enamel coatings. However, application of many of these coating is a difficult task since, no strong bonding between coating and pipe may form. This followed by formation of voids, pinholes, and imperfections which led to their degradation over time [9]. In 1970s and 1980s, new wax or grease products were introduced to accommodate irregular shaped components such as valves and fitting. In 1990s, dry powders and wet-applied epoxies with much higher quality were discovered

and utilized for protection of pipelines. These coatings possess good dielectric properties and degraded relatively slowly over time. However, the mechanical strength of these coatings was noticeably low such that rough handling would cause failure in the coating. Polyolefin coating was also introduced in this decade with acceptable adherent to the steel pipes. Two-layer and three-layer polyolefin coatings were also very commonly used outside of the United States. An epoxy-based coatings known as Fusion Bond Epoxy (FBE) which is also called "thin-film epoxy" is currently used to protect pipeline against corrosion. FBE is basically a thermoset polymer coating and its name originated from resin cross-linking and the method of application which is different from that of conventional liquid paint. The process of FBE coating is shown in Figure 1.8 schematically [10].
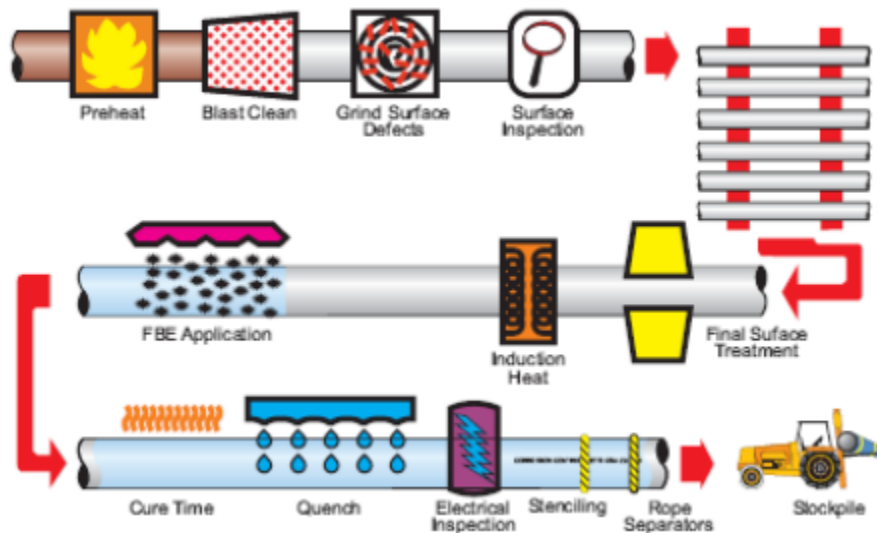
Figure 1.8. Schematic of Fusion Bonded Epoxy powder application process [9].

As it is shown in Figure 1.8, at the typical temperature range of 180°C-250°C the powder will be melted and wet the steel surface, and finally become a solid coating by chemical cross-linking. This process is known as fusion bonding.

Field-applied is another type of the polymer coatings having been used to protect pipelines. Earliest version of this type of coatings was a "granny ragged" hot tar coating which was applied using a saturated cloth. Cold-applied tapes, were another type of field-applied coatings which had limited success. The tape is wrapped around the field joint which sometimes did not adhere well to the joint due to the configuration and promoted localized corrosion.

In 1990s, field epoxy system was used to complement FBE coatings on piping systems. However, if coating failed then they were unable to provide required shielding, and consequently the current could reach to the bare pipe during cathodic [10].

The imperfection and degradation of the polymer coatings inside the soil reduces the pipes resistivity against moisture and strain. It has been trying to find a substitution to be replaced by polymer coatings which pertains longer and provides higher service life. This laid the groundwork to introduce the metallic coatings as a substitution. Among coating technologies, thermal spray technique has been vastly used to deposit hard coatings generally made from metallic materials (i.e. aluminum and zinc for corrosion protection) in submerged offshore applications and pipelines due to the affordable cost and also the excellent corrosion resistance over a wide range of temperature. Following are some information about this technique and their benefits.

1.4.3.2. Hard Coating Technology

1.4.3.2.1. Conventional Methods

There are some methods having been used for decades to apply metallic coatings. Electroplating, conversion coatings (Electroless plating), hot dipping, etc.

1.4.3.2.2. Thermal Spray

This technology for deposition of protective coating was heavily commercialized due to the advantages which will be described later. Thermal spraying is a general term for a group of

coating techniques which rapidly deposit various materials available in powder or wire forms as molten or semi-molten particles onto the surface of a substrate [11]. Very thin protective coatings (tens of micrometers) as well as thick layers (tens of millimeters) can be deposited using thermal spraying techniques. The fundamental feature of thermal spraying process is the heating up of the powders or wires above their melting point and carrying them in the form of individual splats in a hot gas stream toward a substrate. The coating forms by impact, flattening, and solidification of the splats on the substrate. There are several available thermal spray technologies such as Wire Arc Spray, High Velocity Oxy-Fuel (HVOF), and Vacuum Plasma Spray (VPS) or Atmospheric Plasma Spray (APS) processes can be used for different materials with specific properties. There has been a growing interest in using HVOF coating technology due to high quality of the generated coating, low porosity, low cracks, and high mechanical bonding strength between the coating and the substrate. Wire arc spraying has also been center of attention to be used for deposition of protective coatings due to its low cost and flexibility. Both HVOF and Wire arc spraying are easy to operate, require minimum preparation, with inexpensive components. These 2 technologies were selected for this study and will be explained in more details.

1.4.3.2.2.1. High Velocity Oxygen Fuel (HVOF)

HVOF is a process that utilizes supersonic acceleration of material up to several orders of magnitude above speed of sound. The schematic of HVOF process is demonstrated in Figure 1.9.
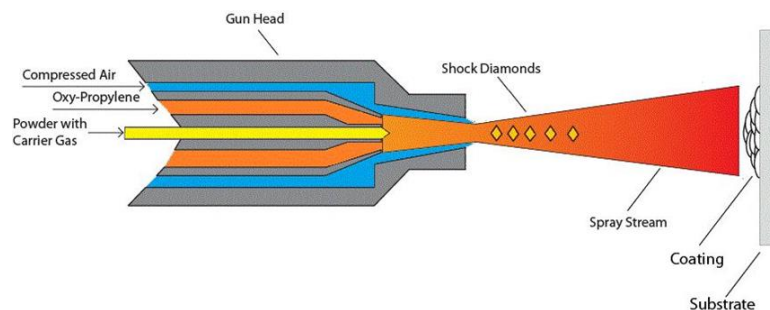
Figure 1.9. Schematic of HVOF spraying process [11].

The desired material in powder form is injected into the stream from a controlled feeder, where it gets heated and accelerated as it's exiting the nozzle. The material stream reaches velocities of several times the speed of sound as it impacts the work surface to form a solid homogenous coating. The tremendous impact energy (with particle speed of between 400 and 650 m/s) [12] attaches particles to each other to form a strong coating. Particles are practically forge welded onto the surface and onto each other to form the coating. Compressive stresses within the coating ensure very high adhesion even for the case of deposition of thick coatings. This characteristic makes HVOF a unique technique for generating a coating with desirable quality and properties [11].

1.4.3.2.2.2. Wire Arc Spraying

Electric arc spray, which is known as twin-wire arc, arc spray, or wire arc spray has been commercially introduced to the market in early 1960s [4, 5]. Unlike the other thermal spraying techniques, in which feedstock particles are indirectly heated by hot gas jet, in electric arc spray process direct current (DC) is used to strike between two consumable electrode wires to effect direct melting. An electric arc is formed in the gap between the wire tips as the two wires are continuously fed together. There is a high velocity air jet located behind the intersection of the wires which shears away the molten particles and propels them toward the substrate. The velocity of in-flight particles in arc spray technique is ranged within 0.8-1.8 m/min which is much lower than that of HVOF. Figure 1.10 shows the schematic of the wire arc spray technique.
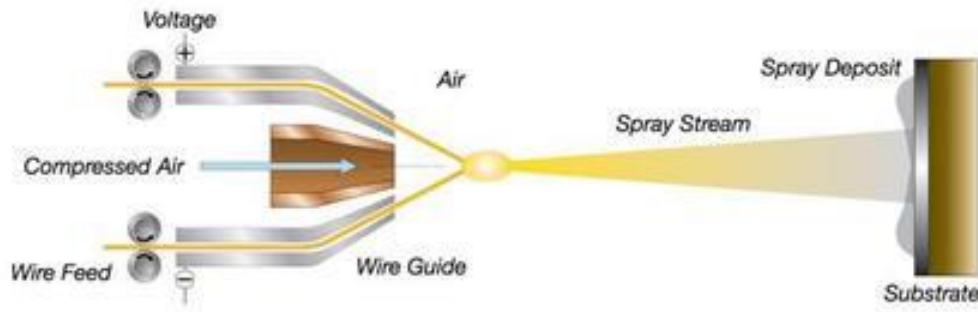
Figure 1.10. Schematic of wire arc spray technique [11].

Both HVOF and Arc Spray techniques have been selected among the other thermal spray methods for the coating deposition. These methods proved to have outstanding characteristics such as high density, high bond strength, optimum hardness, improved toughness, higher coating thickness, beneficial residual stress, excellent wear resistance, superb corrosion resistance, and fine surface finish with more uniform edges [11].

1.5. An Overviw on Corrosion Monitoring Technology

1.5.1. Non-Destructive Techniques (NDT)

Conventional inspection techniques such as ultrasonic measurements, X-ray radiography, eddy current, magnetic test, and penetration test are commercially used in industry, but they are associated with problems such as being very time consuming and/or expensive. There are some other advanced non-destructive techniques including infrared thermography, and optical techniques yield in 3-dimentional mapping. Various types of sensors were used for structural health monitoring and corrosion detection as explained in the following.

1.5.2. Sensor Technology for Corrosion Detection

In this study, it has been tried to introduce different concepts that have been used for detecting and monitoring the external corrosion of pipelines. In this regard, the fundamentals of different types of sensor systems including optical (fuse-like) sensors, capacitive sensors, and

resistive sensors have been discussed and studied in this chapter to stimulate and propose the possible sensor designs for corrosion detection [12-27].

1.5.2.1. Optical or Fuse-like Sensor

Optical sensors are based on transmission of light between a light source and a light detector. The transmission light can travel along either an air path or a fiber-optic cable. Either forms of transmission give immunity to electromagnetically induced noise and also provide greater safety than electrical sensors when used in hazardous environment [19]. In general, fiber-optic sensors, have long life, low cost, very good accuracy with ± 1% of full scale reading, high reliability and small size [19]. The fiber section of fiber-optic cables can be made of plastic, glass, or combination of both materials. This type of sensor is proved to be able to detect pressure, displacement, pH, and smoke. Recently it has been several papers reported the succession of using fiber-optic as corrosion sensor [19, 21-24]. According to the study by S. A. Wade, et al [22], fiber optic corrosion can act as fuse-like sensor which two operating modes (on and off). In this study, they tried to address the proof-of-principle tests carried out on commercially available aluminum-coated optical fiber. The sensors were exposed in both non-corrosive environments (aqua region) and in sea water. The principal of using fiber-optic sensor as a fuse like sensor has been shown in Figure 1.11.
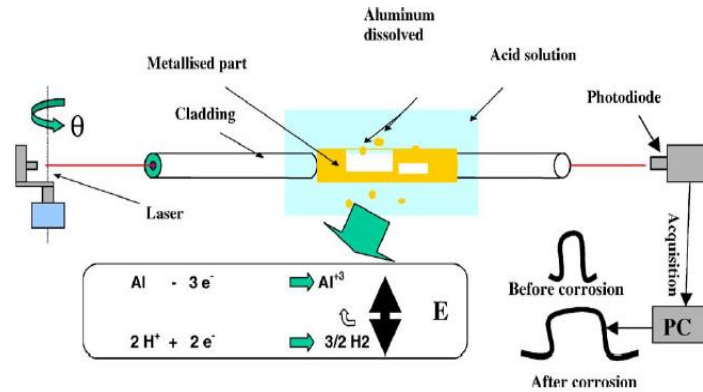
Figure 1.11. Principal of fuse-like corrosion sensor [22].

The metallized part of the optical fiber is immersed in an acidic solution. When corrosion occurs in aluminum coating, part of metallic cladding around the core was removed and the core came in direct contact with acid solution. Hence, attenuation of the higher guided modes should decrease significantly and this phenomenon could be determined by a simple measurement of the electrochemical potential [26]. To conclude, by exposing to the corrosive environment the cladding around the core was removed and the output signal of the fiber will drop accordingly. Therefore, two conditions would take place for the optic sensor which are: 1) the cladding was on the sensor (no effect from corrosive environment on the output) which means the sensor was working and there was an output, and 2) once the clad was removed which means the sensor was damaged and there would be no output signal. In this case, the sensor acts as fuse-like sensor. This prominent of the optic-sensor, makes it a good choice to be used for corrosion monitoring.

However, if the function of using this type of sensor is just to measure strain, temperature compensator is needed to eliminate the temperature interference on the output result. The other issue with fiber-optic is their relatively complicated fabrication process and difficulties of implementation of the sensor to the substrate.

CHAPTER 2. AN OVERVIEW ON CORROSION MECHANISMS OF THERMAL SPRAYED COATINGS

2.1. Corrosion Mechanisms

Various types of corrosive attacks could occur to the coatings developed by thermal spray techniques. General corrosion mechanism, where the average rate of corrosion on the surface is almost uniform, has been responsible for less than 30% of the failure. Localized corrosion, on the other hand, contributing about 70% of the failures in industrial structures and components [28]. Galvanic corrosion occurs when there is a considerable difference between the electronegativity of the materials of the coating and the substrate while they are in contact with an electrolyte. The protection of carbon-steel from corrosion is achievable by either anodic (e.g. nickel) or cathodic coatings (e.g. zinc or aluminum). In the case of anodic coatings, no discontinuity in the coating could be tolerated due to formation of galvanic cell and accelerating the corrosion in the steel part [28, 29]. Selective corrosion may occur when the alloys with noble and reactive components such as WC-Ni and WC-Co with varying quantitative compositions exposed to corrosive environment. Inappropriate heat treatment is another reason for depletion of specific element. For instance, chrome carbide precipitation at grain boundaries of stainless steel could result in Cr-depleted zone with less corrosion protection [29]. Heterogeneous surface of the metals with step, kink, inclusion, cracks, and porosity may also accelerate the corrosion rate in metallic structures [30].

Elevated temperature has usually resulted in more severe oxidation or sulfidation in materials. Hot corrosion has been considered as a two-stage process comprising incubation period exhibiting a low corrosion rate, and propagation of the actual corrosion [30]. The incubation period has been referred to formation of a protective oxide scale and acceleration has occurred when the protective layer broke down. Various mechanisms have been proposed to explain the corrosion

acceleration phenomenon. The most widely accepted corrosion mechanism at elevated temperature was salt fluxing in which oxides can dissolve in the surface as anodic species (basic fluxing) or cationic species (acidic fluxing), depends on the salt composition [30]. Acidic salts are usually high in SO_3 and basics are low in SO_3 [30]. Since, corrosion formation mechanism strongly depends on the type of materials. A complete study in this area is needed to examine corrosion formation in different coating materials. To this end, corrosion mechanism in several common coating materials on steel structures have been studied in this study and special attention has been given to aluminum, zinc, and their alloys, since they are among the most recommended anti-corrosion coatings to protect carbon steel at ambient temperature. Nickel, chrome, tungsten carbide, and their alloys, on the other hand, were the focus of this study, in the case of high temperatures corrosion, due to their wide applications to extend the service life of steel in severe conditions.

2.1.1. Corrosion of Thermal Sprayed Coatings at Ambient and Elevated Temperatures

Table 2.1 has been provided to compare the corrosion mechanism of thermally sprayed coatings deposited on steel to be used for ambient temperature applications. The most common thermal spray techniques used in this case are: D-gun, variety of flame spraying techniques such as HVOF and HVAF, APS, VPS, atmospheric plasma spray+ quenching (APS+Q), and wire arc spraying (WAS). Electrochemical impedance spectroscopy and polarization potential are the most well-known techniques to evaluate the corrosion behavior. The important parameters defined for indication and comparison of corrosion behavior of various materials are corrosion potential (E_{corr}) and corrosion current density (I_{corr}) which are listed in Table 2.1.

Table 2.1. Room temperature electrochemical behavior of some thermal sprayed coatings deposited on steel.

Coating material	Coating method	Corrosive solution	E_{corr} (mV)	I_{corr} ($\mu A/cm^2$)	Observations
Ni-based					
NiTi	APS+Q	3.5%NaCl	-600	3.3	High level of micro-crack and porosity. Corrosion occurred in internal coating [31].
	VPS	3.5%NaCl	-177	0.052	More noble corrosion potentials and lower I_{corr} than that of APS+Q coating due to higher interlamellar cohesion and lower porosity and crack level [31].
	HVOF	3.5%NaCl	-88 to -470	0.085 to 0.3	
	APS	3.5%NaCl	-320	2	More oxide phases, including TiO, and micro-cracks compared to HVOF coating [31].
NiCrBSi	HVOF	3.5%NaCl	-75	14.6	Corrosion along the particles boundary, no change in their morphology [32].
	OAC	3.5%NaCl	-268	0.2838	High amount of corrosion products [33].
Cr-based					
Cr_2O_3	PS	3.5%NaCl	-550	2000	No protection from the coating due to high porosity [34].
Cr_3C_2+NiCr	D-gun	3.5%NaCl	-600	500	Better protection than plasma sprayed Cr_2O_3 due to smaller porosity size [35].
Cr_3C_2-NiCr	HVOF	3.4%NaCl	-210	--	High amount of corrosion product at coating/substrate interface and reduce in corrosion resistance after 12 hr [35].
WC-based					
WC-12Co	HVOF	5% H_2SO_4	-400	10-100	Dissolving the W and Co elements and formation of hydroxides and oxides and poor corrosion resistance [36, 37].
WC-17Co	HVOF	3.5% Na_2SO_4	-330	0.7	Formation of CoO and WO_3 and increase in pit depth to 16μm after 30 days of exposure [38].
WC-10Co-4Cr	HVOF	Sea water	---	3-9	Severe depletion of hard particles contains WC from the coating [39].
WC-10Co-4Cr	HVOF	5%NaCl	-220	0.1	Less micro-galvanic/crevice corrosion than WC-Co [40].
WC-10Ni	HVOF	5% H_2SO_4	--	--	Selective corrosion of Ni binder and falling-off the WC particles after long time exposure [41].
WC-12Ni	HVOF	5%NaCl	-260	60	Red rust spot formation occurred in the longer time compared to WC-20Cr_2C_3-7Ni and WC-10Co-4Cr coatings [42].
Al-based					
99% Al wire	WAS	3.5%NaCl	-1030	5	Formation of passive layer made of Al_2O_3 and $Al(OH)_3$ by increasing the exposure time [43].
Al-Al_2O_3	WAS+PEO	3.5%NaCl	-370	3.5-4.5	Dense coating and excellent corrosion behavior [44].
Al-5Mg	AS	3.5%NaCl	-1070	1	Better corrosion resistance than Zn-Al alloys [45].
Al-Zn-Si	HVAF	3.5%NaCl	-946	2.6	Self-sealing nature and good cathodic protection [46-50].
Al-Zn-Si-RE	HVAF	3.5%NaCl	-965	36.54	Five steps during the corrosion: pitting-dissolution-redeposition, activation corrosion, cathodic protection, physical barriers formed by corrosion products, and the coating failure [48, 49].
Al-Zn-Si-RE	WAS	3.5%NaCl	-965	36.54	Effective cathodic protection and self-sealing behavior [48, 49].
85Al-14.5Zn-0.5Zr	WAS	Sea water	-1884 to -984	1-10	Two reactions: concentration polarization by the reduction of dissolved oxygen, and active polarization by hydrogen gas generation [50].
Al_2O_3-13TiO_2	PS	6%Na_2SO_4	--	--	Corrosion occurred on the steel substrate due to high porosity level through which the electrolyte reached out to the surface and caused the corrosion [51].
Alumina-13Ti	APS	3.5%NaCl	-220	1.9	Lower chance of interconnection with the substrate due to lower porosity level compared to plasma spray [52].
Zn-based					
Zn-15Al	WAS	3.5%NaCl	-1112	40.41	Lower porosity level compared to Zn-30Al and better corrosion resistance [53].
Zn-15Al	FS	Marine solution	-1020	--	Improved cathodic protection, but lower long-term (after 30 days) durability compared to pure Al coating [54].
Zn-15Al	HVAF	SRB	-1040	3.69	Corrosion of surface at first place, formation of ZnS and plugging the pores at the second stage [55].
Zn-Mg-Al	Wire arc	5%NaCl	-992	2.08	Formation of dense corrosion products, clogging the pores and slowing down the corrosion [56].

Table 2.1. Room temperature electrochemical behavior of some thermal sprayed coatings deposited on steel (continued).

Coating material	Coating method	Corrosive solution	E_{corr} (mV)	I_{corr} ($\mu A/cm^2$)	Observations
Zn-Al-Mg-RE-Si	WAS	3.5%NaCl	-687.3	30.9	Self-sealing behavior due to formation of $Al_{3.21}Si_{0.47}$ and $Mg_3Al_2(SiO_4)_{3\ [58]}$.
Zn-Al-Mg-RE	HVAF	5%NaCl	-1010 to -1124	26.66-53.96	Better corrosion resistant behavior than Zn-Al-Mg due to the microstructural refinement of coating by adding RE [57].

2.1.1.1. Aluminum-based Coatings

Aluminum and its alloys have been known as one of the best candidates to be used for protection of steel against corrosion due to their anodic nature respect to steel that eliminates the need for formation of flawless coating. In fact, aluminum coatings act as sacrificial protection to the steel substrate by formation of passive layer which protects both coating and substrate from further corrosion. Plasma spray, wire arc spray, cold spray, and flame spray are typically selected for deposition of aluminum-based coating to perform against corrosive environments, mostly at lower temperatures [43-46, 59-64].

Long-term corrosion mechanism of arc sprayed wire made of 99% aluminum deposited on steel sample and immersed in 3.5 wt.% NaCl solution, at room temperature and also in neutral salt spray test for 1500 h, has been evaluated by Esfahani et al. [43]. The coating contained about 7 vol.% porosity and its corrosion behavior was significantly under the influence of exposure time. By increasing the time of immersion, the electrolyte penetrated through the pores and Warburg impedance observed indicating the corrosion was strongly under diffusion control. By further increase of exposure time, the corrosion products (mainly made of Al_2O_3 and $Al\,(OH)_3$) plugged the defects and hindered higher penetration of the electrolyte into the coating.

The effect of different thermal spray techniques comprising flame spray and electric arc spray on corrosion resistance of aluminum coating deposited on grade C steel substrate has been studied by Regina et al. [59]. Both flame and arc sprayed coatings exposed to saline mist inside a chamber simulating a marine atmosphere for 4000 hours. They have reported that although both

coatings could hinder corrosion formation and propagation on the steel to some extent, better protection was provided by arc sprayed coating since the aluminum oxide/hydroxide phases persisted for longer sputtering time on the lamella. Different corrosion performances of the thermally sprayed coatings were illustrated due to different corrosion products generated after exposing to the marine solution in the flame sprayed coating (mainly bayerite, boehmite and gibbsite) and arc spray deposited coating (aluminum, boehmite, and bayerite phases). According to the work published by Han et al. [61], an increase in the thickness of the arc sprayed Al coating deposited on STS 304 steel could result in even higher corrosion resistance while exposed in sea water for 1260 hours.

Corrosion resistance of Al 7075 coating deposited by cold spraying technique on steel substrates using both air and nitrogen as propelling gas has been addressed by Irissou et al. [60]. They have concluded that cold spray process was more robust than the arc spray due to less complexity that facilitated easier optimization of the coating properties to improve the corrosion protection.

2.1.1.1.1. Al/Al$_2$O$_3$ Coatings

Passive nature of alumina (Al$_2$O$_3$) has turned it to one of the most effective and commonly used coatings to protect steel from pitting corrosion because it can provide more uniform protective layer which is less deteriorated during certain time [44-46, 48-52, 62-69]. Effect of Al$_2$O$_3$ fraction on corrosion resistance of Al-Al$_2$O$_3$ coating deposited by cold spray on steel substrate being exposed to salt spray (3.5 wt.% NaCl) for 1000 h has been studied by Irissou et al. [62]. They have found that addition of Al$_2$O$_3$ to the Al powders improved the deposition efficiency. The optimal deposition quality achieved with addition of ~30 wt.% Al$_2$O$_3$ to the starting powder. The bonding strength between Al and Al$_2$O$_3$ phases was also improved by increasing the fraction of Al$_2$O$_3$/Al.

It has been suggested that a combination of arc spraying and plasma electrolytic oxidation for Al_2O_3/Al coating deposition on steel could significantly enhance the corrosion resistance (Weichao et al. [44]). In this work, aluminum alloy, A7, was deposited on Q235 steel by arc spraying technique, thereafter, it subjected to plasma electrolysis oxidation (PEO) in an aqueous electrolyte containing 5 wt.% NaOH and other additives (pH 11.8). They observed that the duplex coating mainly composed of α-Al_2O_3, γ-Al_2O_3, and θ-Al_2O_3 performed as promising barrier to protect steel substrate, while immersed in a 3.5 wt.% NaCl solution for 1 day.

2.1.1.1.2. Al-Mg Coatings

Magnesium is usually added to Al-based alloys to enhance the durability in corrosive environments for long time exposure as well as mechanical properties such as hardness [45, 63, 64]. Effect of variation of Mg content (Al, Al-3wt.%Mg, Al-5wt.%Mg) on cavitation damage behavior of arc sprayed Al-Mg coating on a mild steel in sea water, at room temperature after 90 min, has been studied by Park et al. [63]. The resultant coatings had porosity level ranged from 6-9%vol. They reported that the weight loss of the Al-Mg coatings was significantly lower than thermally sprayed pure Al coatings. Al-3wt.%Mg coating exhibited the smallest surface damage resulted in better corrosion resistant behavior of the surface. On the other hand, Al-5wt.%Mg has been introduced as a high corrosion protection barrier on steel after 14,000 h exposure to salt water, by Takeyoshi et al. [64].

A comparison between the corrosion performance of arc sprayed Al-5wt.%Mg coating on steel with some other coatings such as: pure aluminum, Zn-35Sn, and Zn-27Al (by mass percent) in a solution contained 3.5 wt.% NaCl, at 25 $^{\circ}$C (by Choe et al.) has shown that Al-5Mg possessed superior corrosion performance compared to the other zinc-based alloys [45].

2.1.1.1.3. Al-Zn Coatings

Pure aluminum coatings function as a good barrier to protect steel substrate but are yet prone to pitting and mechanical damages. Zinc coatings, on the other hand, exhibit highly sacrificial properties that provides cathodic protection, especially when attached to steel substrate. have shown poor durability in weak acid or marine environments [46, 47]. According to the report published by American Welding Society [47], Al-Zn alloys, even without sealing, exposed in marine and industrial environments, provided very high galvanic corrosion protection to steel substrate. In the case of Al-Zn, usually other alloying elements such as Si, RE (rare elements), Zr, and Mg are added to enhance the mechanical and corrosion behavior even better than Al-Zn coatings.

There have been several published works introduced Al-Zn-Si-based alloys as self-sealing material in corrosive environments due to their capability to produce components to clog the pores and prohibit further penetration of corrosive solution in to the coating [46-50]. For instance, the anticorrosion behavior of HVAF sprayed Al-Zn-Si coating on a mild steel substrate in the simulated high concentration ocean environment contained 50 ± 5 gL^{-1} NaCl solution, for 240 h at room temperature, has been investigated by Yang et al. [46]. According to their result, corrosion products mainly contained zinc aluminum carbonate hydroxide hydrate clogged the pores triggered self-sealing behavior and hindered the further corrosion propagation.

Addition of rare element to Al-Zn-Si coating boosted its self-sealing properties [48]. Jiang et al. [48] have assessed the electrochemical behavior of Al-Zn-Si-RE alloy deposited on a mild steel, using HVAF. The corrosion medium used in this study was 3.5 wt.% NaCl solution at room temperature. The corrosion mechanism of Al-Zn-Si-RE explained to be very similar to that of Zn-15wt.%Al, in which five distinct stages were observed: pitting-dissolution-redeposition, activation

corrosion, cathodic protection, physical barriers formation by corrosion products, and finally the failure of the coating. The corrosion results of Al-Zn-Si-RE coating deposited on mild steel by arc spray technique and immersed in 3.5 wt.% NaCl solution reported by Jiang et al. [49] were in good agreement with the ones reported by Jiang et al. [46]. Both studies have described that the presence of the RE in the coating did not affect the phase compositions of the corrosion products, but improved the formation of fine, continuous, and uniform phases in the coating layers, which improved the stability of self-sealing barrier. A Schematic of self-sealing mechanism for a hypothetical metallic based thermal sprayed coating exposed to NaCl solution has been developed in this work as shown in Figure 1.11. This model was created according to findings by Jiang et al. [49]. In the beginning, the pitting occurs on the surface of the coating in the initial stage and metal ion (M^+) is deposited on the coating surface in the form of dissolution and redeposition. This phenomenon has been known as "pitting-dissolution-redeposition period" [49]. At the next stage, corrosive solution gradually diffuses through the pores and voids in the coating, and accumulation of the corrosion products at the surface of the coating hinders further penetration of the corrosive solution which is known as self-sealing behavior. In fact, evolution of the corrosion product film containing M^+ particles resulted in formation of a very good physical barrier which hindered the electrochemical corrosion processes.
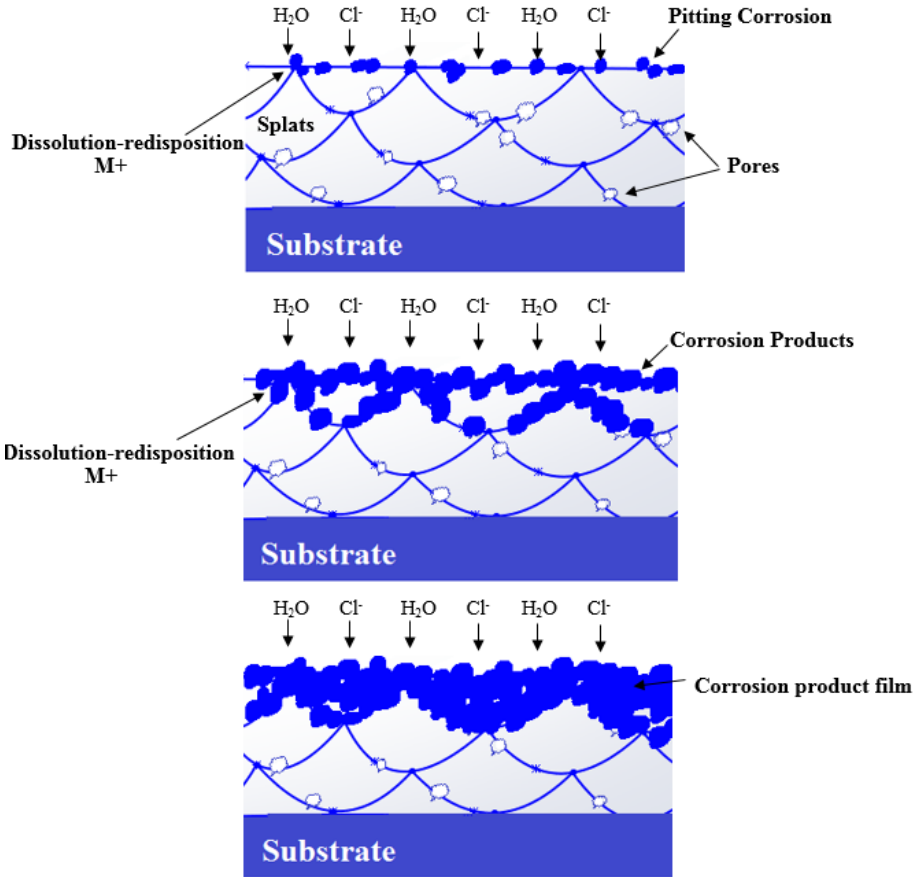
Figure 2.1. A Schematic of self-sealing mechanism of coating in NaCl solution, step by step process starting from top to the bottom.

It has been shown that deposition of 85Al-14.5Zn-0.5Zr (in weight %) coating on steel substrate using arc spraying process could successfully help to prevent corrosion of steel in the ocean environment at room temperature (Kim et al. [50]). In this work, several sealants comprising: water-soluble fluorine (hereinafter W-F), nano-fluorine (hereinafter nano), hybrid ceramic (hereinafter ceramic), salt-tolerant epoxy (hereinafter epoxy), and fluoro-silicon (hereinafter F-Si) have also been used to enhance the corrosion resistance. Electrochemical evaluation of the coating showed two distinct reactions: concentration polarization by the reduction of dissolved oxygen ($O_2 + 2H_2O + 4e \rightarrow 4OH^-$) and active polarization by hydrogen gas

generation ($2H_2O+2e \rightarrow H_2+2OH^-$). It has been suggested that using sealant material could significantly increase the resistance against cavitation.

2.1.1.1.4. Other Al-based Coatings

There are several other published works studied on the effect of addition of other alloying compositions such as TiO_2, SiC, and ZrO_2 to aluminum-based coting on the corrosion resistance. It has been reported different plasma spray techniques could have significant effect on the porosity level of Al_2O_3-TiO_2 coating and the corrosion behavior as a resultant [51, 52, 65, 66]. For instance, corrosion performance of plasma sprayed Al_2O_3-13wt.%TiO_2 coating on a carbon steel to be used in aggressive environments composed of 6 wt.% Na_2SO_4 solution, has been estimated by Wang et al. [51]. All these results have revealed that electrochemical corrosion mainly occurred on the steel substrate during immersion since Fe and O detected in the corrosion products due to high porosity level through which the electrolyte reached out to the surface and caused the corrosion. Habib et al. [65], on the other hand, have reported very low porosity in alumina-titania (Al_2O_3/TiO_2) coating formed by flame spray technique on a steel sample. Liscano et al. [52] have suggested that sealing the atmospheric plasma sprayed alumina-13wt.%titanium coating, exposed in 3.5wt.% NaCl, using different sealants such as phosphoric acid, phenol, and epoxy-based material could help decreasing the interconnected porosities to the substrate and improved the corrosion resistance .

Yttria-stabilized zirconia is another alloy having been added to the alumina-based coatings due to its good adhesion and strong oxidation protection ability [67-69]. There are few works on corrosion resistance of alumina-zirconia coating deposited by thermal spray techniques, which might be due to huge difference in the melting points of the constituents. According to the results reported by Amaya et al. and Campo et al. [67-69], high level of porosity and crack have been indicated in the microstructure of the Al_2O_3-YSZ coating deposited by plasma spray technique that

followed by penetration of electrolyte contained sulfate in to the steel substrate and formation of Fe_2O_3, FeS, and, $FeSO_3$ phases. They concluded that thermally sprayed Al_2O_3 coating have much higher long-term corrosion resistance than Al_2O_3-YSZ in molten Na_2SO_4 due to alkaline dissolution of Al_2O_3 in such an environment [67].

In summary of the thermal sprayed Al-based coatings: wire arc spraying is highly recommended technique for deposition of Al-based coatings. Addition of low amount of Mg to Al could improve their mechanical properties alongside with their corrosion performance. Al-Zn-Si-RE is known as self-sealing material in corrosive environments due to its capability to produce components that could clog the pores and prohibit further penetration of corrosive solution in to the coating.

2.1.1.2. Zinc-based Coatings

Thermally sprayed zinc-based alloys have been widely used to protect steel constructions due to their high stability in the sea water and lower electronegativity compared to steel which makes it acts as a sacrificial anode [53-58, 70-82]. However, if the coating is exposed to high humidity or mediums containing aggressive species such as chloride or sulphate ions, the Zn will dissolve in the solution and result in less dense protective layer following by localized corrosion [70]. This issue has not been significant when Al-based alloys have been used for corrosion protection [70]. Thermal spraying techniques have been employed for over 50 years to spray zinc and its alloys for variety of applications [70]. Twin wire arc has been one of most recommended methods among the thermal spray techniques in the case of using zinc-based materials.

Corrosion resistance of wire arc deposited Zn coating on a steel sample has been compared with those of Al and Zn-15wt.%Al coatings exposed to salt spray contained 5 wt.% NaCl, at room temperature, in the study performed by Gulec et al. [70]. They claimed Zn-15wt.%Al has shown

the best corrosion resistance since it had two protection mechanisms: (1) creating a stable oxide, similar to Al coatings, (2) acting as sacrificial anode, alike Zn coatings [70]. According to the report published by thermal spray committee of Japan Association of Corrosion Control (JACC) [71, 72], flame and arc sprayed Zn coatings developed on carbon steel pipes started to suffer degradation after 7 years of service in the marine environment. They reported that Al and Al-Zn coatings deposited with the same techniques performed with no significant corrosion on the surface after 18 years exposure to the same environment.

Results published by Katayama et al. [55] indicated that Zn coating deposited by gas wire flame spray technique on carbon steel and immersed in 0.1 M NaCl solution effectively retarded the corrosion rate by formation of corrosion products on the surface during long-term exposure. However, when it is compared to aluminum-based coatings, better performance of aluminum-based coatings in the most cases were reported for long-term applications owing to the formation of thin oxide film on the surface [55].

2.1.1.2.1. Zn-Al-based Coatings

Generally, corrosion in alloys containing zinc and aluminum occurs in two different mechanisms which are passivation due to aluminum oxide formation and acting as sacrificial anode due to high electronegativity of the zinc. These characteristics make Zn-Al alloys superior than Al coating and Zn coating for corrosion protection. A comparison of the corrosion experiment results of arc sprayed Zn-15wt.%Al and Zn-30wt.%Al coatings, when subjected to a salt spray environment for 1000 h, has been addressed by Varacalle et al. [75]. The porosity of the Zn-30Al coatings was higher than that of Zn-15Al, thus, higher corrosion resistance observed in Zn-15Al coating. Moreover, corrosion resistance of the both coatings was effected primarily by nozzle diameter, and secondary by current and spray distance. Excellent corrosion resistance has been

29

observed for flame sprayed Zn-30wt.%Al coating on steel during thirty-years exposure to corrosive environment. It is basically, due to the generation of thick layer of corrosion products formed by selective dissolution of zinc [55]. Corrosion resistance of high speed electric arc sprayed Zn/Al (300/100 μm thickness) composite and Zn/Al (100/300 μm thickness) composite on steel exposed to salt spray contained 5 wt.% NaCl at room temperature after 30 days have also been investigated [76]. Mio et al. observed that the porosity of Zn/Al (300/100 μm) was lower than that of Zn/Al (100/300 μm) and consequently Zn/Al (300/100 μm) showed better corrosion resistance. It has been indicated that flame sprayed Zn-15wt.%Al exposed to marine type environment for one year has shown improved cathodic protection capabilities compared to pure aluminum coating tested at the same condition [77]. However, the long-term corrosion durability of pure aluminum coating was yet higher than those of both pure Zn and Zn-15Al coated steels [53, 70, 72, 77]. In other cases, dual system of Zn/Al formed by primer coat of flame sprayed zinc and second coat of aluminum as top coat generated with the same technique showed an excellent corrosion resistance due to cathodic protection ability of zinc and erosion resistance of aluminum [54]. It has been suggested that, using sealant such as wash primer could improve the corrosion behavior and extend its service life. Corrosion performance of Zn-15wt.%Al coating deposited by high velocity arc spray technique in presence of sulfate-reducing bacteria (SRB) in seawater after eight days has been evaluated by Hong et al. [78]. The coating was corroded at the early stage of immersion process mainly by metabolites, thereafter the ZnS formed as corrosion product and plugged the porosity and reduced the corrosion rate. They suggested sealing the coating system with silicon improved the corrosion performance [78].

2.1.1.2.2. Zn-Al-Mg-based Coatings

As it is previously mentioned, magnesium is a potential candidate to be used as the sacrificial anode for protection of industrial components. Addition of magnesium to Zn-Al-based alloy could significantly enhance the corrosion resistance due to self-sealing nature of Zn-Al alloys [78]. This was attributed to formation of intermetallic phases such as $MgZn_2$ and $MgZn_{11}$ and, in some cases, $Zn_5(OH)_8C_{l2}.H_2O$ [78] formation of which plugs the pores and protects the substrate against electrolyte. As the result, Zn-Al-Mg coatings possessed even higher corrosion resistance than that of pure Zn and Zn-Al coatings [78]. It has been reported that the time for red rust to appear in the neutral salt spray test of Zn-Al-Mg coating is 4-20 times higher than that of zinc coatings [78]. In fact, magnesium reacts with CO_2 and forms $MgCO_3$ that hinders formation of hydrozincite $Zn_5(CO_3)_2(OH)_6$ which is drawn to be less protective than simonkolleite $Zn_5(OH)_8Cl_2.H_2O$ [78]. Another reason for superior corrosion resistant behavior of the Zn-Al-Mg coating attributed to buffering effect of dissolved Mg which inhibits formation of ZnO [78]. Formation of Layered Double Hydroxides (LDH) by co-precipitation of the corresponding ions is assumed to be the main contribution to enhance the corrosion resistance of these alloys [78].

Corrosion performance of Zn-Al-Mg coating deposited by wire arc spray technique using a $ZnAl_2$ sheath and $ZnMg_{6.3}$ has been investigated by Bobzin et al. [80]. They noticed that the Zn-Al-Mg coating after 2448 h exposing to neutral salt spray contained 5 wt.% NaCl was remained un-corroded state. This has been explained due to formation of simonkolleite and LDH which provide dense barrier against the electrolyte. It has also been found that the reaction of Mg ions with CO_2 and generation of $MgCO_3$ hindered further corrosion reaction and formation of hydrozincite. Usually, higher mount of hydrozincite on Zn and Zn-15Al coatings after exposure to the same medium detected in comparison with Zn-Al-Mg coatings. Zhu et al. [78] have shown that

wire arc sprayed coating with a composition of Zn-14.9Al-5.9Mg-3O (in weight %) possessed better electrochemical behavior compared to that of Zn-Al coatings which was attributed to the formation of corrosion products, which blocked the pores and prevented further corrosion at room temperature.

Similar to Al-Zn-Mg-based coating, addition of RE to Zn-Al-Mg alloys could improve the self-sealing behavior due to the reduction in the size of atomized molten in-flight droplets and formation of more stable phases that directly affected the corrosion resistance [57, 78, 82]. Corrosion behavior of cored wires and high velocity arc sprayed Zn-Al-Mg-RE coatings immersed in 5 wt.% NaCl solution has been evaluated by Liu et al. [82]. It has been concluded that addition of small amount of RE markedly enhanced the anticorrosion properties of the coating in accordance to the formation of denser, more compact, and uniform corrosion products as result of coating refinement by addition of RE elements. According to the results from study performed by Yan et al. [57, 78], addition of RE element could increase the liquidity of Al and improve the microstructural properties of the coating by decreasing the porosity level. The measured corrosion resistance of the high velocity arc sprayed Zn-Al-Mg-RE coating exposed in 5wt.% NaCl compromised with those reported by [78] advocating the self-sealing nature of the coating due to formation of corrosion products such as Zn, $Zn_5(CO_3)_2 \cdot (OH)_6$, $ZnO \cdot ZnCl_2 \cdot 2H_2O$, $ZnCl_2 \cdot 4Zn(OH)_2 \cdot H_2O$, $Mg_2(OH)_3 \cdot Cl \cdot 4H_2O$ and $Mg_6Al_2(OH)_{18} \cdot 4.5H_2O$ [78]. Effect of addition of silicon (1-6%) on corrosion behavior of high velocity arc sprayed Zn-Al-Mg-RE coating exposed to 3.5 wt.% NaCl solution was investigated by Kuiren et al. [58]. The results indicated that Zn-Al-Mg-RE-Si coating had higher corrosion resistance than Zn-Al-Mg-RE due to presence of glass-like state phase attributed to $Al_{3.21}Si_{0.47}$ and $Mg_3Al_2(SiO_4)_3$ formed on the external surface of Zn-Al-Mg-RE-Si coating which acted as self-sealing barrier, depressed the porosity of coating

32

and hindered reaching the electrolyte to the substrate. They also reported that addition of 3 wt.% silicon to the initial feedstock resulted in the best corrosion resistant behavior.

The characteristics of thermally sprayed Zn-based coatings can be summarized as following: Zinc-based alloys act as sacrificial anode and protect steel against corrosion due to their lower electronegativity compared to steel. Adding magnesium to Zn-Al-based coating resulted in formation of some intermetallic phases that could improve corrosion behavior of the coatings. Moreover, addition of Si to some zinc based alloys containing Al, Mg, and RE could also improve anticorrosion behavior of the deposited coating. Table 2.2 has presented a summary of high temperature corrosion behavior in different thermally sprayed coating materials.

Table 2.2. Hot corrosion behavior of some thermal sprayed coatings deposited on steel.

Coating material	Coating technique	Corrosive environment	Temperature (ºC)	Observations
Ni-based				
Ni–50Cr	CS	$NaSO_4$-$60V_2O_2$	900	Formation of passive layer contained Cr_2O_3 and nickel oxide, but yet high porosity in the coating [58].
Ni-50Cr	D-gun	$8CO_2$+$18H_2O$+$0.1HCl$+N_2	500 and 600	Chlorination and oxidation of the substrate due to high porosity of the coating [58].
Ni-20Cr	APS	$0.7Na_2SO_4$-$0.3NaVO_3$	900	Generation of Cr-rich oxide layer of ~ 30μm as a passive layer [58].
NiCrBSi	HVOF	Na_2SO_4–60 V_2O_5	900	Passive layers made of oxides of silicon/chromium/nickel, and spinel's of nickel and chromium [32, 33, 83-88].
Inconel 718	HVOF	3.5%NaCl	250	Incomplete oxidation, unstable passive layer due to high solubility of chromium oxide in the solution [89].
Cr-based				
Cr_3C_2-25NiCr	D-gun	$75Na_2SO_4$+$25K_2SO_4$	900	Diffusion of elements such as Fe, Cr, and Ni from the substrate to the coating and high gained weight due to high porosity level [32, 33, 83-88].
WC-based				
WC-NiCrFeSiB	HVOF	Na_2SO_4-25NaCl	800	Formation of Cr_2O_3, NiO, $NiCr_2O_4$, and Fe_2O_3 and sealing the pore hindering the aggressive species penetration [58].

It is mentioned earlier that nickel, chrome, tungsten carbide, and their alloys have been the most common-used corrosion protection coatings deposited by thermal spraying techniques such as D-gun, APS, cold spraying, and HVOF for applications at elevated temperatures. The range of the temperature used to evaluate the hot corrosion behavior of the coatings was within 500-900 °C.

The most common parameters considered for hot corrosion evaluation were weight-loss and weight-gain. Electron probe microanalysis (EPMA) is also a promising technique for evaluation of hot corrosion. Porosity is considered as one of the major contributors which significantly interfered in the corrosion mechanism. A comprehensive review of corrosion mechanism of different coating materials at elevated temperature will be discussed in the next sections.

2.1.1.3. Nickel-based Coatings

Nickel-based coatings are often deposited by thermal spraying processes to improve corrosion resistance, wear resistance, and mechanical properties such as toughness and hardness of the surface to function in advanced engineering applications, especially at elevated temperatures [90]. Nickel commonly was combined with other elements such as titanium, chrome, silicon, and boron to increase the passivity behavior and mechanical properties of the coatings. Plasma spraying, HVOF, cold spraying, and flame spraying have commonly been used to deposit Ni-based alloys for corrosion protection application. Among Ni-based alloy, Ni-Cr-based, NiCrBSi, and Ni-Ti-based, attracted high attention to be used as corrosion protection barriers due to their excelled corrosion resistance.

2.1.1.3.1. Ni-Cr Coatings

Nickel-chromium alloys have been mostly used as welded and thermally sprayed coatings in fossil fuel-fired boilers, waste incineration boilers, and electrical furnace due to their elevated temperature mechanical and corrosion resistance behaviors [32, 84, 86, 88, 91-94]. Thus, in the case of Ni-Cr coatings, most of the published works dealt with evaluation of corrosion behavior of these coatings while exposed to high temperature condition ranged within 700-900 $^{\circ}$C. The high corrosion resistance of Ni-Cr-based alloys attributed to the formation of Cr_2O_3 passive layer which could protect the base material from corrosion up to ~1200 $^{\circ}$C [91].

The hot corrosion resistance of the Ni-50wt.%Cr coating deposited on boiler steel SA-213-T22 and SA516 (Grade 70) samples, by cold spraying process, has been investigated by Niraj et al. [91]. The coated samples were exposed to an aggressive environment of $NaSO_4$-60wt.%V_2O_2 under a cyclic condition in which after 50 cycles each sample was hold 1 hour at 900 $^{\circ}$C in a tube furnace followed by 20 minutes cooling in ambient temperature. The authors have reported no indication of spalling in the both coatings after exposed to corrosive environment. Ni- and Cr-oxides were detected in the EDS results of the both coatings which indicated formation of the passive layer.

In the work done by Yamada et al. [92], Ni-50wt.%Cr alloy coating was deposited on boiler tube made of carbon steel using denotation spray method and exposed to corrosive bath in the furnace at temperatures of 500 $^{\circ}$C and 600 $^{\circ}$C. Sample was exposed to refuse incineration ash contained 4.66 Na, 5.11 K, 15.4 Ca, 1.8 Mg, 5.4 Fe, 0.11 Pb, 0.66 Zn, 7.04 S, and 11.3 Cl (wt.%). The feed corrosion gas was made of 8%CO_2+ 8%O_2+ 18%H_2O+ 0.1%HCl+ N_2 into the electric furnace. The EPMA results of revealed the presence of chlorine, which indicated as the main reason of hot corrosion formation in the coating. The high porosity in the deposited coating, allowed chlorine and oxygen diffusion in to the substrate which could led to the internal chlorination and oxidation and weakening of the bonding between the coating and the substrate [92, 93].

Elevated temperature corrosion performances of Ni-20wt.%Cr coating deposited by low pressure plasma spraying (LPPS) method on UNS S30400 stainless steel has been evaluated by Longa Nava et al. [93]. The coating was exposed in thin fused films of sodium sulfate and sodium metavanadate (Na_2SO_4-0.3mol.%$NaVO_3$) at 900 $^{\circ}$C, in a 1% sulfur dioxide-oxygen (SO_2-O_2) atmosphere for 16 hours. The authors have reported the formation of Cr-rich oxide layer of ~30µm

35

on LPPS coating, after corrosion exposure, which effectively prevented sulfidation corrosion of the coating.

In the work presented by Abuali. G et al. [95] electrochemical behavior of Inconel 718 coating deposited by HVOF technique on carbon steel substrate has been examined using an innovative device: High Temperature Corrosion Measurement Device (HTCMD), in 3.5% NaCl solution at 250 ºC. According to their result, the coating was not able to grow a stable passive oxide layer to protect the steel against corrosion effectively. This was explained due to high solubility of the oxide layer (mainly chromium oxide) in the corrosive environment as well as insufficient oxygen content at high temperature condition which resulted in incomplete oxidation on the surface [95].

2.1.1.3.2. NiCrBSi Coatings

NiCrBSi alloys are usually deposited using HVOF, APS, and flame spraying to protect steel against chemical interaction with its environment [96, 97]. This alloy has shown excellent corrosion resistance in alkaline solution, due to the self-passivation of the coating even under very severe corrosive environments [33, 83, 85, 96, 97]. It has been found that the corrosion resistance of NiCrBSi coating deposited with HVOF process was higher than the other commonly-used thermal spraying techniques because of lower level of porosity generated in the coating by HVOF process [96, 97].

Electrochemical behavior of the HVOF and oxyacetylene flame sprayed NiCrBSi coatings on steel substrates have been investigated by Zhao et al. [96]. The coatings were exposed to solutions contained 1.0 N H_2SO_4, 1.0 N HCl, 1.0 N NaOH, 3.5 wt.% NaCl, and 3.5 wt.% NaCl acidified with acetic acid to give a pH of 3. The Tafel polarization results revealed excellent corrosion resistant behavior of HVOF deposited NiCrBSi coating in alkaline solution. They

reported that HVOF sprayed coating possessed lower porosity level than that of oxyacetylene sprayed coating. It resulted in more severe corrosion in the oxyacetylene coating where due to high corrosion rate, particles were separated from the surface of the coating.

In the other work presented by the same group [97], the corrosion mechanism of NiCrBSi coating applied on a low carbon steel substrate by HVOF technique and exposed in 3.5 wt.% NaCl solution for 60 days was studied using EPMA. They reported that after exposure in the corrosive environment, no selective corrosion of favored element was observed. Corrosion in the coating was mostly attributed to the presence of un-melted particles, pores, inclusion and micro-cracks, and laminar structure of the coating. They also acknowledged that penetration of Cl^- ion in to the coating accelerated the corrosion process. The authors reported that optimization of spraying parameters could significantly improve the quality of the coating and consequently the its corrosion resistant.

Corrosion performance of NiCrBSi coating deposited by HVOF on Fe-base substrates at elevated temperatures in molten salts contained Na_2SO_4-60 wt.%V_2O_5 for 50 cycles has been speculated in multiple works published by Sidhu et al. [32, 33, 83-88]. They found that the coatings were very effective in decreasing the corrosion rate of the steel samples at high temperature (900 $^\circ$C). It was mentioned that this effect was attributed to the formation of passive layers made of silicon/chromium/nickel oxides as well as nickel and chromium spinel's [32, 33, 83-88, 98].

2.1.1.3.3. Ni-Ti Coatings

Titanium has been one of the most well-known elements having been added to nickel-based alloys to protect the surface of engineering alloys including steel [99-103]. Ni-Ti intermetallic compounds are famous due to their shape memory effect (SME). This compound have also shown excellent corrosion resistance in various environments [104]. The high corrosion resistance of

titanium alloys is attributed to formation of TiO_2 that acts as passive film on the surface [105]. However, manufacturing process of NiTi alloy is very complicated and expensive. Thus, coating techniques such as thermal spraying methods have been used to generate this alloy on the surface of engineering components [31, 106, 107]. NiTi has been developed by several thermal spraying techniques such as HVOF, VPS, and atmospheric plasma spray quenching (APS+Q) [31, 108-111]. This alloy drawn to be very susceptible to react with oxygen, hydrogen, and nitrogen during exposition to high temperature conditions. Thus, in the case of deposition of this alloy in low pressure mode, the spray chamber is filled with inert gas and maintained at low pressure (~ 100 mbar) to avoid oxidation. Ni_3Ti, and Ti_2Ni are two undesirable intermetallic phases formed during deposition of NiTi coating due to their poor corrosion and mechanical properties [31, 106, 107]. NiTi coatings possess lower electronegativity compared to steel substrate. Thus, in the case of formation of galvanic corrosion between the coating and the steel substrate, NiTi coatings will act as cathode and accelerate the corrosion in steel [31].

It has been shown that pitting potential of NiTi deposited on AISI 316 steel were comparable to that of the substrate (Chiu et al. [102]), but the protection and corrosion potential were somehow lower. The authors have claimed that laser surface modification of NiTi alloy in order to produce a crack- and porosity-free layer resulted in a significant corrosion resistant improvement due to reduction in the corrosion current density (I_{corr}) [102].

Thermally sprayed NiTi has been introduced by Guilemany et al. [31] as an alternative corrosion resistant coating to stainless steel. They have developed the NiTi coating by three different thermal spraying techniques including HVOF, VPS, and APS+Q and evaluated their corrosion behavior using potentiodynamic polarization test in 3.5 wt.% NaCl solution. They have shown VPS and HVOF deposited coatings presented more noble corrosion potentials and lower

38

I$_{corr}$ than those of APS+Q coating due to higher interlamellar cohesion and low porosity and crack level of VPS and HVOF coatings. VPS and HVOF coatings exhibited potential fluctuation during the time course test which was attributed to irregular electrolyte penetration and/or depassivation/ repassivation process as a consequence of a pitting attack of chloride to the regions near oxides or new phases, where localized attack is favored. No oscillation observed in Tafel curve of APS+Q coating which was explained due to higher porosity and cracks presence in APS+Q deposited coating through which higher penetration of the electrolyte directed to the substrate causing homogeneous wettability of the whole system and resulted in no potential oscillation in its Tafel curve which indicated lower corrosion resistance.

Corrosion performances of HVOF and APS thermally sprayed NiTi intermetallic coatings on 316L stainless steel in 3.5 wt.% NaCl solution have been compared, in the works published by Verdian et al. [106, 107]. According to these reports, HVOF deposited coating has contained less oxide phases, including TiO, and micro-cracks compared to APS deposited coating. Tafel polarization indicated that the corrosion performance and passive ability of HVOF deposited NiTi coating were higher than those of APS coating. The results of EIS test have illustrated one time constant (one semi-circle in Nyquist plot) for the HVOF coting confirming perfect coating passivation. On the other hand, they have reported two time constants (two semi-circles in Nyquist plot) observed in the EIS result obtained from APS deposited NiTi coating representing that corrosion occurred in interior coating. They have concluded that different thermal spraying techniques effect on level of micro-cracks and inter-splat oxides governing the electrolyte penetration in to the coating and accelerate/decelerate the localized corrosion mechanism [31, 106, 107].

In summary of the thermal sprayed Ni-based coatings: In general, nickel rich coatings protect steel against corrosion by formation of a passive layer. The high corrosion resistance of Ni based coatings containing Cr/Ti-based has been attributed to the formation of Cr_2O_3/TiO_2 passive layers. HVOF is the highly recommended thermal spraying technique to deposit Ni-based coating due to the lower oxide and porosity content. Most of the available literatures for thermally sprayed Ni-based coatings speculated the appearance of the coating and the amount of formation of the new products (weight-gain) or reduction in the weight of the coating (weight-loss) as the indications to corrosion behavior. Thus, electrochemical behavior of Ni-based coating at high temperature still remained to be elucidated.

2.1.1.4. Chrome-based Coatings

Chromium has been used for many years as an effective protection by electroplating for repair applications, corrosion protection, and to reduce the surface friction. Due to low deposition rate of the electro-plating, thermal spray techniques such as plasma spray and denotation gun were introduced as the alternative coating processes [98]. However, it has been reported that plasma-deposited chromium has not shown good wear resistant properties compared to electroplated chromium at ambient temperature. This could be due to high residual stress induced in the coating during the thermal spraying process [98]. To improve the mechanical properties of the chrome-based coating deposited by thermal spraying techniques, alloys comprised chromium carbide dispersed in a chromium matrix have also been examined. The majority of the published works dealing with thermally sprayed Cr-based coatings, suggested Cr_2O_3 [34, 98, 112, 113] and Cr_3C_2-NiCr [35, 43, 59, 114-120] as two high corrosion resistant coatings while their mechanical properties pertained in a good condition as well.

2.1.1.4.1. Cr_2O_3 Coatings

Chromium oxide coatings considered as one of the best corrosion resistant coatings among the other Cr-based alloys to hinder the possible chemical attack on metallic components especially while exposed in alkaline and acidic environments. Corrosion behavior of Cr_2O_3 coating, has found to be very high especially at elevated temperature in severe environments [34, 112, 113]. However, their relatively higher cost compared to other corrosion resistant alloys such as aluminum, zinc, and tungsten carbide has limited Cr-based alloys' applications. Using thermal spray techniques such as plasma spraying to deposit chrome oxide mostly demands surface modification due to high porosity evolution.

For instance, the electrochemical and long-term corrosion behaviors of plasma sprayed Cr_2O_3 on steel samples in 3.56 wt.% NaCl solution and in accelerated salt spray test, for 500 h at room temperature, have been investigated by Ashby et al. [112]. They indicated that, the coating possessed relatively high level of porosity (~3 vol.%) triggered no significant protection compared to the bare steel. This was explained due to the fact that high level of porosity provided a channel through which the salt solution reached out to the substrate and accelerated the galvanic corrosion of the steel. To resolve this issue, they suggested using either a crevice-corrosion-resistant substrate or applying an epoxy sealant to close of the porosities in the case that corrosive environments are encountered.

Atmospheric plasma sprayed Cr_2O_3 coating sealed by aluminum phosphate has been introduced by Leivo et al. [34]. In this work, aluminum phosphate sealant has been used to close out the open porosities and aid the corrosion resistance behavior of the substrate. In the other study performed by Ashby et al. [113] electrochemical behavior of the chrome oxide coating was compared to that of Cr_3C_2+NiCr coating and explained that chrome carbide dispersed in the NiCr

41

matrix could significantly enhance the corrosion resistance due to smaller porosity size and better quality of the coating.

2.1.1.4.2. Cr$_3$C$_2$-NiCr Coatings

There was an interest during 1990-2010 in deposition of coatings made of nickel chrome matrix contained chrome carbide particles uniformly dispersed in the matrix [35, 114-120]. The most common thermal spray techniques used to deposit Cr$_3$O$_2$-NiCr coating on steel substrate have been HVOF [35, 114-120] and denotation gun [119, 120]. However, HVOF is found to be the most desirable thermal spraying technique to substitute chrome plating due to the low porosity, good oxidation resistance, high bonding strength, and high deposition rate [35, 114-120].

The corrosion resistance of hard chromium coating has been compared to that of HVOF deposited Cr$_3$C$_2$-NiCr in 3.4 wt.% NaCl solutions at room temperature, for long immersion time [114]. Hard chromium stands for the corrosion resistant coating developed by electroplating processes [41]. The result of potentiodynamic polarization and EIS test advocated superior corrosion resistance of HVOF sprayed Cr$_3$C$_2$-NiCr coating compared to that of hard chromium coating. In the case of hard chromium coating the electrolyte attacked the surface of the steel substrate through cracks and Fe could penetrate to the coating, whereas that did not happen for Cr$_3$C$_2$-NiCr coating. However, immersion in corrosive environment after 12 hours showed a continuous decrease in the corrosion resistance of thermal sprayed coating with time, while hard chromium coating exhibited small variation in the experiment time course. Higher amount of corrosion products was detected at coating/substrate interface of Cr$_3$C$_2$-NiCr coated sample, only after long immersion time, while hard chromium coating underwent localized corrosion at cracked regions [35, 114-120].

Corrosion performance of Cr_3C_2-NiCr coating deposited on a UNS-G41350 steel substrate using HVOF technique has been speculated by Espallargas et al. [116]. According to the results of electrochemical measurements, Cr_3C_2-NiCr coating has exhibited even better corrosion resistance compared to WC-Ni under corrosive conditions. Guilemany et al. [118] have studied the effect of thickness of coating (151, 285, 430, 542, and 715μm) on the electrochemical behavior of the HVOF sprayed Cr_3C_2-NiCr coating on UNS G11200 steel immersed in 3.4 wt.% NaCl solution. The author reported low amount of porosity (1-2%) for the all coatings with various thicknesses. However, the results showed that although higher thickness diminished the probability of pore interconnection with the substrate, it resulted in higher number of cracks, interlayer separation, and residual stress distribution that may have adverse effect on the corrosion behavior. They suggested an optimized thickness value to improve the corrosion resistant.

The effect of gun transverse speed on electrochemical behavior of HVOF sprayed Cr_3C_2-25wt.%NiCr coatings on SAE4140RH steel in 0.5 M H_2SO_4 solution has been studied in the work published by Suegama et al. [35]. No significant corrosion formation was observed on the coating surface during immersion in the corrosive environment. The higher transverse speed of the gun resulted in formation of denser coating structure with lower level of cracks and porosity which triggered better corrosion resistant. They have also witnessed after longer time, when the electrolyte could reach to the substrate, the galvanic cell was formed between the coating and the substrate and since the coating possessed nobler potential, steel was corroded.

Hot corrosion resistance of Cr_3C_2-NiCr coating deposited by denotation gun spraying technique has also been investigated [119, 120]. Kamal et al. [119] have evaluated cyclic hot corrosion resistance of denotation gun sprayed Cr_3C_2-25wt.%NiCr coating on superfer 800H in the presence of mixture of Na_2SO_4+25wt.%K_2SO_4 film at 900 °C for 100 cycles. The detection of

the phases such as NiO, Cr_2O_3, $NiFe_2O_4$, $NiCr_2O_4$, Fe_2O_3, Ni_3S_4, and Ni_2FeVO_6 in the XRD pattern of the corroded coating indicated that all the major elements from the substrate (e.g. Fe, Cr, and Ni) diffused into the coating [120]. The author described that concentration gradient helped this inter-diffusion of the substrate elements into the coating. Thus, the weight gained after corrosion was relatively high.

In summary of the thermal sprayed Cr-based coatings: Formation of passive layer mainly consist of Cr_2O_3 is the major mechanism responsible for excellent corrosion resistance of the Cr-based coatings. Again, HVOF has been introduced as the most desirable thermal spray technique to generate Cr-based coating as a substitution to chrome plating due to low porosity, low oxidation, high bonding strength, and high deposition rate. Since most of the Cr-based coatings deposited with thermal spraying techniques possessed high level of porosity, effect of post-heat treatment on their corrosion behavior could be an interesting topic for the future research. An accurate optimization of spraying process parameters such as: plasma gas composition, flow rate, energy input, torch offset distance, and substrate cooling could significantly improve coating quality by reduction of the porosity content which are needed to be studied. The electrochemical behavior of the Cr-based coatings at high temperature has also remained unknown and requires further attention.

2.1.1.5. Tungsten Carbide-based Coatings

Tungsten carbide based alloys usually used due to their excellent abrasion, corrosion resistance, high temperature durability, and insulation properties [121]. These alloys are also considered as an alternative replacement to the more traditional hard chrome plating to reduce the pollution issue [41, 42, 121, 122]. Pure WC coating has not shown good corrosion resistance and mechanical stability and for this reason some other elements such as Co, Co-Cr, Cr_3C_2-Ni, and Ni

were usually added as mechanical binders to resolve this issue. The most common thermal sprayed WC-based alloys used to protect steel components are WC-Co, WC-Co-Cr, and WC-Ni which will be explained in detail in following.

2.1.1.5.1. WC-Co Coatings

It has been reported that HVOF sprayed WC-Co coating on steel substrate has superior long-term atmospheric corrosion resistance compared to electrochemical hard chrome coatings [42]. The results of corrosion test reported by Takeda et al. [122] taken from WC-12wt.%Co deposited by HVOF on a steel sample in 0.05 kmol.m^{-3} Na$_2$SO$_4$ indicated that oxides and hydroxides of W and Co formed on the coating surface due to dissolution of these elements after long-term immersion which resulted in weak corrosion resistance of the coating system. HVOF deposited WC-12wt.%Co on steel, reported by Cho et al. [41], exposed to 5 wt.% H$_2$SO$_4$ solution after 120 hour also confirmed poor corrosion resistance behavior due to considerable micro-galvanic corrosion occurred between WC particles and binder metal and poor corrosion resistance of binder materials [41]. The schematic of galvanic corrosion has been shown in Figure 2.1, where the particles with lower electronegativity (anode) were dissolved in the electrolyte and caused separation of the cathodic particles from the surface of the materials. WC-17wt.%Co, as another common-used coating composition ,was examined in both 0.5 M H$_2$SO$_4$ and 3.5 wt.% NaCl by Ward et al. [42] and have shown active corrosion process due to inhomogeneous binder comprising a Co(W, C) matric with varying compositions. The active dissolution of WC-17wt.%Co coating in 0.5 M H$_2$SO$_4$ solution has been attributed to anodic polarization of the binder phase (Co), which followed by pseudo-passivity associated with oxidation of W, Co, and C [42, 123, 124]. It has also been reported that the corrosion resistance measured by potentiodynamic scanning study indicated weaker performance of HVOF sprayed WC-12wt.%Co compared to the stainless steel substrate

[42]. In general, it has been drawn that the corrosion behavior of thermal sprayed WC-Co coatings has been lower than that of WC-Co-Cr and WC-Ni-based coatings [36-39, 123-129].
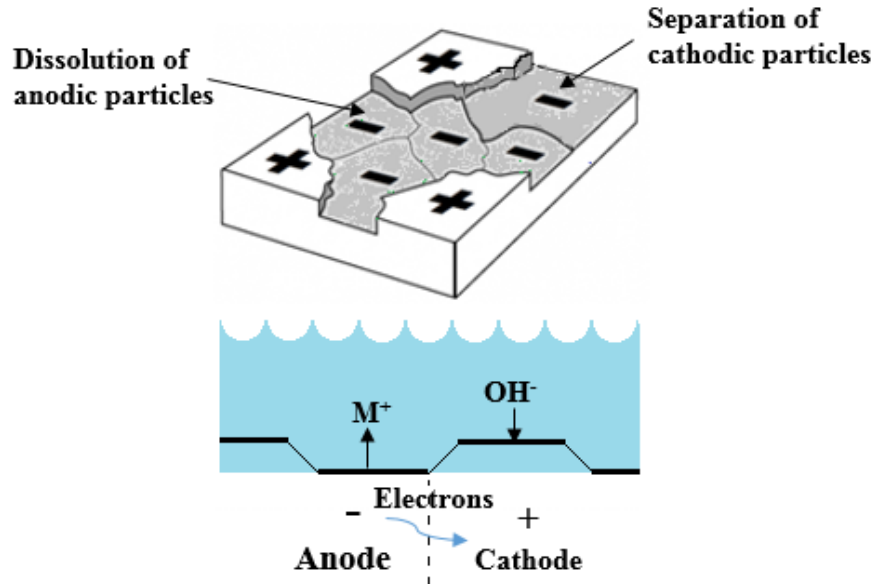
Figure 2.2. Schematic of micro-galvanic corrosion occurred in thermally sprayed coatings.

2.1.1.5.2. WC-Co-Cr Coatings

It is well-documented that addition of Cr to WC-based alloys has resulted in formation of Cr_2O_3 and significantly improved the corrosion resistance [36-40, 123-130]. However, there have been some controversial reports on the corrosion behavior of WC-Co-Cr compared to WC-Co. For instance, corrosion assessment of HVOF sprayed WC-Co-Cr and WC-Co coatings on stainless steel exposed in artificial seawater, by Bjordal et al. [123, 124], has showed that addition of Cr binder to a cobalt matrix increased the corrosion resistance of HVOF deposited WC-based cermet. However, they reported higher localized corrosion occurred at 18 °C on WC-10Co-4Cr compared to WC-Co. As the temperature increased to 50 °C the more Co content dissolved in the solution and the corrosion resistance considerably decreased, which has been explained due to higher selective corrosion of Co content by increasing the temperature.

46

It has been reported that, HVOF deposited WC-10Co-4Cr coating on steel substrate in the neutral saline of 5 wt.% NaCl solution has performed better than WC-Co deposited with the same technique (Wang et al. [131]). It has been observed that potential gap between WC particles and binder matrix in WC-Co has been higher than that in WC-10Co-4Cr has resulted in more significant micro-galvanic corrosion in WC-Co coating. Voorwald et al. [39] have also confirmed that HVOF sprayed WC-10Co-4Cr coating possessed much better corrosion resistance, while exposing to salt spray test contained 5 wt.% NaCl, compared to WC-17wt.%Co deposited with the same technique and tested at the same condition.

Presence of Cr_2O_3 in HVOF sprayed WC-10Co-4Cr coating, detected by Takeda et al. [122], have suppressed dissolving of coating components in the corrosive solution. The effect of metallic matrix composition and particle size distribution on corrosion behavior of different HVOF deposited WC-10Co-4Cr coatings has been studied by Berget et al. [132]. According to their observations, smaller powder size distribution range resulted in better quality of the coating. Moreover, corrosion resistance of the coating in sea water increased when the Cr content in the metallic binder increased from 5 to 8.5 wt.%.

A closer look to corrosion mechanism of HVOF sprayed WC-Co-Cr coating in static and liquid-solid impingement saline environment has been taken by Perry et al. [133]. They reported that corrosion mostly occurred at the carbide/matrix interface resulted in extensive removal of the hard phase. By increasing the temperature, more severe corrosion took place on the overall surface and promoted severe attack in random localized regions not associated with specific microstructural features. According to their findings, temperature played an important role in the electrochemical corrosion rate of the coating.

2.1.1.5.3. WC-Ni Coatings

It has been reported that addition of Ni as binder to WC-based coating has resulted in lower porosity and better corrosion resistance when deposited on mild steel substrate [129, 134]. It has been speculated that subjecting the WC-12wt.%Ni coating, deposited by HVOF process, in salt spray test after 397 hour resulted in the red rust spot formation [42]. However, these features appeared in shorter immersion duration for the WC-10Co-4Cr and also WC-20Cr_2C_3-7Ni coatings tested at the same condition.

According to the work published by Cho et al. [41], micro-galvanic cell generated between the WC particles and Ni binder phases in the HVOF sprayed WC-10wt.%Ni coating exposed in the 5 wt.% H_2SO_4 resulted in corrosion of anodic binder materials. In such a case, the galvanic corrosion has even been more sever if large cathode and small anode was presence, considering the area ratio effect. They observed the selective dissolution of Ni binder at the first stage of corrosion process followed by separation of- the WC particles.

Corrosion resistance of composition matrix made of 50 (WC + 12Co) balance with Ni9Cr2Si3.5Fe2B.5C coating deposited by HVOF technique, as Bjordal et al. [123, 124] explained, has been much higher than WC coating with pure Co binder due to higher corrosion rate of cobalt in the electrolyte solution. Oxidation and hot corrosion resistance of HVOF deposited WC-NiCrFeSiB coating on a Fe-based superalloys at 800 ℃ while exposed to the air and molten salt contained Na_2SO_4-25wt.%NaCl, under cyclic condition, has been evaluated by Sidhu et al. [87]. The coating consisted of protective oxides of mainly chrome and less protective oxides of nickel and cobalt and their spinels formed in the surface scale and the boundaries of Ni and W rich splats. These oxides plugged the pores and hindered the possible diffusion paths in the coatings

for penetration of aggressive species. The WC-NiCrFeSiB coating showed better resistance to oxidation as compared to hot corrosion.

The SEM micrographs of three WC-based HVOF deposited coatings with different binding materials have been shown in Figure 2.3. This figure has illustrated the effect of using various binders on the severity of micro-galvanic corrosion formation in tungsten carbide based coatings. The black regions on the micrographs has represented voids resulted from separation of WC particles from the surface. It can be concluded that WC-Co-Cr coating possessed the lowest level of micro-galvanic corrosion compared to the other coatings. For both WC-Co and WC-Ni coatings, a selective dissolution of the Co/Ni binder has first occurred in the HVOF deposited coating and led to separation of the WC particle [41]. Presence of Cr in HVOF deposited WC-Co-Cr coating has resulted in the formation of a stable chromium oxide passive layer, detected by XRD [41], which reduced the amount of Co dissolution and led to less separation of WC particle.
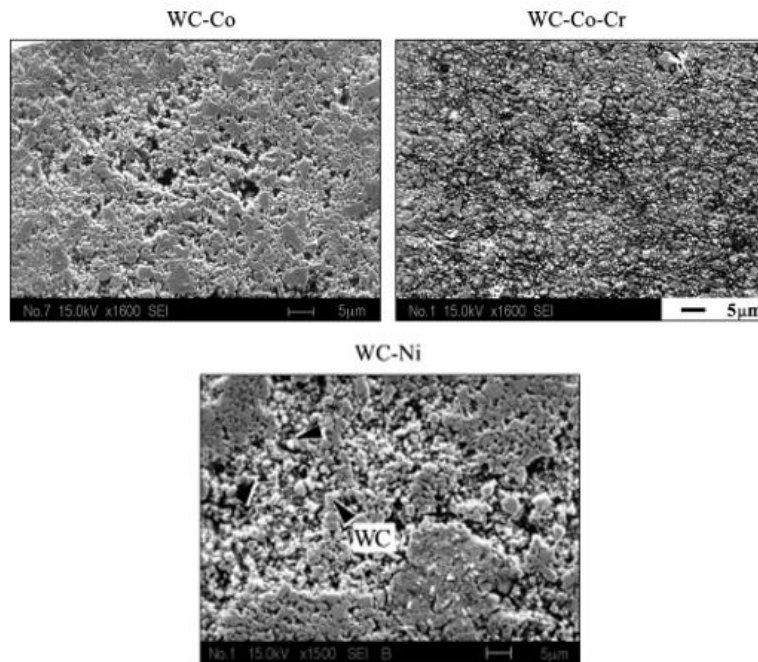
Figure 2.3. The representative SEM micrographs of HVOF deposited WC-based coatings after 120 h immersion in the aerated 5 wt.% H_2SO_4 solution [41].

In summary of the thermal sprayed WC-based coatings: Binders such as Co, Co-Cr, and Ni have usually been added to WC-based coatings deposited by thermal spraying techniques for increasing their stability. Micro-galvanic corrosion is the most common corrosion mechanism which usually occurred due to potential gap between the constituents. Selective dissolution of the binder materials at the different stages of corrosion was followed by falling off the WC particles. Addition of Cr to WC-based alloys has resulted in formation of Cr_2O_3 and significantly improved the corrosion performance. In general, the chemical composition of metallic binder materials and occurrence of micro-cracks and micro-galvanic cells were the most crucial factors affecting the corrosion behavior of the HVOF sprayed WC coating. Thus, possibility of introducing new binders with smaller potential gap respect to the WC matrix could drastically improve the corrosion resistance.

2.2. Schematic of the Corrosion Mechanisms Map for Thermal Spraying Coatings on Steel

Figure 2.4 has shown a summary of possible corrosion mechanisms at room and elevated temperatures for thermal spray coatings. As could be seen in this graph, formation of passivation layers (e.g. oxides of chromium, Ni/Cr/Ti/Si, and Al) have played an important role in the corrosion behavior of the coatings either in high or ambient temperatures. Self-sealing is another favorite mechanism dominated, especially, in thermally sprayed Zn-based and Al-based coatings, through which the pores and cracks were clogged and the corrosion rate has been significantly decreased. Galvanic corrosion between the coatings constituents can be considered as dominant corrosion mechanism in thermally sprayed WC-based coatings. The galvanic corrosion rate can be hindered by addition of Cr which could reduce potential gap between the constituent and resulted in the formation of Cr_2O_3 layer which is considered a good protection for metallic surfaces against corrosion.
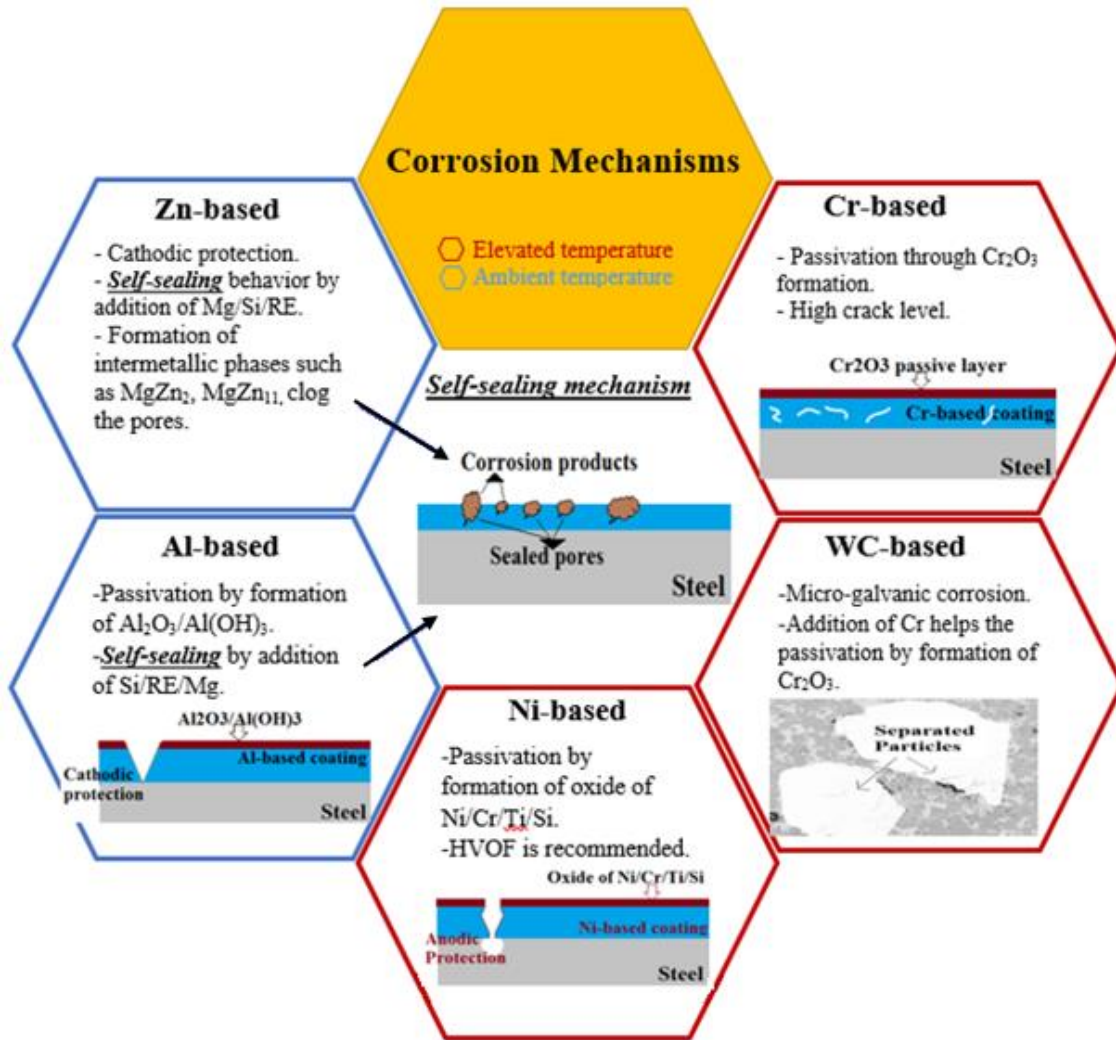
Figure 2.4. A Comparison between the corrosion mechanisms of various thermally sprayed coatings at room and elevated temperatures.

CHAPTER 3. A NEW CONCEPT OF SELF-SENSING CORROSION RESISTANT COATING

3.1. A New Concept of Self-Sensing Corrosion Resistant Coating

To search for an effective mitigation approach for on-shore pipeline external corrosion, in this study, a composite self-sensing thermal sprayed coating is proposed. The materials to be used for the protective coating were selected such that could address both room and high temperatures service conditions. Figure 3.1 shows the structure of the proposed coating. As it can be seen from Figure 3.1, the self-sensing system contained 1) sensors embedded inside the coating, 2) thermally sprayed coating as an interior layer of the coating system, and 3) protective polymer coating as an exterior layer. The thermal sprayed coating has a thickness around 200-600 µm and consists of a combination of various high corrosion resistant metal materials including Al, Zn, and Cu to be used at room temperature and WC and Ni-base coatings to perform at elevated temperature. The best material combination which would present the best corrosion resistance and at the same time lowest cost were investigated in this project. The corrosion effectiveness of the individual thermal sprayed coating was also studied in this study. Figure 3.1 has shown the self-sensing capability of the proposed coating by embedding fiber optic corrosion sensors developed by Dr. Ying Huang's group at Civil Engineering department of NDSU. These fiber optic corrosion sensors enabled the coating to monitor their corrosion status remotely in real time.
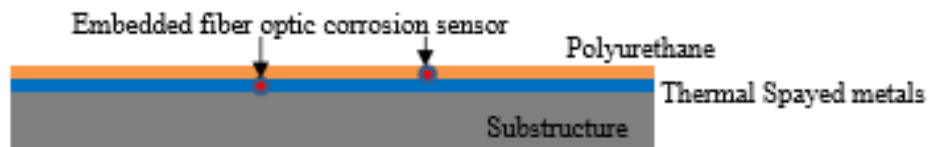
Figure 3.1. Structure of the composite self-sensing thermal sprayed coating.

The main objective of this project is to conduct fundamental and interdisciplinary research that will lead to the future development of a composite self-sensing thermal sprayed coating system

for on-shore buried pipeline corrosion mitigation. The developed coating system consists of three innovative components: 1) an optimized thermal sprayed metallic coating for corrosion prevention, 2) an embedded corrosion monitoring system to enable self-sensing capability of the coating for pipeline corrosion, and 3) a documented coating procedure, combination, and sensor characteristics for future field applications. This idea brought together an interdisciplinary research team to establish a design framework and demonstrate the feasibility of an integrated solution. Two teams of experts in the areas of mechanical engineering (expert on thermal sprayed coating) and civil engineering (expert on structural health monitoring) at North Dakota State University were collaborating closely. The proposed composite self-sensing thermal sprayed coating system was intended to provide a promising solution for an improved corrosion mitigation of the on-shore pipeline with lower costs, at the same time provide the real-time corrosion assessment, which has always been a challenge in pipeline safety consideration. The main focus of this thesis was to develop the metallic corrosion resistant layer by using thermal spray techniques on the surface of pipeline.

As mentioned, thermal spray technique including HVOF and wire-arc spray were selected as the coating techniques to be studied by Dr. Azarmi's research group in Mechanical Engineering Department at NDSU. The suitable materials for the coating were selected and under studied using materials selection methods and considering the available references.

3.1.1. Material Selection Procedure for Optimum Coating

Traditionally, steel components were protected by painting for ordinary applications and in some cases with epoxy type coating for applications in more corrosive service conditions. Application of coating on the exterior surface of the gas and liquid transmission pipelines is a common method to protect the surface against corrosive environment [135-137].

Material selection process for the coating must satisfy some prerequisites. In this regard, the investment and operational/ maintenance costs were minimized while providing acceptable safety and reliability. In general, some factors must be taken into the consideration for material selection of the coating materials:

-Design life and system availability requirement.

-Failure probabilities, failure modes and failure consequences for human health, environment, safety and material assets.

-Inspection and corrosion monitoring possibilities.

-Mechanical properties of the material should satisfy the conditions.

For the final stage of material selection process, the following aspects shall be included in the evaluation:

-Priority should be given to materials with good market availability and documented fabrication and service performance.

-The number of screened materials shall be minimized during ranking procedure considering stock, cost, interchangeability and availability of relevant spare parts.

In current work, a computer program known as CES EduPack has been used for material selection. This software was developed by Granta Design (Professors Mike Ashby and David Cebon as a spin-out from Cambridge University Engineering Department in 1994) to develop and apply material intelligence, making better material decisions, saving time and money, and reducing risk during product optimization. This software grounded on material and process database presenting comprehensive information on technical, economical, and environmental properties.

3.1.2. CES Software

To systemically select the optimum materials used as a coating for pipeline corrosion mitigation to be deposited by thermal spraying technique, CES software had been used in this study. Following is a short description about the material selection fundamental using CES software and Ashby's method.

The first step in tackling the material selection is translation which means examining the design requirements to identify the constrains imposed on material selection [138]. In the next step, the massive wide choices is narrowed down by screening-out the materials which cannot meet the constrains. Further narrowing is gained by ranking the candidates based on the highest performance. The aspects to be considered for ranking and screening are derived from the design requirements for component by analysis of function, constrains, objectives, and free variables. Simply, function means "what does component do", constrains stands for "what non-negotiable conditions must be met", objective represents "what is to be maximized or minimized", and free variables are "the parameters of the problem that are free to be changed". The property or property-group that maximizes performance for a given design is called its material index. After applying these steps, supporting information which are usually descriptive, graphical or pictorial, should be considered to make the task viable [138].

In the case of material selection for corrosion protection to be deposited by thermal spraying techniques, the function, constrains, and free variables were defined. Function in this case was corrosion protection and constrains were low price and high fracture toughness.

Two leading formulas were considered to define the materials index:

$$\sigma_f = \frac{F}{A} = \frac{c.K_c}{\sqrt{(\pi.a_c)}} \qquad \text{(Eq. 3.1)}$$

$$Mass = \rho.v \qquad \text{(Eq. 3.2)}$$

Where σ_f is yield strength, F is load, A is the area, c is constant, K_c is fracture toughness, a_c is the crack length, and ρ is density.

Assuming a pipe with a length equal to L the following relations could be defined:

$$v = 2.\pi.r_0.L.t \qquad \text{(Eq. 3.3)}$$

$$A = 2.\pi.r_0.t = \frac{F.\sqrt{(\pi a_c)}}{CK_c} \qquad \text{(Eq. 3.4)}$$

$$t = \frac{F.\sqrt{(\pi.a_c)}}{C.K_C.(2\pi.r_0)} \qquad \text{(Eq. 3.5)}$$

By knowing that the thickness is the free variable, the universal equation could be defined as follow by plugging in the above equations in the mass equation:

$$Mass = \left(L.\sqrt{a_c}\right)_{geometry} \left(\frac{\sqrt{\pi}}{c}.F\right)_{constant} \left(\frac{\rho}{K_c}\right)_{materials\ properties} \qquad \text{(Eq. 3.6)}$$

$$\text{Materials index} = \left(\frac{k_c}{\rho}\right) \qquad \text{(Eq. 3.7)}$$

Therefore, the slope of the line considered in the CES software (Figure 3.2) was equal to one which is the power of the materials index in the equation (7). After applying more limitations including material durability in fresh water, alkali, and acidic soil, material process ability (ability to be thermal sprayed), cost, flammability, and mechanical properties such as hardness and fracture toughness the chart shown in Figure 3.2 were obtained.

According to the results obtained from CES software (Figure 3.2), several material groups were found to be effective in corrosion prevention for steel pipelines including WC-based, zinc alloy, aluminum alloys, Nickel-based, and copper-based alloys. Taking the price into the consideration, copper, aluminum, and zinc alloys could be a promising coating material for corrosion prevention of the steel pipes performing at low temperature. These materials, however, has shown very limited performances at high temperature environment as discussed in previous

section. Thus, WC, and Ni-base coatings that proved better performances at elevated temperatures have been chosen to resolve this issue.
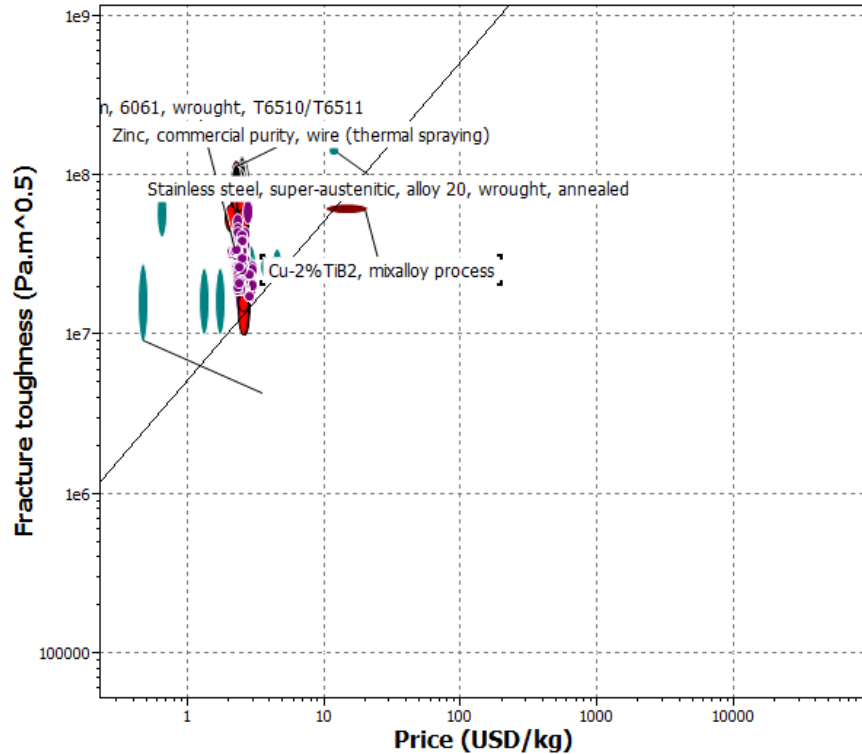
Figure 3.2. A screen shot from CES program as used for materials selection.

3.2. Literature Review on CES Result

3.2.1. Selecting Material Based on Corrosion Mechanism

Several types of corrosion can occur in buried steel pipelines including bimetallic corrosion, general corrosion, pitting corrosion, hydrogen embrittlement, and stress corrosion cracking (SCC). The most common corrosion mechanism in buried pipelines is galvanic corrosion (bimetallic corrosion) which requires special attention. Bimetallic corrosion occurs when two metals, with different potentials are in electrical contact while immersed in an electrically conducting corrosive environment [139, 140]. The basic requirements to initiate bimetallic corrosion are an electrolyte bridging between the two metals, electrical connection between the two metals, a sufficient difference in potential between the two metals to provide galvanic current,

and a sustained cathodic reaction. In the case of bimetallic corrosion, the potential difference is created by the presence of dissimilar metals. Due to the dissimilar natural potentials, a current will flow from the anode (more electronegative) metal to the cathode (more electropositive) which will increase the corrosion on the anode. Since the materials of coating and the pipe could have dissimilar electronegativity, likelihood of the bimetallic corrosion should be considered during materials selection process. The schematic of the bimetallic corrosion is shown in 4.3 [3].
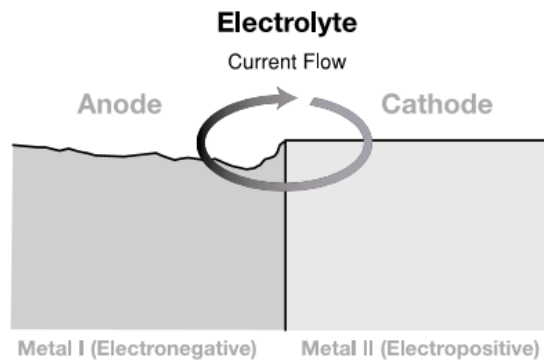
Figure 3.3. Bimetallic corrosion [3].

In general, the formation and growth of corrosion cells are similar to uncoupled metals, but the rate of attack can drastically increase. An appropriate materials selection could play an important role in maximize the service life of pipelines. In the case of using a coupled material (bimetallic) system, combination of some metals with different electronegativity could alter the total electrical balance of the system resulting in induce of corrosion that would not have occurred in the uncoupled state (e.g. pitting). List of the galvanic series is shown in. Although the ranking in was derived for seawater, it is very similar for many other near neutral aerated aqueous solutions.

Table 3.1. List of galvanic series [139].

Electronegativity	Elements
Low	Nickel chrome
	Copper
	Steel
	Aluminum
High	Zinc

As shown in the table, some materials like stainless steel (e.g. 316) have a thin protective layer (passive state) which is maintained while the corrosion rate is very low. Figure 3.4 shows two different types of coatings that can be selected for steel pipes for providing anodic and cathodic protections [141]. In the first case, no discontinuity in the coating can be tolerated, while it has no importance for the case of cathodic coating, as illustrated in Figure 3.4 The coating material and its microstructure play an important role in this type of corrosion. Anodic coatings such as austenitic stainless steels, aluminum bronze, nickel-base alloys, super-alloys MCrAlY materials, cermets (metal matrix re-enforced with WC), Cr_2C_3, and Ni or Co based composites are used against corrosion, often when it is associated with wear. However, such coatings, presenting no galvanic protection, will never protect the substrate if connected porosities and oxide networks exist, which is the case in most of thermal-sprayed coatings [142]. Therefore, the substrate protection requires using a protective bond coat or improve coating quality by deposition of dense coatings or seal the voids and porosities.
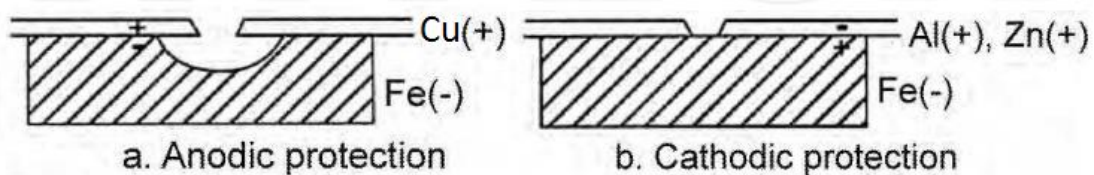
Figure 3.4. Examples of protective coatings; a) Anodic (no discontinuity possible in the coating), and b) Cathodic (discontinuity possible in the coating, resulting in no corrosion of iron) [141].

On the other hand, cathodic coatings act as sacrificial anode due to their higher electronegativity respect to the steel. Hence, if the coating breaks and steel pipe be exposed to the corrosive environment, steel will act as cathode and remains un-corroded. In the case of coating steel for corrosion protection, it is recommended that the coating material with higher electronegativity state be selected. Thus, in this case, coating will act as sacrificial anode and will

protect the steel pipe against corrosion. As sacrificial coatings (cathodic behavior relatively to ions, i.e. Zn or Al on steel): the thicker they are, the longer protection they provide (typical thickness varies between 50 and 500 µm, the most frequent one being around 230 µm) [141].

A general idea of the qualitative risk of bimetallic corrosion can be gained by putting these effects together into a form as shown in Figure 3.5. According to Figure 3.5. alloys that are coupled to metals with more electropositive potentials are the ones, which suffer bimetallic corrosion. To avoid initiation of the bimetallic corrosion of a metal, the couple with higher electronegativity should be selected. As it can be seen in Figure 3.4 coupling the steel with Zinc, Aluminum, and Magnesium could not cause additional corrosion in steel. Using copper may slightly increase the chance of the additional corrosion in steel as its electronegativity is slightly lower than steel. However, copper proved to be much Nobel metal with higher stability in corrosive area once it is used alone (uncoupled).

The potential difference is not the sufficient factor to predict the risk of bimetallic corrosion, and it provides no information on the kinetic of bimetallic corrosion. There are some crucial factors including area ratio, temperature, flow rate, composition of the electrolyte, etc., which define if the bimetallic corrosion is possible for any combined metallic system [143]. For instance, it has been reported that in the case of magnesium and its alloys, even though they have higher electronegativity state compared to steel, there is a possibility of a significant amount of hydrogen evolution at the cathode in neutral solutions. This process resulted in hydrogen embrittlement and disbanding of the coating and failure of the pipe [137].

Metal in Contact — columns: Magnesium, Zinc, Aluminium alloys, Carbon Steel, Cast iron, Lead, Tin, Austenitic Cast Iron, Brasses, Gunmetals / Tin Bronzes, Copper Nickel Alloys, Nickel Aluminium Bronze, Alloy 400/K-500, Low alloy stainless steel, Nickel-chrome moly alloys, Titanium, High Alloy Stainless Steel, Graphite

Metal being considered (a) — rows: Magnesium, Zinc, Aluminium alloys, Carbon Steel, Cast iron, Lead, Tin, Austenitic Cast Iron, Brasses, Gunmetals / Tin Bronzes, Copper Nickel Alloys, Nickel Aluminium Bronze, Alloy 400/K-500, Low alloy stainless steel, Nickel-chrome moly alloys, Titanium, High Alloy Stainless Steel, Graphite

Legend:
- Additional corrosion unlikely
- Additional corrosion may occur
- Additional corrosion possible

Figure 3.5. Risk of additional corrosion from bimetallic contact in neutral aqueous electrolytes. The degree of corrosion refers to the metal on axis.

Locally excessive cathodic protection potentials known as "overprotection" is possible to occur in a pipe with a large population of external coating defects [144-148]. Overprotection in the CP system is generally contributed to two possible damages which are cathodic disbanding and hydrogen-related damages to the pipeline body due to the production of hydroxide at the cathode and the release of hydrogen. The actual generation of hydrogen gas takes place only at fairly high-negative potentials but, under rare conditions, it could literally strip off a coating in a matter of hours whilst hydrogen production may cause hydrogen embrittlement in the carbon steel [149].

The important parameter that is required to be considered in materials selection is the change of potential due to exposure to some environments, which might introduce new problems including hydrogen embrittlement [149]. The effect of PH is even far-reaching and depends upon the composition of both metals forming the couple. For instance, by using magnesium and its alloys, considerable amount of hydrogen evolution at the cathode in neutral solution might cause failure. Hence, extra care is required for selecting a suitable material to avoid severe hydrogen evolution. One of the methods of preventing SCC on pipeline structures include minimizing the operation temperature and controlling the CP levels to values more negative than -850mV CSE [139]. The other method is selecting a material with lower possibility of hydrogen embrittlement. Metallic thin films can hinder hydrogen penetration into the metallic substrate by virtue of their low solubility, diffusivity, or surface effects involving adsorption of hydrogen or combination of these mechanism [150]. They compiled permeability data for hydrogen through a number of metals and compared these value to those for hydrogen through low alloy austenitic steels. The summary of their results, in decreasing order of hydrogen permeability, are listed as follow: Nickel (Ni), Platinum (Pt), Copper (Cu), Molybdenum (Mo), Aluminum (Al), Silver (Ag), Gold (Au), and Tungsten (W). Except for Nickel, all the mentioned metals had less hydrogen permeability compared to steel at temperature less than 300°C. According to ISO 4964 [151], the risk of hydrogen induced cracking mainly exists with a local tensile strength greater than 1200 N/mm^2, a hardness bigger than 34 HRC or a surface hardness larger than 340 HV. Notches, present in the microstructure of the surface, or material inhomogeneity increase the risk of damage.

3.3. Cost Estimation

Several factors including galvanic series, hydrogen embrittlement, corrosion rate and cost of the process were considered to propose a suitable material as coating being compatible with the pipeline and the soil environment. listed the estimation of the material cost and the experimentally measured corrosion rates in quiet seawater. Melting point of the materials was also taken to the account to estimate the energy (cost) required for deposition of each listed materials.

Table 3.2. Selected important properties of the Al and Zn alloy coating materials.

Material	Melting point °C	Price USD/kg [152]	Corrosion rate in quiet seawater mm/year [153-155]	Electronegativity
Cu-alloys	1080-1090	6-7	<0.018	~1.9
Al-alloy	570-670	1.5-1.6	<0.030	~1.61
Zinc-alloy	375-490	1.7-1.9	<0.031	~1.65
WC-based	2800-3000	5-15	<0.025	~2.1
Ni-based	1400-1600	10-20	<0.020	~1.91

As seen in Table 3.2 both Zinc and Aluminum alloys expected to act as sacrificial anode when coupled with steel pipe in order to corrosion protection. Both of these metals are more electronegative with respect to the steel. This makes them as sacrificial anode to steel resulting in providing protection for the steel surface. Considering their relative lower price range, these two materials can be considered as an economical protective coating for the room temperature applications. Zinc performs better than aluminum in alkaline conditions, while aluminum works better in acidic conditions. The aluminum-zinc coating with high zinc content and the zinc coating possessed the best anti-corrosion and anti-fouling properties [141]. According to Davis (2004) the lifetime of a 255-µm thick zinc or zinc aluminum coating is about 25 years and it can be extended by 15 years by sealing it with vinyl paint [137]. Besides painting, impregnation with special compositions (epoxy resin, silicon resin, etc.) is currently utilized as one of common sealing materials. Copper coatings estimated to be relatively more expensive due to higher melting point and also the higher cost of the copper powders. However, it showed considerably higher corrosion

resistance compared to zinc and aluminum due to its nobler nature once exposed to corrosive environment (e.g sea water).

To summarize, as far as room temperature applications, zinc and aluminum alloys could be considered as very comprising candidates to be used as protective coating for steel pipe due to their good corrosion resistance, low possibility of inducing additional bimetallic corrosion on steel, and low hydrogen permeability. It is speculated that application of these two metals are economically justified due to relatively low cost of materials. Copper, on the other side, could also be a very high corrosion resistance coating with anodic protection performance. In the current project, it has been speculated that using HVOF technique to deposit copper coating will provide very low level of flaws in the coating microstructure that might lead to very high corrosion performance. Thus, copper coating selected to be deposited by HVOF technique. Zn-based and Al-based coatings also will be generated by wire-arc spray technique, which is the most recommended spraying technique in this case. The resultant coatings will be examined by material characterization techniques and the result will be compared to suggest the best coatings which meets the requirements.

Copper and copper alloys shown an excellent corrosion resistance in most atmospheric and aqueous environments. For service in marine and other aqueous environments, historically, copper and its alloys have shown good results. They have proved high resistant against corrosion specially, biofouling, and crevice corrosion. The important point is that copper-based coatings provide anodic protection once placed in contact with steel. HVOF is capable of generating very dense coating with low porosity level and for this reason it has been used widely for deposition of anti-corrosion copper coatings.

As far as higher temperature applications, WC and Ni-base coatings have also been selected to be deposited by HVOF technique. The corrosion mechanisms of the deposited coatings as well as their mechanical properties have been evaluated and compared throughout this study.

CHAPTER 4. EXPERIMENTAL DETAILS

4.1. Development of the Self-Sensing Coating System for Corrosion Assessment

To enable the self-sensing capability of the thermally sprayed coatings on steel pipes for corrosion assessment, Fiber Bragg Grating (FBG) sensors embedded inside the coating was developed. The FBG based corrosion sensor shown in Figure 4.1 operated by monitoring the corrosion induced visual property change of the coated iron-particle thin film. The effective refractive index of the fiber cladding and the thickness of the coated thin film changed when the coated iron particles were corroded. As a result, the resonant wavelength of the FBG changed correspondingly. Therefore, monitoring of the change in the resonant wavelength of the FBG sensor provided key information about the mass loss and the material property change of the iron particles over time in a corrosive environment.
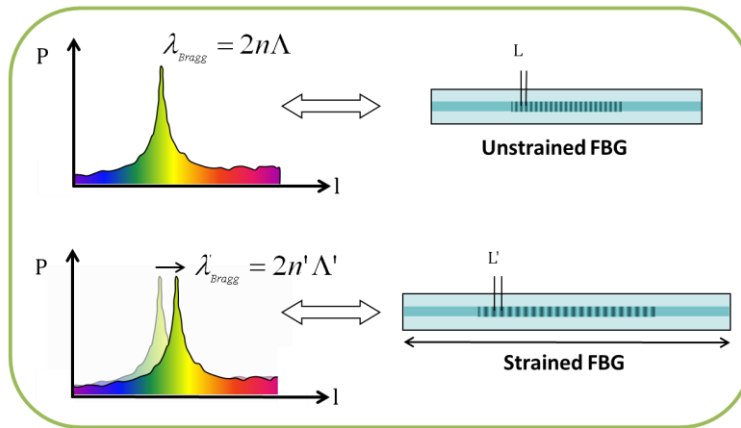
Figure 4.1. Illustrative structure of an FBG spectrum under strain.

4.2. Development of Automatic Rotational Fixture

An automatic rotating fixture capable of holding round objects in front of spraying gun was previously designed and optimized in HCRL at NDSU. This fixture can hold and rotate pipes in front of spraying gun during coating deposition. Figure 4.2 (a) illustrated the spraying set-up for deposition process. The new fixture includes an adjustable pipe fixing holder, a rotational axle

connected to a speed-controlled power supply, and a screw driver custom made movable spraying gun holder. Pipes with inner diameter from 1 inch to 12 inches were placed on the holder for coating deposition. The pipe could be rotated at various speeds from low to high during the spraying process to meet the requirement for different spraying thickness. The spraying gun holder could move horizontally at constant speed to provide a uniform deposition on the surface of the pipe samples. The spraying setup containing the pipe and gun holder were shown in Figure 4.2 (a) while spraying process was illustrated in Figure 4.2 (b).
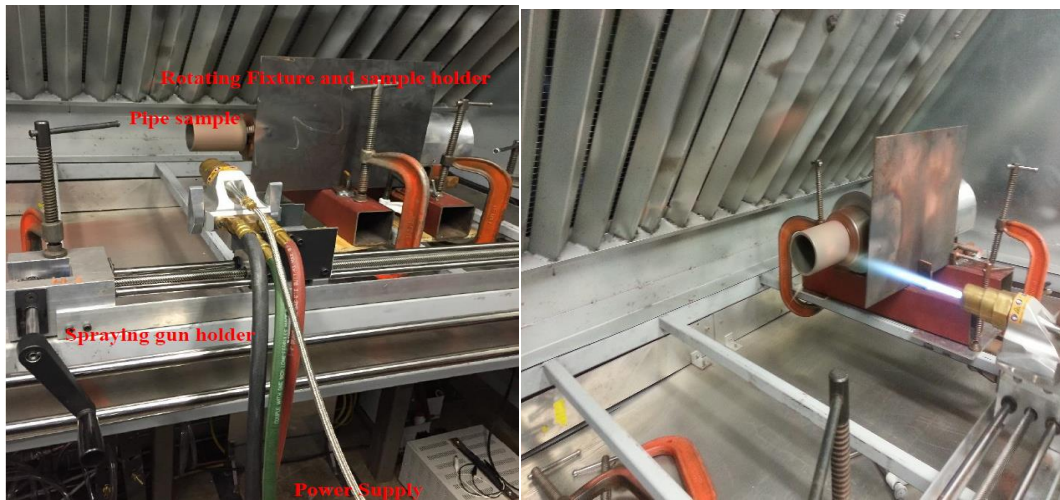
Figure 4.2. (a) Setup for automatic rotational fixture for HVOF spraying and (b) spraying process.

4.3. Sample Preparation for Self-Sensing Development

After testing many adhesions, the challenges of embedment were resolved by applying stainless-steel-based metallic adhesive (Durabond 954) in combination of steel tube. Experimental results confirmed that the adhesive can survive the coating process as shown in Figure 4.2 (a) using thermal sprayed copper coating. Samples were prepared accordingly with embedded sensors and also some without sensor as a reference samples and subjected to the thermal spraying coatings. Figure 4.2 (b) showed the dimensions of the sensor embedded samples with a length of 8 inches,

67

a width of 4 inches, and a thickness of ¼ inches. To have the fiber optic sensors embedded inside the samples, a small groove has been made on the surface of each sample. The sensors were enclosed in hypodermic tubes for protection and embedded using stainless-steel-based metallic adhesive (Durabond 954).
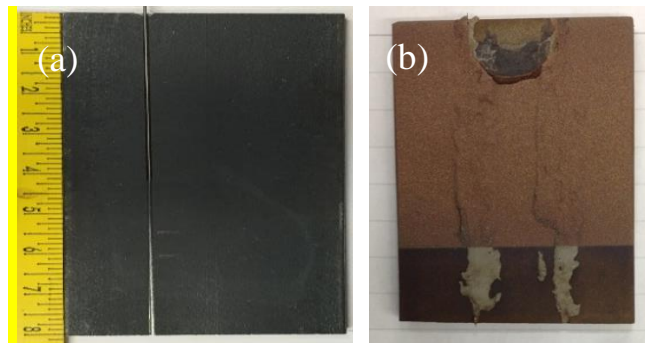
Figure 4.3. Successfully thermal coated sample (a) before and (b) after coating.

To ensure a successful protection of the fiber optic strain sensors during the HVOF thermal spraying coating process, two different sizes of hypodermic tubes had been used. A smaller-diameter hypodermic tube was applied to protect the sensing unit with 0.006 in. of inner diameter and 0.010 in. of outer diameter. A slightly larger diameter hypodermic tube was applied to protect the communication optical fibers from the high velocity of HVOF thermal spraying process with an inner diameter of 0.028 in. and an outer diameter of 0.0425 in. For fiber optic temperature sensor, since a relative thicker steel tube was applied by manufacturers for sensor protection, no future protection was taken. After the documentations of the sensor locations, the sensors were embedded using stainless-steel-based metallic adhesive (Durabond 954). Figure 4.3 (a) has shown all the prepared samples for HVOF thermal spraying coating and Figure 4.4 (b) shown the samples after sand blasting process. As it can be seen from Figure 3.9. (b), only the top half of the samples where the sensors located will be thermal sprayed.

Figure 4.4. Prepared samples (a) after sensor embodiments and (b) after sand blasting.

4.4. Thermal Spraying Coating for Samples with the Embedded Sensing Systems

The prepared samples were then thermal sprayed by the selected materials selected for elevated temperature applications: WC-based, Nickel-based including, and room temperature applications: pure copper, Al-Zn, and Al-bronze alloys (Figure 4.4). HVOF technique with automatic robotic spraying arms in mechanical department at NDSU has been used to develop Ni-base, WC-base, and copper coatings. Al-Zn coating has been generated by wire-arc spray technique. The elemental compositions of the powder used were shown in Figure 4.3.
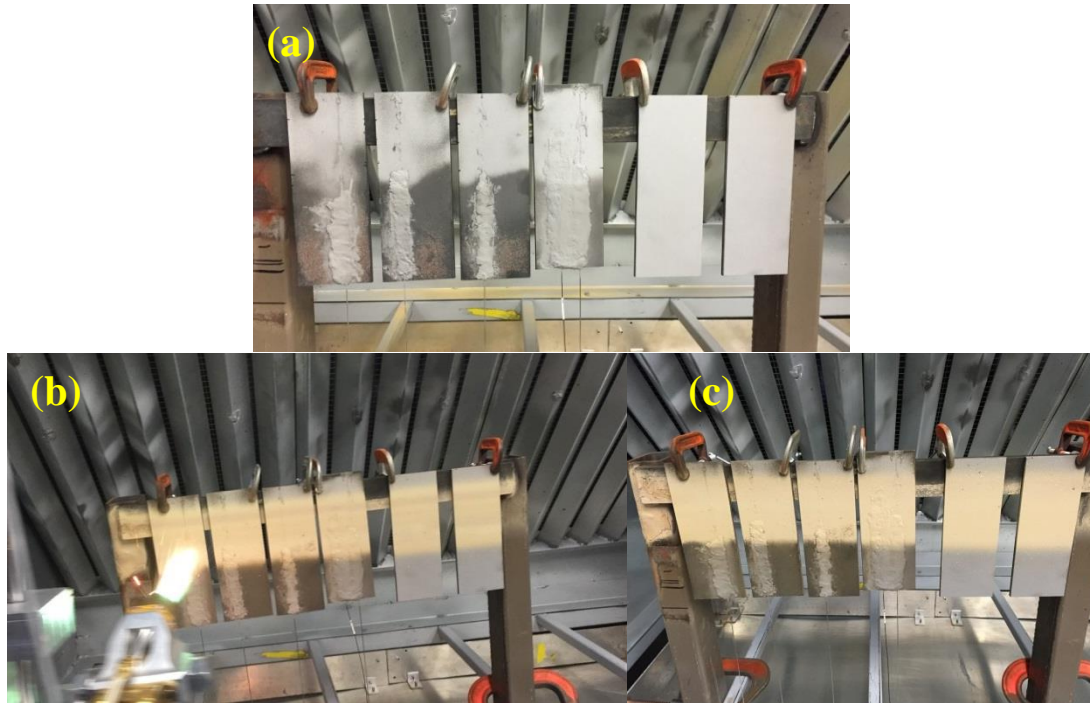
Figure 4.5. (a) Sample setup, (b) thermal spraying process (c), and samples after successful thermal spraying.

To keep on consistency of the thickness, a total of six traverses were made for all the HVOF spray coating process. The responses of the sensors on the samples were fully recorded during the thermal spraying process. All the sensors successfully survived the thermal spraying coating process and monitored the coating process. This thesis however emphasis on the resultant coating properties.

Table 4.1. Information of the powder used for HVOF coating

Product	Weight Percent							
	Cu	Zn	Al	Fe	WC-Ni	Ni	Cr	Other
Al-bronze (Dimalloy 1004)	Bal	--	8.5-10	0.5-2	--	--	--	0.5
Cu (Dimalloy 1007)	99	--	--	--	--	--	--	0.7
Al-Zn	--	Bal	15	--	--	--		1
Ni-Cr	Bal	--	--	--	--	50-55	17-21	3
WC-based	--	--	--	1	75	8-10	--	5

Figure 4.4 shows the samples prepared to be coated with aluminum and zinc coating using arc spray technique.

70

Figure 4.6. Schematic of sample preparation for arc spray coating.

Prior to the spraying, surfaces of the substrates were sand blasted using fine Alumina (Al_2O_3-10-50µm) particles to degrease the surface and improve the adhesion between the substrate and coating.

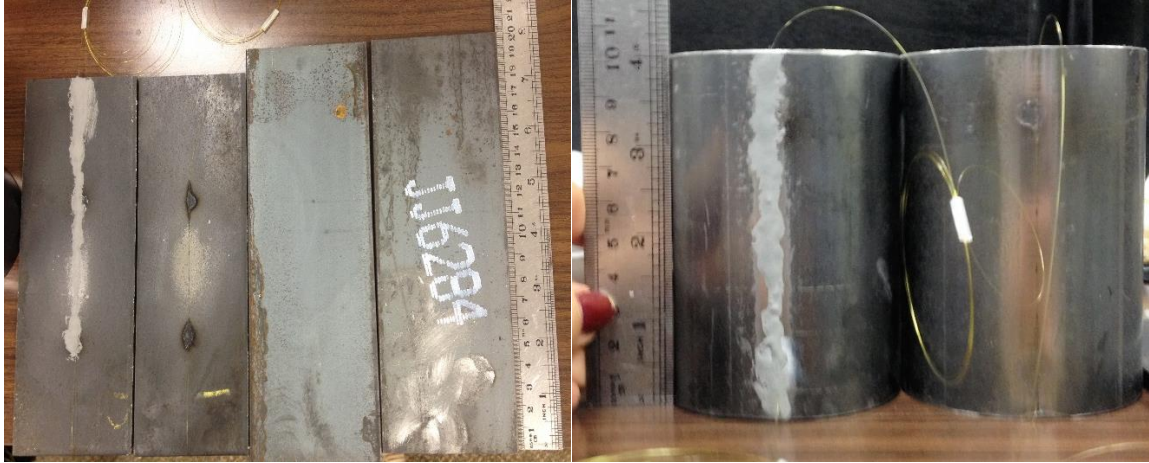## 4.5. Microstructural Characterization

Microstructure was studied by Scanning Electron Microscopy (SEM) using a JEOL JSM-6490LV scanning electron microscope (JEOL USA, Inc., Peabody, MA, USA). The SEM was also equipped with a Nanotrace EDS detector with a NORVAR light-element window and Noran System (Thermo Fisher Scientific, Madison, WI, USA). The accelerating voltage used for EDS was 15 keV to investigate the elemental distribution of the coatings before and after corrosion. XRD was conducted to identify the phase composition for better understanding of the corrosion mechanism by using a Rigaku Ultima IV diffractometer (Cu Kα radiation, voltage 40 kV, current 44 mA, and a fixed incident angle of 1.5 degree in a parallel beam geometry).

4.6. Corrosion Test

The corrosion resistance of Cu, Al-bronze, and Al-Zn coatings were studied and compared to the bare (uncoated) steel (low carbon steel) at ambient temperature. The corrosion performances were tested through accelerated corrosion test using electrochemical method, specifically, the

Potentiodynamic Polarization Technique. The accelerated corrosion tests were performed by placing the coated and uncoated steel samples in 3.5% NaCl solutions. A Gamry Reference 600 Potentiostat-Galvanostat-ZRA instrument as shown in Figure 4.7 was used to analyze the corrosion performance.

Figure 4.7. Electrochemical Accelerated Corrosion Tests Equipment Set-up.

The corresponding electrochemical kinetics parameters such as corrosion potential (Ecorr), anodic Tafel slopes (βa) and corrosion current density (Icorr) obtained by extrapolation of the Tafel lines and corrosion rate were estimated accordingly.

For the elevated temperature corrosion resistance evaluation, HTCMD employed in this study. This device was designed and developed in HCRL[1] (NDSU, ND, USA) was used to elevate the temperature and pressure to 250˚C and 6.9 MPa, respectively.
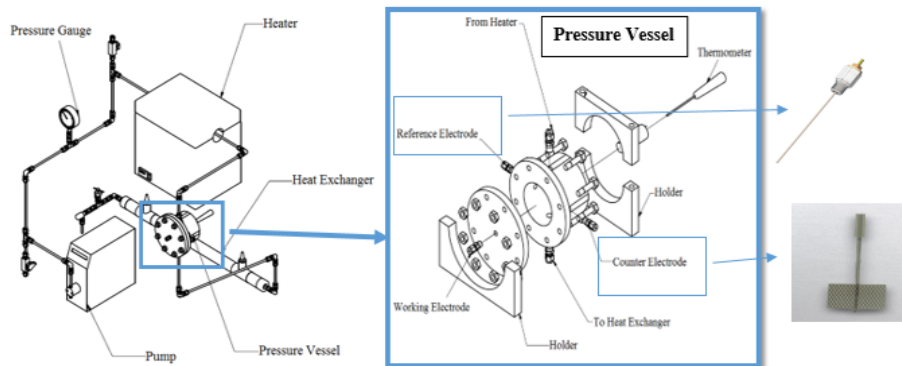

Figure 4.8. Schematic of the HTCMD assembly.

As shown in Figure 4.9, the device consists of five main parts including: (1) pump assembly, (2) heater, (3) pressure gauge, (4) heat exchanger, and (5) pressure vessel assembly. Inconel 718 and WC-Ni coated steel with exposed area of 1.6×1.9 cm^2 was used as the working electrode. The sample was embedded in the pressure vessel as illustrated in Figure 4.9.

Figure 4.9. Sample and electrode placement inside the pressure vessel.

After securing the sample embedded in the ceramic holder by use of glass-coated springs (Figure 4.9), the pressure vessel was sealed and tightened by bolting the cap accordingly.

Reference 600 Potentiostat by Gamry Instruments was connected to the sample prior to conduct the corrosion test. Three-electrode cell set-up was employed to evaluate both EIS and Potentiodynamic Polarization tests. A glass coated wire electrode made of platinum was used as a pseudo reference electrode. The counter electrode depicted at the right side of the test panel (Figure 4.9). It was made of platinum meshes which was part side coated with glass to avoid any connection with the chamber. A thermometer (Type K, Model 701, from JENCO Instruments) was embedded to the chamber to monitor the temperature during the process. A container filled of 3.5 wt.% NaCl solution was connected to the pump to provide the corrosive environment. The solution

was pumped to the heater with a flow rate of 15 mL/min to elevate the temperature and thereafter it passed to the corrosion chamber. After reaching to the desired temperature, the specimen was placed and held in the hot solution for 30 minutes in order to establish the free corrosion potential (E_{corr}).

For the reason of comparison, a low carbon steel sample (1.9×2.2 cm^2) was also subjected to the similar corrosion test at the same environmental parameters. The measurement of EIS spectra was recorded 30 minutes after the corrosion potential was stabilized. The range of frequency varied from 0.2 Hz up to 100 KHz and the amplitude wave of excitement signal was ± 10 mV with respect to the free corrosion potential.

The corrosion rate was also evaluated by means of electrochemical measurement in 3.5 wt.% NaCl solution. Once the open circuit potential was established, a linear polarization was performed in the small potential range around the open-circuit potential with the scan rate of 1 mV/s and finally the potentiodynamic curves were recorded. From the classical Tafel analysis, the value of corrosion rate was estimated by identifying the corrosion current density (i_{corr}), corrosion potential (E_{corr}) and Tafel slopes (b_c and b_a). These values were estimated by plotting the linear anodic and cathodic curves in the potential (E (mV)) versus the logarithm of current density (A/Cm^{-2}).

4.7. Hardness Indentation

To further investigate the influence of the porosity on mechanical property of the thermally sprayed coatings, the hardness value has been evaluated using the Knoop micro indentation test. The CLARK CM-800AT machine was specifically used for the testing. For thermal sprayed coatings, hardness tests were performed based on ASTM E2109-01.

CHAPTER 5. RESULTS AND DISCUSSION

5.1. Low Temperature Application

5.1.1. HVOF Sprayed Copper Coating

The micrograph of HVOF deposited copper coating were shown in Figure 5.1 The coating thickness was approximately 800µm. Image analysis showed existence of only 3% porosity within the microstructure, indicating a dense coating. In addition, a good cohesion between copper splats was indicated from the microstructure.
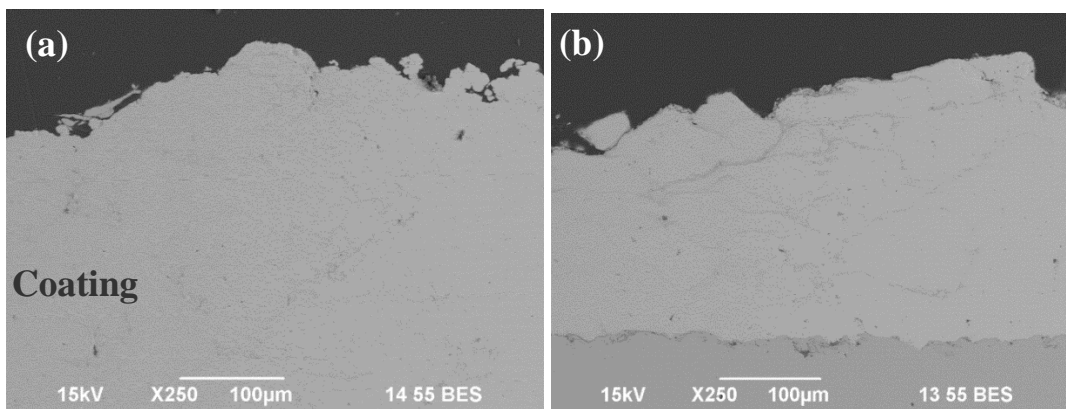
Figure 5.1. SEM images of (a) HVOF deposited copper coating before corrosion and (b) after corrosion.

There was no observable change in the microstructure of the cross section of the coatings, preferably near the surface, when before and after corrosion conditions compared, in the magnification scale the images were taken. This means very slim change (or if it happened in very small scale, less than few micrometers) in the composition of the Copper coatings once exposed to the corrosive environment. The elemental distribution in the coatings' microstructures was studied by EDS mapping technique and were presented in Figure 5.1 The major aim of EDS mapping was to detect the depth of the penetration of the deleterious elements, preferably Cl⁻, to estimate the effectiveness of the coating to act as a barrier to hinder diffusion of such deleterious

elements in to the coatings. The map for Na penetration in to copper coating has also been shown in Figure 5.1.
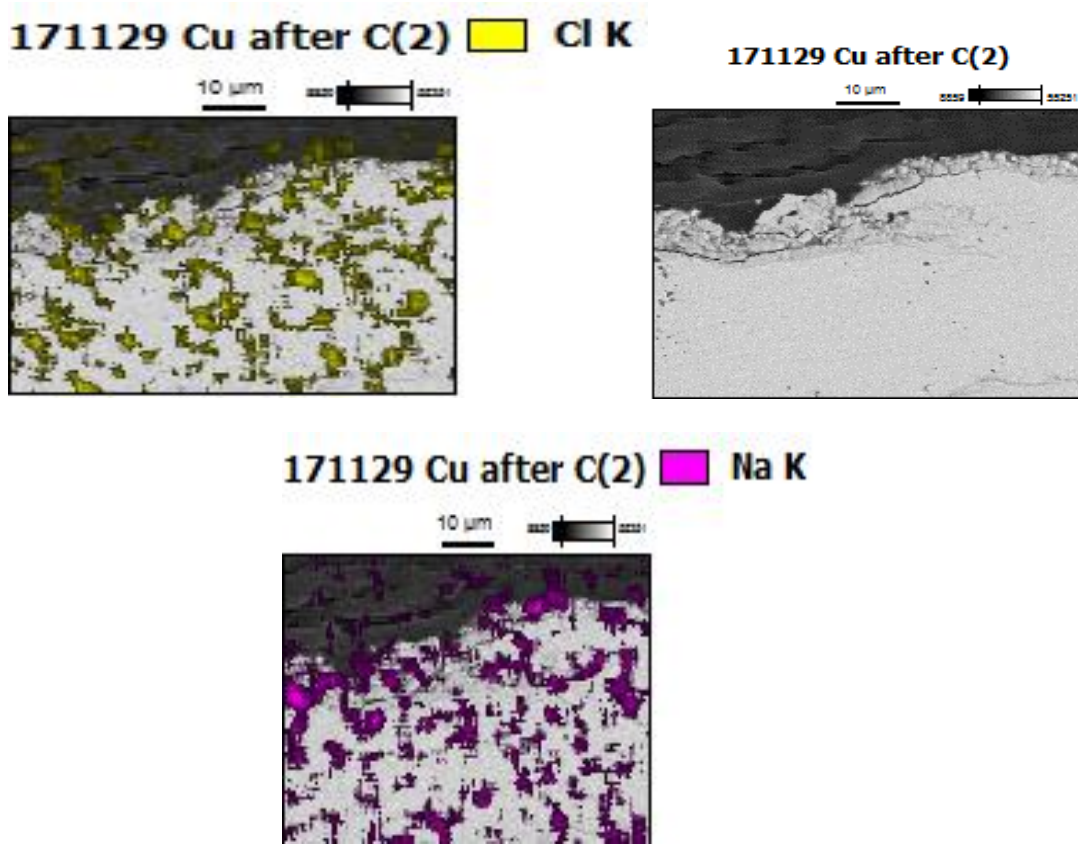
Figure 5.2. EDS maps of Cl⁻, and Na elements penetrated in the HVOF sprayed copper coatings after corrosion experiment.

As the EDS result demonstrates, chlorine and sodium could considerably defuse in the copper coating for less than depth of 50μm. XRD-pattern of the HVOF sprayed copper coatings also exhibited some dissimilarity when before and after corrosion conditions compared. The XRD pattern shown in Figure 5.3 demonstrated that copper oxide was the main composition appeared after corrosion whilst it was not detected in the coating structure before the corrosion experiments.
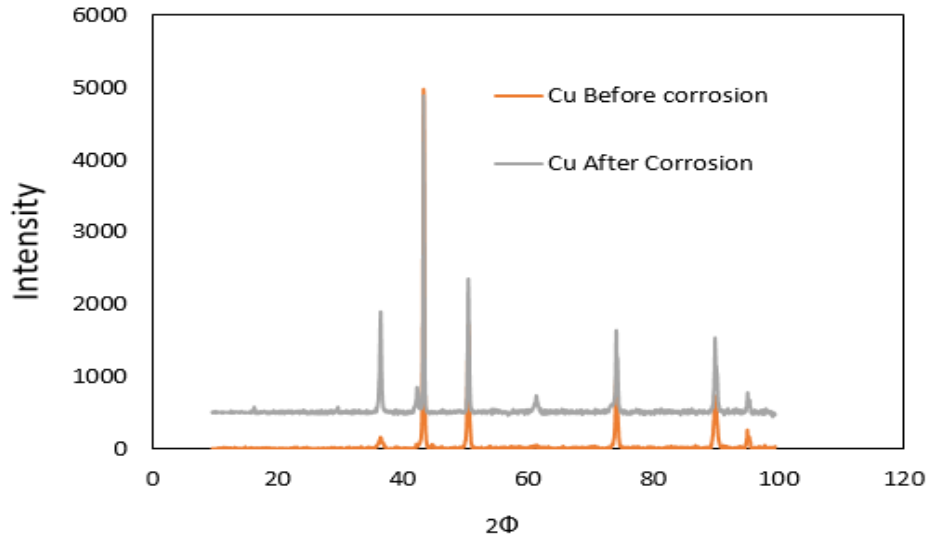
Figure 5.3. X-Ray pattern of HVOF sprayed Copper coatings before and after corrosion.

To further investigate the influence of the porosity on mechanical property of the thermally sprayed Cu coating, the hardness indentation has been examined and presented in Figure 5.3. The average hardness of the Cu coating is 96.5 HK (≈83Hv).
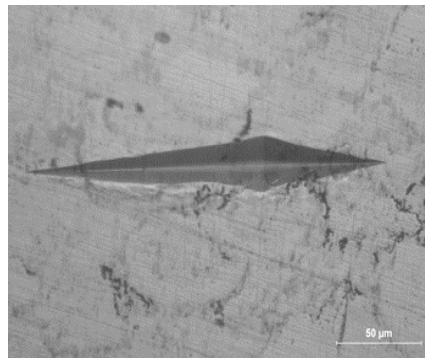
Figure 5.4. Knoop indentation on HVOF deposited Copper.

Corrosion behavior of the HVOF deposited copper coating was investigated using polarization technique in 3.5% NaCl solution. The Tafel curve and some important corrosion parameters extracted from this experiment has been reported in Figure 5.5, and, respectively. As the data summarized in Figure 5.4 advocated, copper coating deposited by HVOF resulted in higher corrosion resistance of the surface.

77
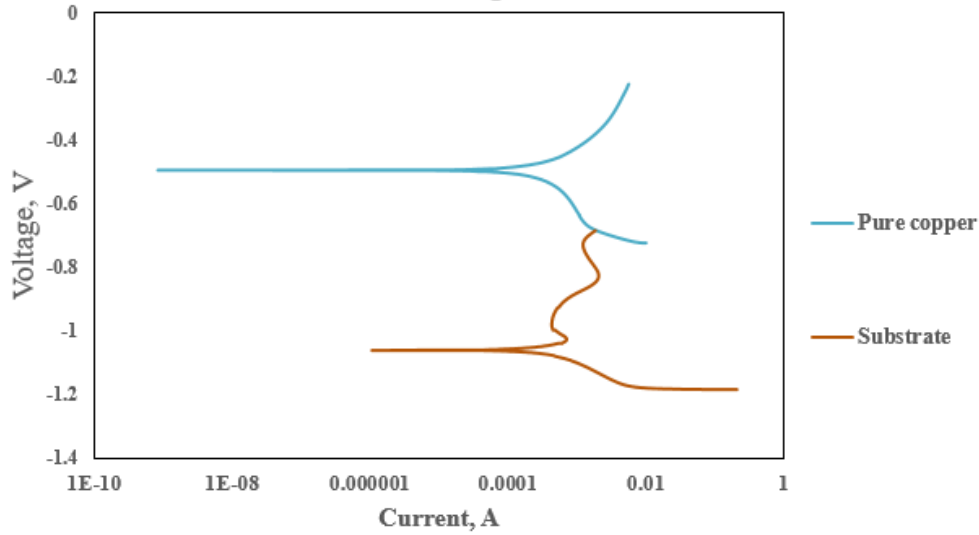
Figure 5.5. Tafel curves of copper coated and uncoated steel samples in 3.5% NaCl solution.

As the corrosion results demonstrated, copper coating could improve the corrosion resistance almost 80 times better than unprotected steel substrate. Corrosion current density has been drastically decreased that advocated effectiveness of applying the HVOF copper coating in terms of corrosion protection.

Table 5.1. Corrosion parameters extracted from Tafel curve.

Material	Corrosion Potential, E_{corr} (mv)	Corrosion Current Density, i_{corr} ($\mu A/cm^2$)	Anodic Tafel Constant, β_a (mV/dec)	Cathodic Tafel Constant, β_c (mV/dec)	Corrosion Rate (mm/year)
Substrate	-1062	638.3	435.4×10^{-9}	104.3×10^{-3}	0.46
Cu	-495.1	1.956	5.586×10^{-3}	4.923×10^{-3}	0.0056

5.1.2. HVOF Sprayed Cu-Al Bronze Coating

Figure 5.6 (a) has shown the SEM image of the HVOF deposited Cu-Al Bronze coating before and after being subjected to the corrosion reaction. The Diamalloy1004 powder was used as the coating materials which is golden-colored and produced using gas atomization technique in inert gas environment. Aluminum and Iron are considered as major alloying elements to be used in Cu-Al-Bronze alloy.
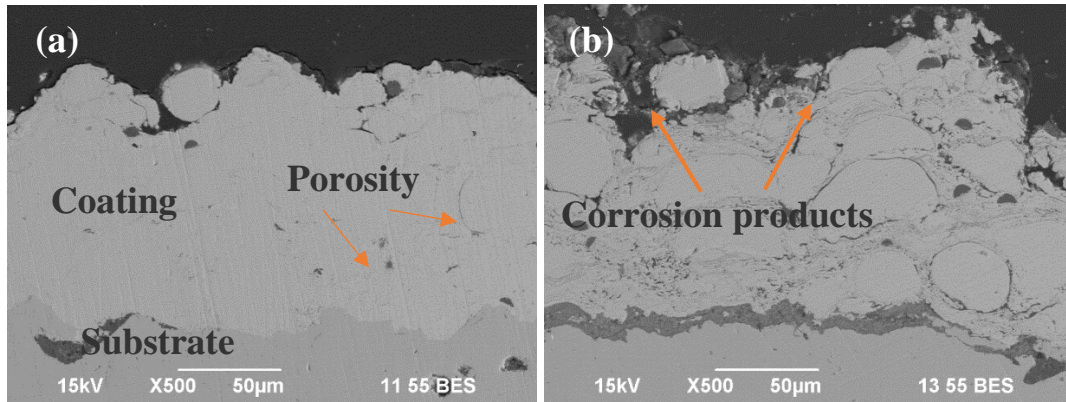
Figure 5.6. SEM images from (a) HVOF deposited Cu-Al-Bronze coating before and (b) after corrosion.

Figure 5.6 (a) shows the microstructure of Cu-Al Bronze coating deposited on steel substrate using HVOF technique before corrosion. The deposited Cu-Al-Bronze coating was dense with no visible delamination in interface of the coating/substrate which indicated good bonding and adhesion between the coating and the substrate. The thickness of the coating was approximately 90µm. However, as it can be seen in Figure 5.6 (a), there are several circular and wire shape pores in the coating. According to the data, the porosity level was estimated near 5.5±1.2% of the cross-section area, which is very small ratio and may also have neglectable influence on material mechanical property.

By comparison the SEM micrograph before and after corrosion, as demonstrated in Figure 5.6 (a, b), it could be concluded that corrosion products significantly were formed on the surface of the HVOF deposited Al-bronze coating due to its reaction with the corrosive solution. The dark gray areas presented very close to the surface of the coating were observed after corrosion which did not exist in the SEM micrograph of the HVOF deposited Al-bronze before corrosion test.
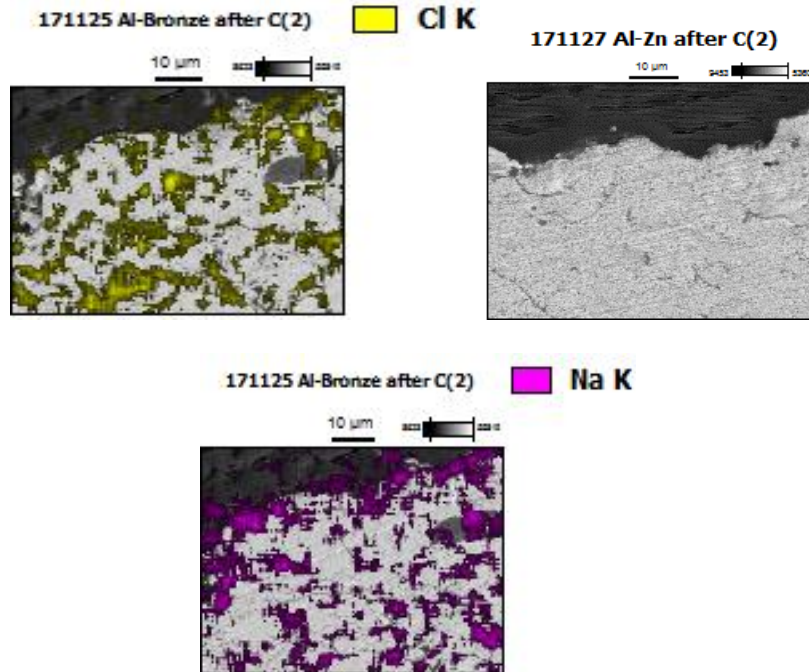
Figure 5.7. EDS maps of Cl$^-$, and Na elements penetrated in the HVOF thermal sprayed deposited coatings after corrosion experiment.

The colored area shown on Figure 5.8 representing for Cl$^-$ and Na elements diffused into the surface. According to the EDS map shown in Figure 5.7, Al-bronze acted less effective compared to the other coatings studied in this thesis in terms of blocking the sodium elements inside the coating.
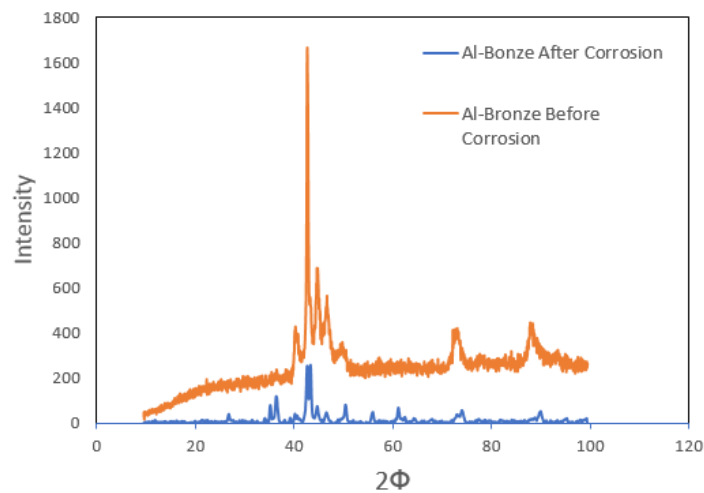
Figure 5.8. X-Ray pattern of HVOF sprayed Al-bronze coatings before and after corrosion.

The composition change after corrosion reaction was examined by XRD experiment. As Figure 5.8 showed, HVOF deposited Al-bronze was mainly contained $AlCu_3$ and $Ni_3ZnC_{0.7}$ before corrosion. After exposing to the corrosion environment there were more compositions identified in the Al-bronze coating microstructure including $AlCu_3$, Cu_2O, and $FeO(OH)$.

For the thermally sprayed Cu-Al Bronze coating, hardness tests were carried out on the coatings cross section based on ASTM E384 -1. Figure 5.9 illustrates the Knoop indentation on Cu-Al Bronze coating. The average hardness of the Cu-Al Bronze coating was estimated near 139.4HK ($\approx$125Hv) from 10 hardness measurement which was higher than the Cu coating. Thus, no reduction of mechanical property was identified for the Cu and Cu-Al Bronze coatings.
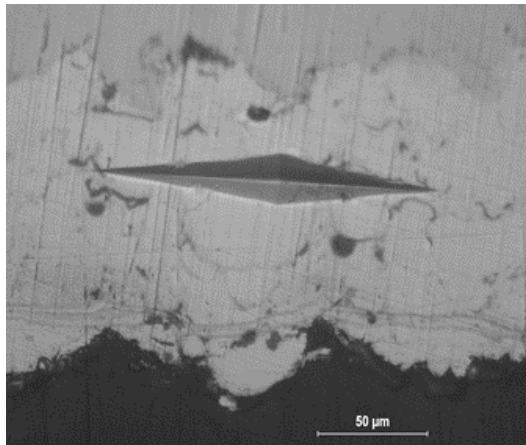
Figure 5.9. Knoop indentation on HVOF deposited Cu-Al-Bronze.

As the corrosion parameters extracted from the Tafel curve (Figure 5.10) of HVOF Al-Bronze coated and uncoated samples exposed to 3.5% NaCl solution exhibits, this coating could improve to corrosion resistance of the surface to some extends, however the influence was significantly less than that of resulted by HVOF deposited copper coating.
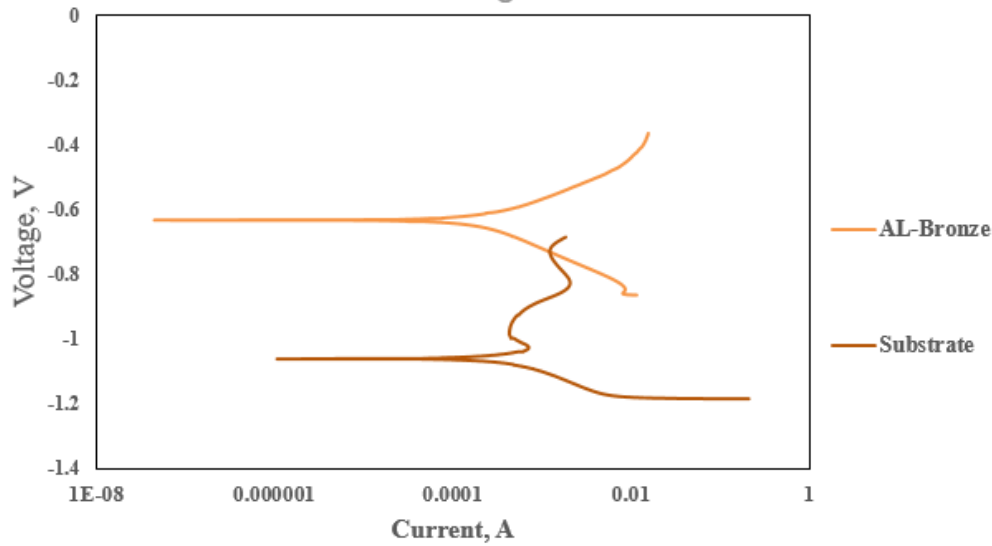
Figure 5.10. Tafel curves of Cu-Al-Bronze coated and uncoated steel samples in 3.5% NaCl.

This could be attributed to higher porosity level in Al-bronze microstructure compared to that of copper deposited coating. The corrosion parameters are listed in Table 5.2. As the table represented the corrosion rate estimated for Cu-Al-Bronze was almost three times more than estimated for the copper coating deposited by HVOF technique.

Table 5.2. Corrosion parameters extracted from Tafel curve of Al-bronze coating.

Material	Corrosion Potential, E_{corr} (mv)	Corrosion Current Density, i_{corr} ($\mu A/cm^2$)	Anodic Tafel Constant, β_a (mV/dec)	Cathodic Tafel Constant, β_c (mV/dec)	Corrosion Rate (mm/year)
Substrate	-1062	638.3	435.4×10^{-9}	104.3×10^{-3}	0.46
Al-Bronze	-632.7	0.641	3.74×10^{-3}	3.39×10^{-3}	0.0168

5.1.3. Wire Arc Sprayed Al-Zn Coating

As discussed earlier in the previous overview of corrosion mechanisms of various alloys, Al-Zn-based materials proved to be good candidates to operate in corrosive environment such as soil, and underground condition. Wire arc is the most recommended technique, among the other thermal spray techniques, to deposit Al-Zn-based alloys due to low porosity level of the consecutive coating. In this study, Al-Zn (84.25Wt.% Al-15.71%Zn) was selected to be deposited

on carbon steel using wire arc spraying technique. Microstructural properties, porosity level, mechanical properties, and corrosion resistant of the coatings were evaluated and compared.

Figure 5.11 exhibited the SEM images taken from wire arc Al-Zn coatings before and after corrosion. The porosity level of the Al-Zn coating estimated near $3\pm0.6\%$ of the cross-section area. As Figure 5.11 revealed, the both coatings before and after corrosion had dense structure with no delamination in the interphase of the coating-substrate indicating good bonding between the coating and the substrate. According microstructural characterization, there was no observable change in the microstructure of the cross section of the coatings, preferably near the surface, before and after corrosion. This means very slim changes occurred due to chemical reaction of the Al-Zn coating in the corrosive environment.
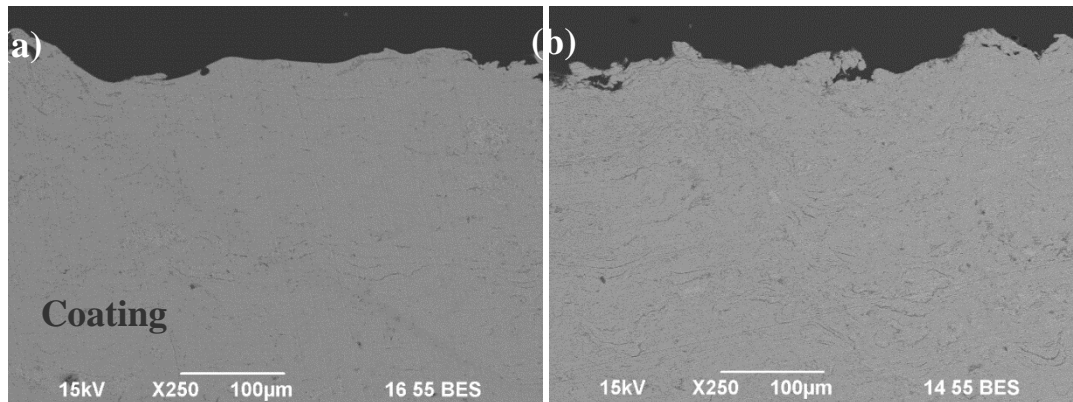
Figure 5.11. SEM micrographs of (a) Wire arc deposited Al-Zn coating before and (b) after corrosion.

Figure 5.12 demonstrated the EDS map indicating the depth of the penetration of Cl^- and Na^+ ions. Comparing to the EDS map from the thermal sprayed coatings addressed in this research, it was concluded that Al-Zn coating acted more effectively in terms of blocking these ions from defusing to the surface. Due to lower porosity level, smaller amount of the Cl^- and Na^+ could diffuse into the surface and therefore the ratio of the grey to colored area was greater in coating.
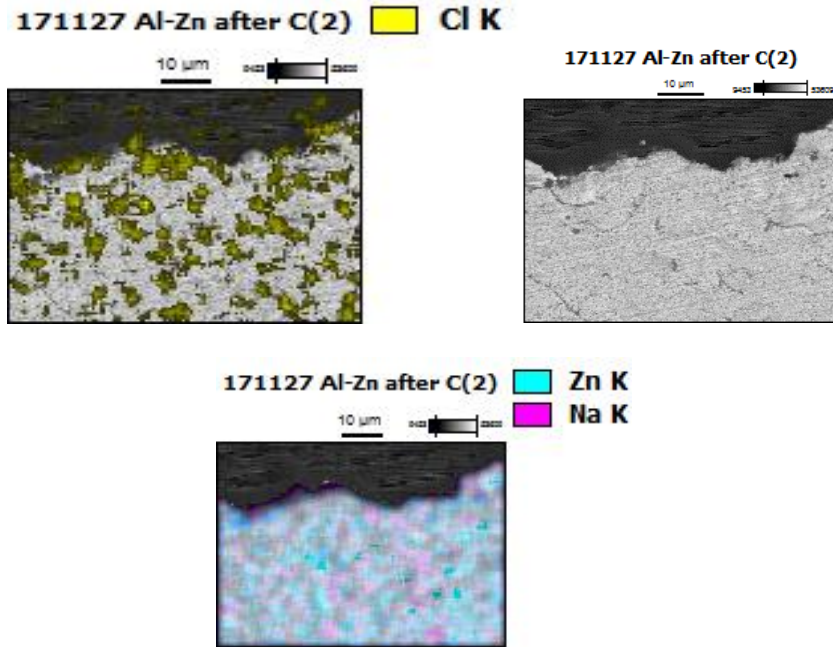
Figure 5.12. EDS maps of Cl⁻ and Na+ elements penetrated in the wire-arc deposited Al-Zn coatings.

After analyzing the XRD pattern of wire arc sprayed Al-Zn coating (Figure 5.13) before corrosion, it was observed that the coating was mainly made of Aluminum and Zinc constituents. After corrosion, some other peaks belonged to aluminum oxide and zinc oxide detected which were formed as the result of the passivation process of the surface. Presence of the oxide phases detected in the XRD pattern of the coating subjected to the corrosive environment has also been identified by observing passivation process observed in anodic slope of the Tafel curve (Figure 5.12). Indeed, change in the anodic slope advocated the formation of the passive layer during the corrosion reaction.
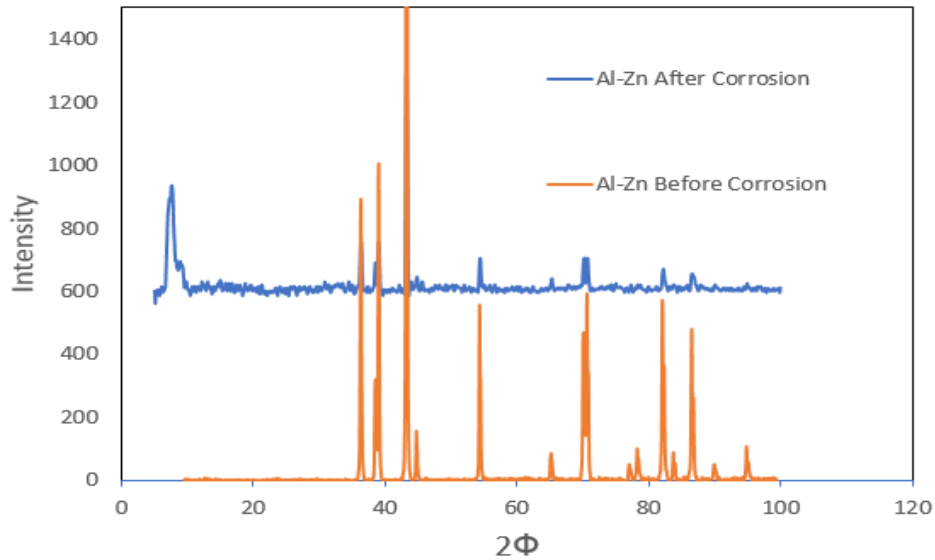
Figure 5.13. X-Ray pattern of wire-arc sprayed Al-Zn coatings before and after corrosion.

The Knoop hardness estimation was also carried out on the surface of the Al-Zn coated sample to indicate the mechanical properties of the surface (Figure 5.14). The value of the hardness was estimated approximately 41.2±1 HK that was lower compared to those of the other coatings such as copper and Al-Cu-Bronze.
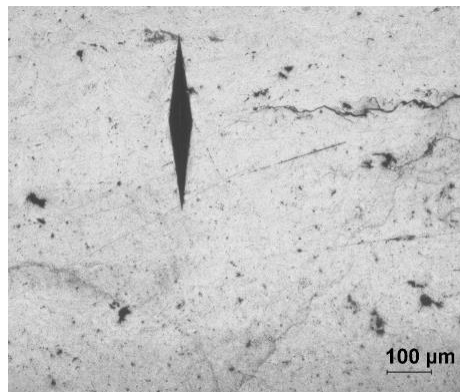
Figure 5.14. Knoop indentation carried out on wire arc sprayed Al-Zn coating.

Presence of the oxide phases detected in the XRD pattern of the coating subjected to the corrosive environment has also been identified by observing passivation process observed in anodic slope of the Tafel curve (Figure 5.15). Indeed, change in the anodic slope advocated the formation of the passive layer during the corrosion reaction.
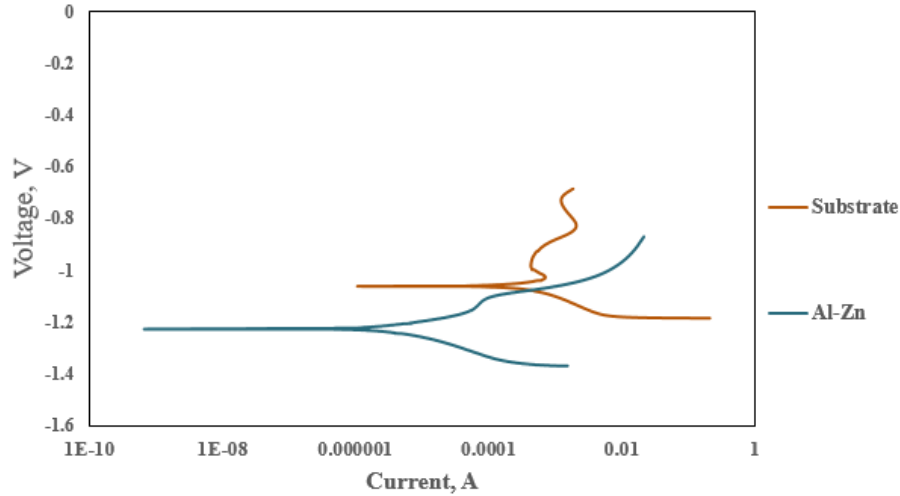
Figure 5.15. Tafel curves of Al-Zn coated and uncoated steel samples in 3.5% NaCl.

The corrosion parameters listed in Figure 5.16 led to the fact that, Al-Zn coated surface possessed the lowest corrosion rate compared to those of copper and Al-Cu-Bronze.

Table 5.3. Corrosion parameters extracted from Tafel curve of Al-Zn coating.

Material	Corrosion Potential, E_{corr} (mv)	Corrosion Current Density, i_{corr} ($\mu A/cm^2$)	Anodic Tafel Constant, β_a (mV/dec)	Cathodic Tafel Constant, β_c (mV/dec)	Corrosion Rate (mm/year)
Substrate	-1062	638.3	435.4×10^{-9}	104.3×10^{-3}	0.46
Al-Zn	-1226	0.79	35.24	40.2	0.003

The estimated corrosion rate for the Al-Zn coating was near 0.003 mm/year having been one third that of Cu-Al-Bronze and almost one tenth of the HVOF deposited copper coating. This could be due to lower porosity level of the Al-Zn coating and also the successful passivation process including formation of protective oxide layer on the surface that inhibited further diffusion of the corrosive agents.

5.2. Elevated Temperature Application

5.2.1. HVOF Sprayed Inconel 718 Coating

5.2.1.1. Microstructural Characterization

In this study, it has been tried to evaluate the corrosion performance of Ni-based coating on the surface of the steel and also examine the effect of different substrate on the bonding strength

of the deposited coatings. To this aim, steel and Inconel 718 substrates were coated by Inconel 718 coating through HVOF deposition technique. SEM micrographs of the cross-section of HVOF deposited Inconel 718 coatings on Inconel 718 and Steel substrates were shown in Figure 5.16 (a and b). SEM micrographs exhibited similar microstructural features for both Inconel 718/Inconel 718 and Inconel 718/Steel.
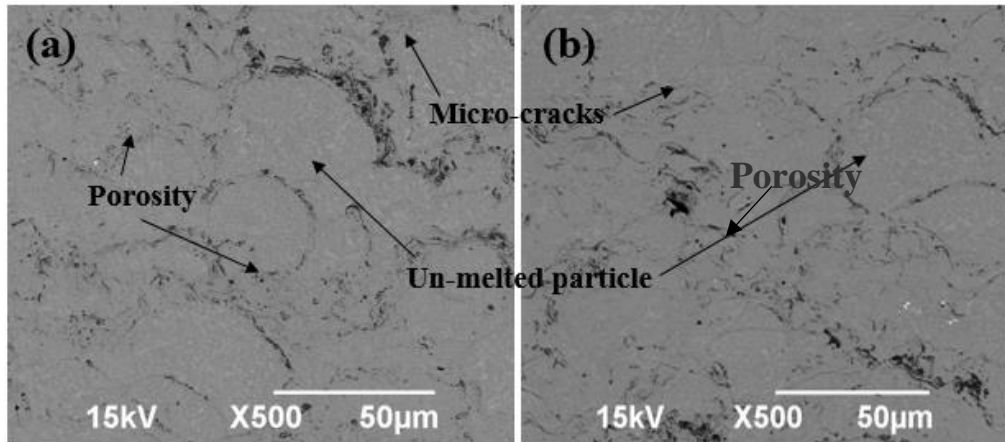
Figure 5.16. SEM micrographs of (a) Inconel 718/Inconel 718 and (b) Inconel 718/Steel coating cross-sections.

According to the micrographs of Inconel 718/Inconel 718 similar to the ones shown in Figure 5.16 (a and b), coating possessed a very dense microstructure with very low porosity and micro-cracks. Porosity values of the coatings were in a very close range, being approximately 1.15%±0.20 and 1.22%±0.25 for Inconel 718/Inconel 718 and Inconel 718/Steel, respectively. Lamellae structures which is typical for thermal sprayed coatings were seen in those micrographs. Detailed microstructural observation indicated existence of un-melted particles similar to that of marked in Figure 5.16 (a and b). There were three discernable contrasts observed in the microstructure of the both coatings: black, dark gray, and light gray regions. The black regions that were distributed through the microstructure and along the interface between splats, were identified as the remnant porosity and voids [24, 25]. Small voids, pores, and micro-cracks were

marked in Figure 5.17 (a and b). To identify the elemental distribution of the dark and light gray areas, EDS was conducted at the higher magnifications from five random locations on the regions of interest (Figure 5.17).
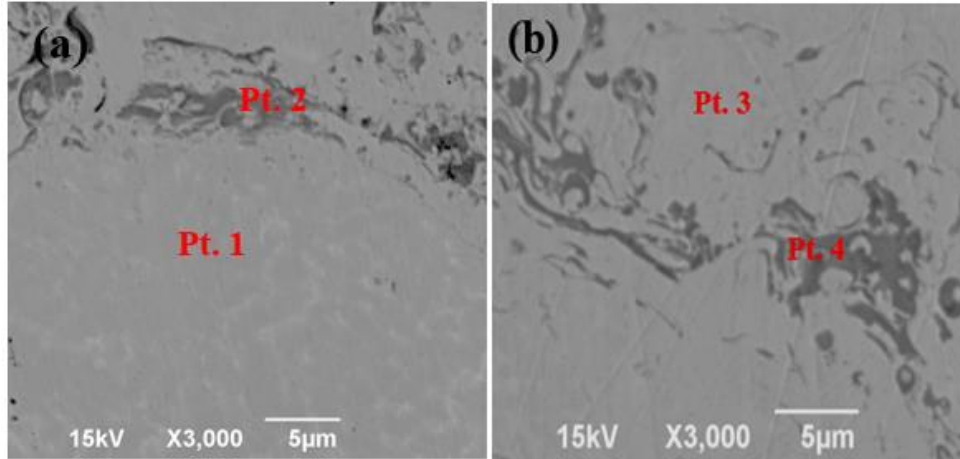
Figure 5.17. High magnification SEM micrographs of (a) Inconel 718/Inconel 718 and (b) Inconel 718/Steel.

Table 5.4. Elemental distribution of the Inconel 718 coating on(a) Inconel 718 and (b) Steel substrates.

	O-K	Al-K	Si-K	Ti-K	Cr-K	Fe-K	Ni-K	Nb-L
(a) Inconel 718/Inconel 718								
Pt. 1	-	0.02±0.01	2.28±0.2	0.38±0.18	12.01±0.67	13.17±1.03	40.00±2.03	4.70±0.63
Pt. 2	20.78±1.3	0.76±0.21	-	1.91±0.23	26.20±0.92	18.28±1.25	9.39±1.57	11.11±0.7
(b) Inconel 718/Steel								
Pt. 3		0.51±0.20	1.23±0.3	0.77±0.08	16.70±2.13	15.16±1.08	44.91±2.13	5.25±0.64
Pt. 4	17.65±0.2	0.52±0.22		1.07±1.24	25.21±1.72	17.57±1.24	12.76±1.72	10.7±0.71

The average of EDS results taken from the light gray regions (Pt.1 and 3) and dark gray areas (Pt. 2 and 4) of both coatings were listed in Figure 5.17 According to the EDS results reported for point 1 and 3, the interior region of the lamellae mostly contained Ni, Fe, and Cr elements. The darker regions around the splats (designated by Pt. 2 and 4) were made of considerable amount of O as well as Cr, and Fe elements. Azarmi et al. [24, 25] previously reported the existence of such elements in dark splat boundary regions of thermal sprayed nickel superalloys.

XRD pattern of the coatings were exhibited in Figure 5.18 Inconel 718/Inconel 718 and Inconel 718/Steel structures had very similar XRD-pattern with no significant difference. This agreed with the SEM and EDS results indicating that different substrates did not have notable effect on composition of the corresponding coatings. In both coatings, three main compositions detected were: chrome oxide (Cr_2O_3), FCC-matrix, and other cubic (Ni, Fe)-rich phases. Comparing the result of EDS with XRD, led to the conclusion that in the lamellae core (Pt. 1 and 3), which was rich of Ni and Fe elements, could be made of cubic (Ni, Fe) phases and FCC-matrix, that was previously reported as γ phase by Normand et al. [27]. There was a significant amount of oxygen detected in dark gray areas between the lamellae which represented that oxide phases (mainly chrome oxide) mostly formed in these regions (Pt. 2 and 4). The formation of oxide phases could be due to the oxidation during the spraying process when molten particles were traveling between gun and substrate. Since oxide are generally form on the outer surface of in-flight particles, they will remain in interlamellar regions after solidification of splats [25]. The existence of oxide phases may increase the chance of the crack propagation within splat boundary regions due to brittle nature of oxides. Thus, it is expected that the splat boundaries experienced weaker bonding strength compared to splat cores due to presence of considerable amount of oxide phases as well as voids and porosities.
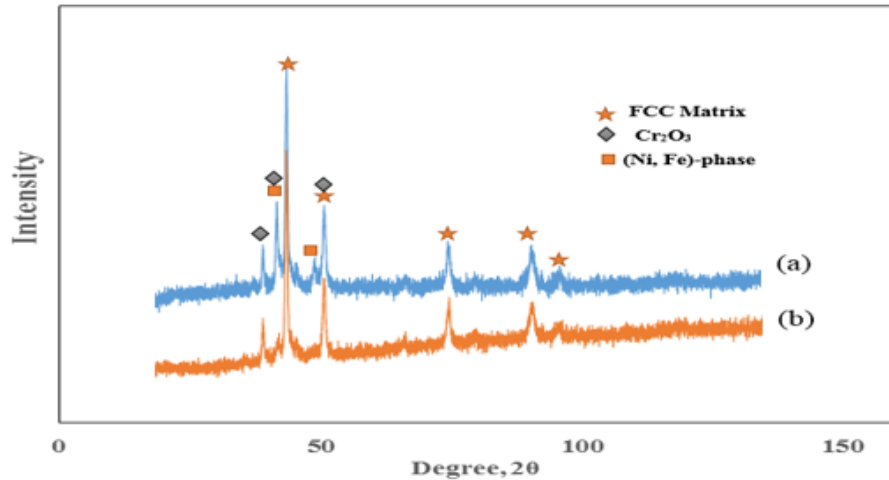
Figure 5.18. XRD results of the Inconel 718 coatings deposited on (a) Inconel 718 and (b) Steel substrates.

5.2.1.2. Effect of the Substrate on Interfacial Mechanical Properties

5.2.1.2.1. Hardness and Fracture Toughness Estimation

Vickers indentation tests at different applied loads were conducted to understand the effect of the substrate material on hardness and fracture toughness of the coating-substrate interface. This method is one of the most common techniques to measure the hardness of thermally sprayed coatings [156, 157]. A Clark micro-hardness tester (model: CM-800AT) was used for indentation test. Five sets of indentation were carried out at different loads (200, 300, 500, 1000, and 2000 g) on coating-substrate interface of each sample. The indentation test was repeated ten times at each applied load to minimize the possible error due to inhomogeneity in the coating microstructure. To increase the accuracy, only the indentations located appropriately on the coating-substrate interface region were taken to the account for the calculation [156, 157]. This procedure was repeated four more times on various distances from the coting-substrate interface (150, 300, 450, and 600 μm) to evaluate the hardness and fracture toughness variation across the coating microstructure. The dwell time for the indentation was set to 15 s. Eventually, the average hardness values obtained from interface and different distances apart were calculated. To avoid any

90

interaction of neighboring indentations, they were spaced far enough as recommended by the standard [23, 158, 159].

Based on earlier reports, there were two main types of crack occurred during the Vickers indentation which were either surface-radial cracks (Palmqvist cracks), or radial-medium cracks (half-penny cracks) [156, 159]. In the case of Palmqvist crack, $l_a/a \leq 2.5$ and $c/a \leq 3.5$. Where, l_a is the average of the radial corner crack length, a is the average indent half-diagonal size, and c is the radial crack length around the indentations. On the other hand, half-penny is favored to use when $c/a \geq 2.5$. The conventional method entitled as "direct straight-line method" was used to measure the crack length [19]. According to this method, l_a is given by $l_a = c - a$, where a is obtained by $a = (2a_1 + 2a_2)/4$ [156, 159]. The crack length is measured, considering radial crack at the corners, edge cracks, ring shape cracks, and other small cracks around the indentation according to the definition given by A. G. Evans [160]. In this work, most of the cracks were radial and edge crack. Since the geometry of the cracks created after indentations met the requirements mentioned for Palmqvist model (Eq. 5.1), this method was selected to estimate the fracture toughness.

$$K_{IC} = 0.0319 \left[P/(a\sqrt{l_a}) \right] \qquad \text{(Eq. 5.1)}$$

Where K_{IC} is the fracture toughness (in units of MPa.m$^{1/2}$), P is the indentation load (in Newtons), a and l_a are in meter.

Fig. 5.19 (a and b) exhibited example of the Vickers indentations on the interfaces of the Inconel 718/Inconel 718 and Inconel 718/Steel samples, respectively. As it was observed from the micrographs (Figure 5.17), the type of cracks created by indentation were mostly radial and edge cracks. The indentation induced asymmetric fractures in both Inconel 718/Inconel 718 and Inconel 718/Steel interfaces. This could be attributed to the presence of voids and inhomogeneity in phase

distribution around the contact regions [23, 26-28]. This asymmetry is more obvious in Inconel 718/Steel interface (Figure 5.19 (b)) as Steel substrate underwent higher plastic deformation compared to the coating, which led to wider indent in the substrate region. There were considerable radial cracks appeared exactly at the coating-substrate interfaces of the both samples, which can be vividly seen in Figure 5.19 (a and b). Some edge micro-cracks propagated mostly in the splat boundaries of the both samples, which was attributed to the weaker bonding strength between the splats due to the presence of brittle oxide phases, voids, and porosities in the splat boundary region. However, the amount of those visible micro-cracks in the splat boundary regions were higher in the Inconel 718/Steel coating. It could be due to thermal mismatch and residual stress build up because of the difference in coefficient of thermal expansion between the coating and the substrate. The higher residual stress concentration intensified the resilience of these regions for crack propagation [8, 9, 28].
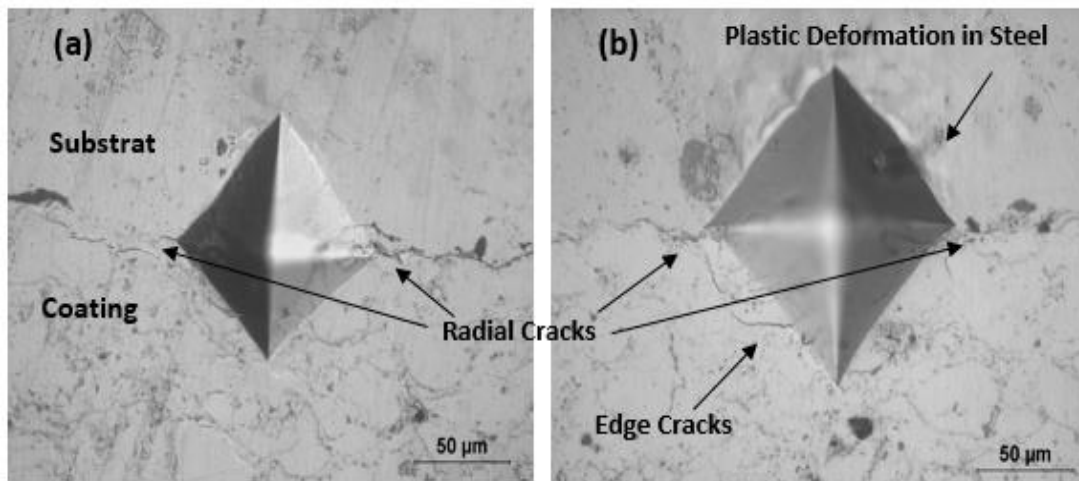
Figure 5.19. Vickers indentation on the interfaces of (a) Inconel 718/Inconel 718 and (b) Inconel 718/Steel samples.

According to the results of the Vickers indentation test, the average hardness values obtained from Inconel 718/Inconel 718 interface regions at each applied load condition was significantly higher than that of Inconel 718/Steel. Since the value of the hardness obtained at load

500 grf had better compromising with the average value, the corresponding data obtained by this load was selected and was shown in Table 5.5 The average hardness value at 500 grf load for the Inconel 718/Inconel 718 was 286.81±10 HV while this value for Inconel 718/Steel was 194.33±8 HV.

Table 5.5. The results of the average hardness and fracture toughness.

Materials	Hardness (HV) at 500grf	Fracture Toughness (MPa.m$^{1/2}$)
Inconel 718/Inconel 718	286.81±10	0.57
Inconel 718/Steel	194.33±8	0.41

The plot of $a\sqrt{l_a}$ against the load yields a straight line from which the fracture toughness could be determined. Figure 5.20 demonstrated this line for both Inconel 718/Inconel 718 and Inconel 718/Steel samples.
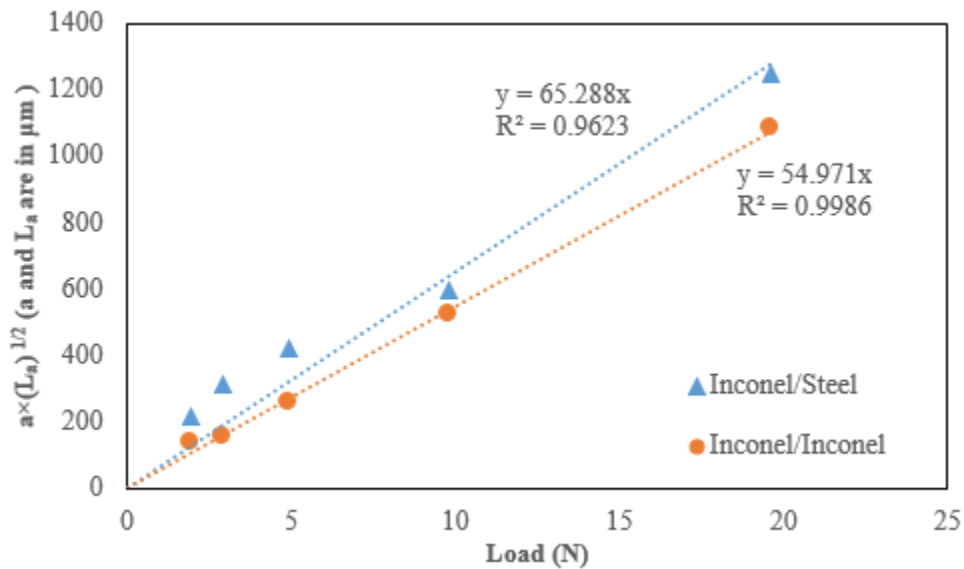
Figure 5.20. Fracture toughness assessment based on crack length indication.

The results illustrated that the interface fracture toughness of the Inconel 718/Inconel 718 measured approximately 0.57 MPa.m$^{1/2}$ which was significantly higher than that of Inconel 718/Steel (0.41 MPa.m$^{1/2}$). This could be due to contribution of higher thermal stress built up in Inconel 718/Steel interface during the cooling because of the dissimilarity in their coefficient of

thermal expansion [26]. The higher residual stress followed by more crack propagation in the interface of Inconel 718/Steel compared to the Inconel 718/Inconel 718 could be considered as the reason for the weaker fracture toughness and bonding strength of Inconel 718/Steel coating system.

Figure 5.21 depicted the optical images of the indentations carried out at different locations of Inconel 718/Inconel 718 across the coating.
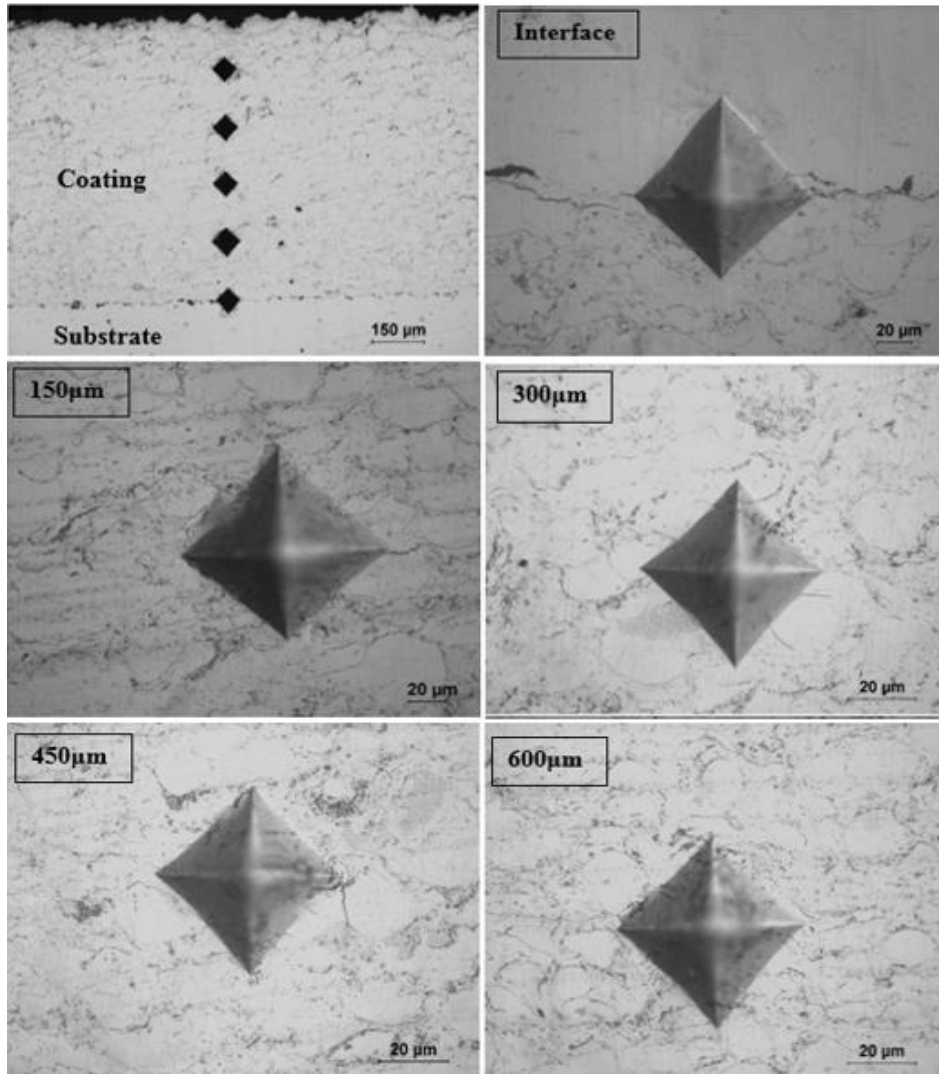
Figure 5.21. Crack propagation by Vickers indentation at interface and distances of 150, 300, 450, and 600μm from the interface.

According to the optical images, there was a slight drop in the size of the cracks created as distance from the interface of coating-substrate increased. The highest average crack length and

indentation diagonal size occurred in the interface, which resulted the lowest calculated fracture toughness and hardness in this region. Similar results were obtained when this study was performed on Inconel 718/Steel coating system.

The distributions of the hardness and fracture toughness values across the coatings were compiled in Figure 5.22 (a) and (b), respectively. Figure 5.22 (a) indicated that with moving from interfacial region toward coating core there is a drastic increase in hardness values of Inconel 718/Steel samples. No significant increase in hardness was observed for Inconel 718/Inconel 718 system in the same condition. The measured hardness values for both samples after 150 μm showed similar trend. The range of measured hardness values were 286±11-314±8 HV and 194±13-315±11 HV for Inconel 718/Inconel 718 and Inconel 718/Steel samples, respectively. There was a good indication of weaker interface in Inconel 718/Steel sample due to its lower hardness and fracture toughness values (Figure 5.22 (a and b)).
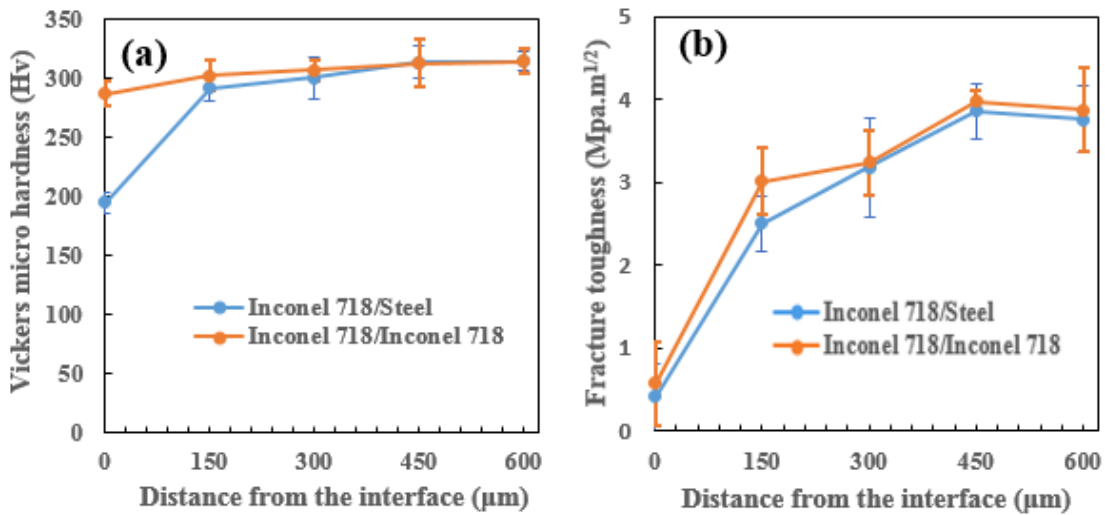
Figure 5.22. Distribution of (a) Vickers hardness and (b) fracture toughness across the coatings.

According to Figure 5.22 (b), the values of fracture toughness for the both coatings were increased with increase in the distance of the indentation from the interfacial region. The lowest values of fracture toughness obtained at the coating-substrate interface while the highest value

obtained at the last measurement point before the nearest one to the coatings surface for both samples. As can be concluded from Figure 5.22 (b), there was a jump in the fracture toughness values once indentation shifted from the interface to the distance of 150 μm away from interface. As the distance increased, the value of the fracture toughness for both coatings varied in the smaller ranges. Inconel 718/Inconel 718 possessed much higher hardness and fracture toughness values in its interfacial region compared to those of Inconel 718/Steel sample. However, the measured hardness values were only slightly higher for other measured distances. In general, the main reason of lower fracture toughness of the interfacial regions for both samples could be due to presence of oxide phases, porosities, cracks, regions of incomplete bonding, and also contribution of higher residual thermal stress at interfacial regions. The higher value of the hardness and fracture toughness of the Inconel 718/Inconel 718 compared to Inconel 718/Steel, especially near the interface, could be attributed to the effect of the substrate material in thermal mismatch stress build-up.

5.2.1.2.2. Adhesion Test

The shear strength values of the Inconel 718/Inconel 718 and Inconel 718/Steel coating systems were evaluated in order to compare their bonding strength and validate the results that previously obtained for fracture toughness. The shear strength was calculated from the maximum shear force divided by the representative sample square area [15]. The maximum shear force stands for the maximum load supported by the coatings before completely peeled-off from their substrates. It is worth to clarify the terminology, which has been used in this study regarding ″cohesion″ and ″adhesion″ in the coating systems. Cohesion is referred to the strength of the bonds between the splats within the coating microstructure, while adhesion is known as the strength of the bonds between the coating material and the substrate. Three different modes of failure were

suggested for the coating-substrate systems; mode I: adherence is smaller than coherence, mode II: adherence is equal to coherence, and mode III: adherence is greater than coherence [29]. In the first mode, the coating detaches completely at maximum shear load and fracture occurs in the interface between the coating and substrate [29]. At mode II, if the shearing occurs close to interface region the coating will detach along the interface area, whereas if shear happens at larger distance from interface, fracture occurs within the coating. In the last mode (mode III), in the case of hard coatings, failure mostly occurs in the mode of splinter in small particle, while soft and often porous coatings crumble and loaded layer of the coating may delaminate [29].

Figure 5.23 (a and b) exhibited the failure modes after adhesion and cohesion tests, respectively. The results indicated that both Inconel 718/Inconel 718 and Inconel 718/Steel failed at the same mode, in which the coating was separated from the substrate without breaking during the test. In this mode, the fracture path propagates along the coating-substrate interface until the complete separation of the coating from the substrate (Figure 5.23 (a)). The average value of shear stress measured for Inconel 718/Inconel 718 sample was 92±2 MPa which was two times larger than that of Inconel 718/Steel one which calculated as 45±2 MPa. These results are in a good agreement with the fracture toughness estimations obtained by application of Palmqvist model, which illustrated the higher bonding strength in Inconel 718/Inconel 718 sample compared to Inconel 718/Steel sample.

The results of the lap shear test on freestanding coating samples revealed that cohesive strength of both coatings was higher than the shear strength of the adhesive material, since the failure occurred in the adhesive with no visible fracture in the coatings. Figure 5.23 (b) exhibited the failure mode of the freestanding coatings under lap shear tests demonstrating there was no coating residue remained on the adhesive.
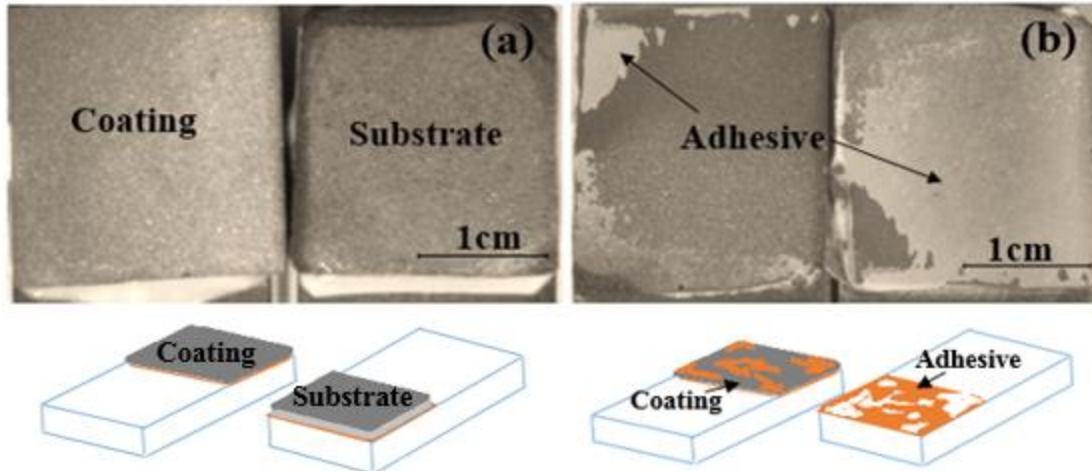
Figure 5.23. Macroscopic and schematic of the interfaces and failure modes in (a) Inconel718 coating-Steel substrate and (b) free-standing Inconel 718 coating.

It was concluded that the failure mode observed for both Inconel 718/Inconel 718 and Inconel 718/Steel samples met the criteria as defined for mode I. In other words, no separation of coating layers was observed in the freestanding coatings under lap shear test. Furthermore, the entire coating was peeled off from the substrates without any noticeable residue particles on the surface of substrates. Both results supported that the cohesive strength between the coatings layers (lamellae) was greater than adhesion between the coatings and substrates.

5.2.1.3. Corrosion Test

Corrosion mechanisms of HVOF Ni-base coating has been evaluated using the potentiodynamic electrochemical technique at elevated temperature near 250ºC. Materials characterization by SEM, EDS, and XRD were conducted to evaluate the effectivity of the Inconel coating to protect the surface in the corrosive environment. As can be seen in Figure 5.24, two new oxide phases were detected after corrosion formation. The main peaks of the new oxide phases attributed to iron niobium oxide ($FeNb_2O_3$) and chromium molybdenum oxide ($Cr_2Mo_3O_{12}$). Mahobia, et al., previously reported formation of these two compositions as a result of hot corrosion of Inconel 718 in chloride solution indicated formation of chromium oxide rich unstable

passive layer resulted in localized protection of superalloy material that was not sufficient to provide corrosion protection for the entire surface, during the service at high temperature condition.
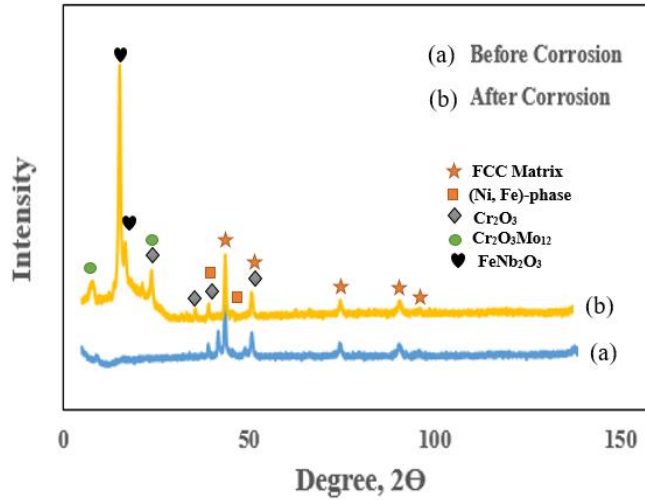
Figure 5.24. XRD patterns for the HVOF Inconel 718 coatings (a) before and (b) after corrosion.

Table 5.6. Elemental composition of Inconel 718 coatings before and after corrosion obtained by EDS.

Before Corrosion				After Corrosion			
Element	Pt. 1	Pt. 2	Pt. 3	Element	Pt. 1	Pt. 2	Pt. 3
O-K	25.76±0.67	8.90±0.60	8.71±0.91	O-K	1.38±0.23	6.74±0.36	11.34±0.43
Mg-K	-	-	-	Mg-K	-	0.03±0.05	-
Al-K	0.18±0.07	0.71±0.10	-	Al-K	-	0.38±0.09	0.46±0.14
Si-K	-	-	0.21±0.09	Si-K	-	0.43±0.04	-
S-K	-	-	-	S-K	0.15±0.03	0.58±0.30	0.16±0.38
Cl-K	-	-	-	Cl-K	-	1.03±0.16	-
Na-K	-	-	-	Na-K	-	0.85±0.17	-
Ti-K	0.28±0.13	-	0.75±0.18	Ti-K	-	0.44±0.09	0.83±0.25
Cr-K	1.16±0.16	8.29±0.38	13.55±0.66	Cr-K	4.89±0.40	3.16±0.29	14.57±0.51
Mn-K	0.30±0.25	-	-	Mn-K	1.11±0.55	-	-
Fe-K	54.78±1.27	0.77±1.77	15.60±1.00	Fe-K	14.47±2.46	3.07±0.42	13.78±0.74
Ni-K	0.69±0.40	16.08±1.75	43.38±1.99	Ni-K	67.36±1.01	5.72±0.70	40.17±1.46
Nb-L	2.2±0.43	-	2.92±0.48	Nb-L	-	0.53±0.22	3.60±0.41
Mo-L	0.27±0.21	-	2.29±0.38	Mo-L	0.70±0.25	0.27±0.66	2.21±0.92

Resulted Tafel curve indicated higher corrosion resistance behavior of the HVOF deposited Inconel 718 coating compared to the bare substrate. SEM results also showed that Inconel 718 coating had a very dense and clustered structure that mostly contained FCC-matrix and cubic (Ni,

Fe)-rich phases. Table 5.6 listed the elemental distribution of the Inconel coatings before and after

corrosion reaction. These results were also validated by XRD experiments where peaks of all those

elements were detected in the microstructure. Some oxide phases were observed in the coating

microstructure, which probably formed due to in-flight oxidation of molten metallic particles

during the spraying process.
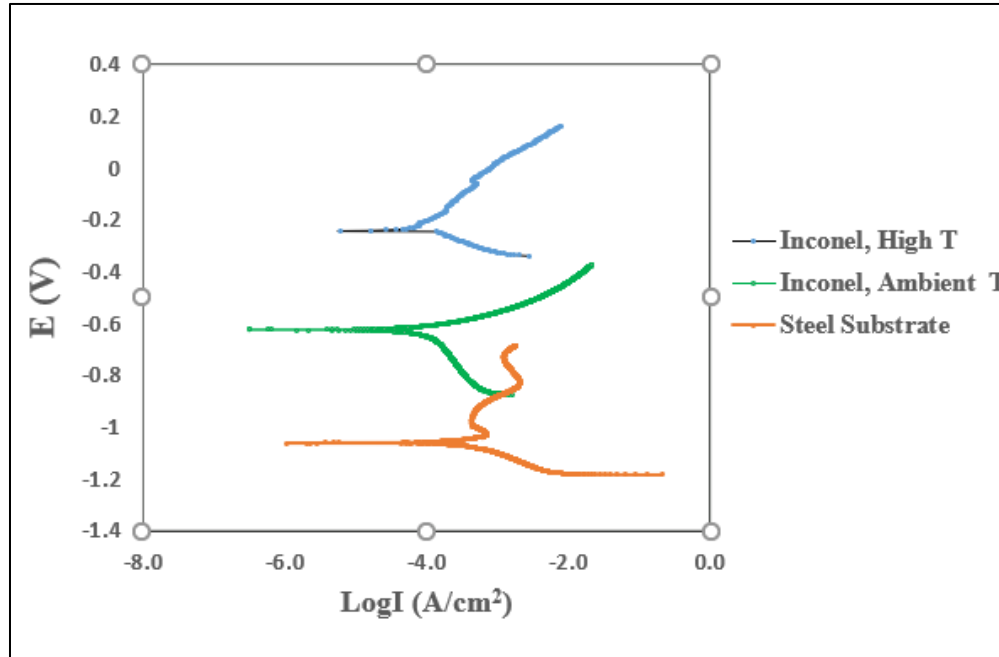
Figure 5.25. (a) Polarization curves of Inconel 718 coating at 250°C and ambient temperature
and carbon steel substrate at ambient temperature in 3.5wt% NaCl solution.

Table 5.7. Corrosion parameters extracted from Tafel curve of HVOF Ni-base coating.

Material	Corrosion Potential, E_{corr} (mv)	Corrosion Current Density, i_{corr} ($\mu A/cm^2$)	Anodic Tafel Constant, β_a (mV/dec)	Cathodic Tafel Constant, β_c (mV/dec)	Corrosion Rate (mm/year)
Substrate	-1062	638.3	435.4×10^{-9}	104.3×10^{-3}	0.46
Ni-based at 250°C	-235	14.68	13.6×10^{-3}	16.5×10^{-3}	0.0124
Ni-based at Ambient T	-624.2	5.2	40.5×10^{-5}	16.5×10^{-3}	0.0095

The majority of the oxide phases detected after corrosion formation were made of

chromium and iron oxide containing low amount of Mo and Nb. However, as revealed and

supported by Tafel curve, SEM, and EDS results, the chromium oxide layer could not act like stable passive layer at the elevated temperatures.

5.2.2. WC-based Coating

Thermal sprayed coatings are classic examples of materials with inhomogeneous microstructure and normally include porosity, micro cracks, voids, and oxides which affect their mechanical and tribological properties. A combination of optical microscopy and SEM followed by image analysis were used to examine the microstructural properties of the coating. The average thickness of WC-Ni coatings was measured to be $350\pm5\mu m$. Backscattered electron SEM images of cross-sections of WC-Ni coatings were shown in Figure 5.26. The measured porosity for HVOF deposited WC-Ni coating was approximately $3.32\pm0.1\%$. To evaluate the accuracy of the porosity measurement by image analysis, the actual densities of the coatings was calculated and compared with the theoretical density. SEM micrograph of the HVOF deposited WC-Ni coating (Figure 5.26) illustrated that the microcracks in this coating was low and mostly located between the splats.
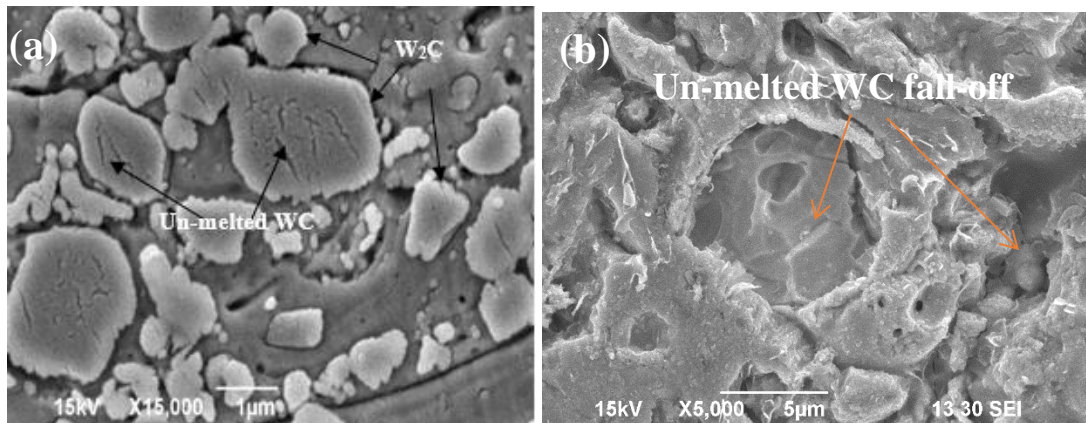
Figure 5.26. SEM micrographs of WC-Ni coatings (a) before and (b) after corrosion.

HVOF sprayed WC-Ni contains un-melted powders which were seen as angular particles within the microstructure (Figure 5.26). Existence of such un-melted particles in the microstructure of the same type of coating has also been previously observed and reported for WC based coatings

101

by S. Usmani, et al. and C. Pornthep, et al. [165, 166]. The average size of un-melted WC particles in the coating was less than 1.17 ± 0.71 μm (Figure 5.26 (a)). Higher magnification micrograph of etched coating (Figure 5.26 (b)) indicated a lighter contrast shell around the WC grains. Since melting point of WC (2870°C) was much higher than that of Ni (1455°C), it was expected that Ni was completely melted, and the edge of WC irregular shaped grains were overheated and consequently decarburized which could result in formation of W_2C at the outer shell of particles. It has been drawn that during the deposition of WC-based coatings some new crystalline phases are formed - mainly W_2C and W which has also previously reported for the same type of coating [167]. Formation of W_2C after decarburization resulted in higher density and hardness of coating but its brittleness leads to lower fracture toughness and abrasive wear resistance [167]. Similar results were also reported by J. Yuan, et al. [168]. Comparison of the SEM image of the corroded surface of the WC coating indicated separation of the un-melted WC particles from the surface as a result of selective corrosion.

EDS map of chlorine and sodium ions diffusion to the surface (Figure 5.27) during the corrosion experiment also indicated the fact that the WC coating could not effectively act as a protective barrier and block these destructive ions from penetration to the surface.
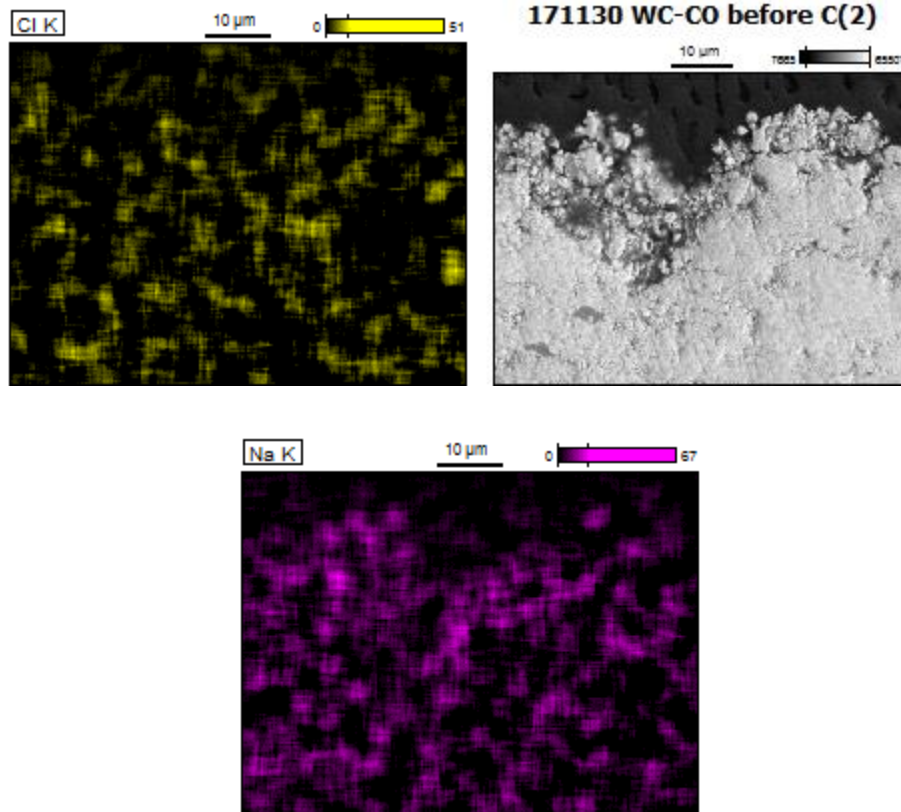
Figure 5.27. EDS maps of Cl$^-$ and Na$^+$ elements penetrated in the HVOF deposited WC coatings.

The data induced that both coatings before and after corrosion contained WC, W$_2$C, Ni, and W. In fact, according to XRD pattern in Figure 5.28, no significant change observed in chemical composition of the HVOF deposited WC-Ni coatings before and after corrosion test. This means the coating materials did not contribute in chemical transformation during the corrosion reaction. However, low corrosion performance illustrated in the Tafel curve shown in Figure 5.28, shows that other mechanisms altered the corrosion reaction. Galvanic corrosion between the WC and Ni particle and/or selective corrosion of the WC particle due to having lower electronegativity compared to Ni might significantly contribute in the corrosion mechanisms. The areas where the separation of the WC particle from the surface occurred after corrosion were observed in SEM micrograph which is another indication for the phenomenon discussed above. The other factor for the high corrosion rate of the WC-Ni coating could be attributed to the existence of high level of

cracks and porosity that provided higher chance of diffusion of the corrosive environment to the substrate.
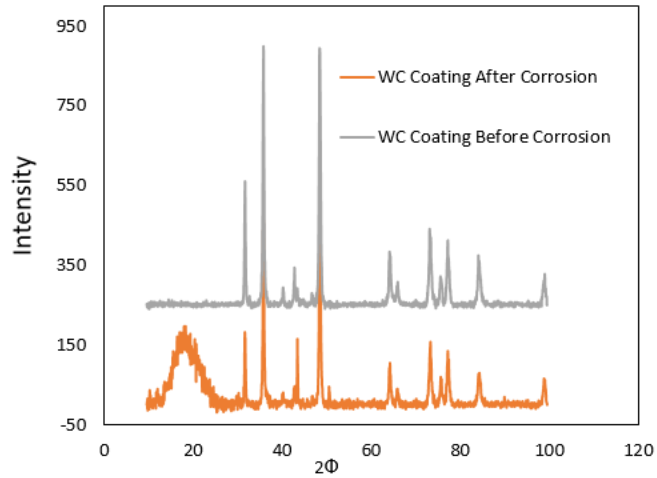
Figure 5.28. XRD pattern of WC coating before and after corrosion test.

The hardness value of the HVOF deposited WC-Ni coating was 370.01±40.41 HK. The hardness indentation image has been shown in Figure 5.29.
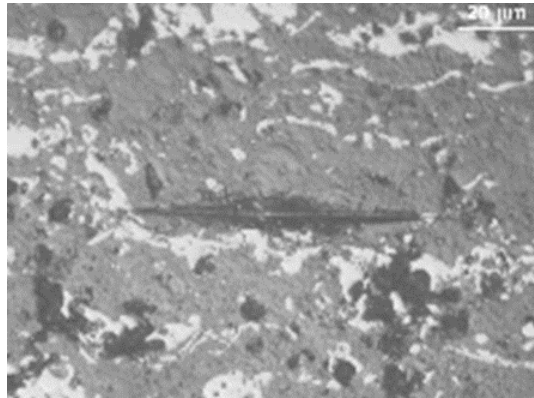
Figure 5.29. Knoop hardness indentation on HVOF deposited WC-Ni coating.
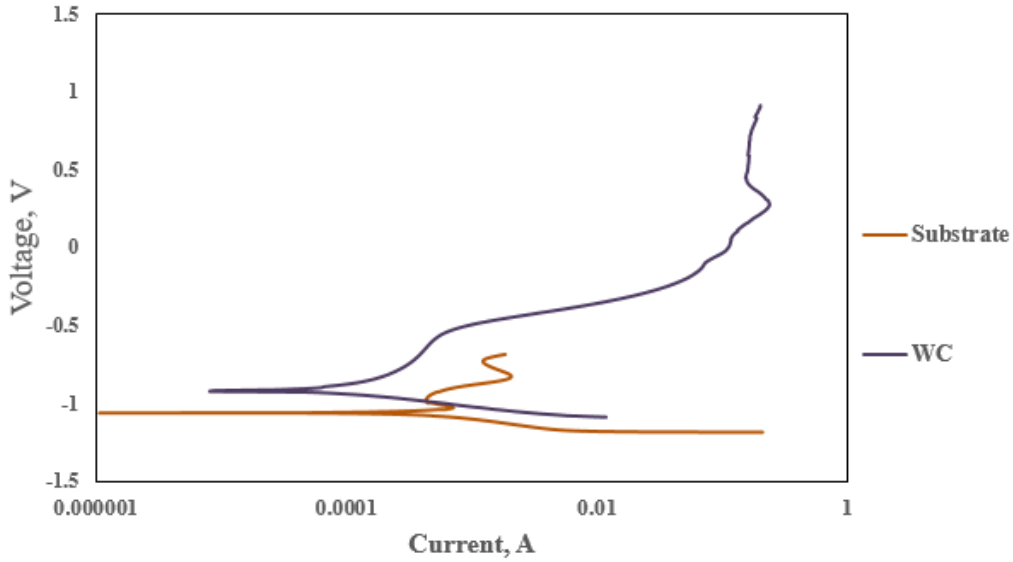
Figure 5.30. Tafel curves of HVOF WC coated and uncoated steel samples in 3.5% NaCl at 250ºC.

Some important corrosion parameters obtained from potentiodynamic polarization technique have been listed in Table 5.8.

Table 5.8. Corrosion parameters extracted from Tafel curve of HVOF WC coating.

Material	Corrosion Potential, E_{corr} (mv)	Corrosion Current Density, i_{corr} ($\mu A/cm^2$)	Anodic Tafel Constant, β_a (mV/dec)	Cathodic Tafel Constant, β_c (mV/dec)	Corrosion Rate (mm/year)
Substrate	-1062	638.3	435.4×10^{-9}	104.3×10^{-3}	0.46
WC	-920	106	419.4×10^{-3}	95.9×10^{-3}	0.39

WC coating could not provide effective protection for the underneath surface, according to the Tafel curves from corrosion tests performed at elevated temperature (~250ºC) as shown in Figure 5.30 and listed in Table 5.8 The measured corrosion rate after deposition of the coating on the surface was slightly reduced from 0.46 mm/y to 0.39 mm/y.

Table 5.9 has summarized and compared the corrosion resistance of the various thermal spray coatings deposited and studied in this thesis.

Table 5.9. Corrosion performance comparison between different thermal sprayed coatings.

Material	Corrosion Potential, E_{corr} (mv)	Corrosion Current Density, i_{corr} ($\mu A/cm^2$)	Anodic Tafel Constant, β_a (mV/dec)	Cathodic Tafel Constant, β_c (mV/dec)	Corrosion Rate (mm/year)
Ambient Temperature					
Substrate	-1062	638.3	435.4×10^{-9}	104.3×10^{-3}	0.46
Cu	-495.1	1.956	5.586×10^{-3}	4.923×10^{-3}	0.01
Al-Bronze	-632.7	0.641	3.74×10^{-3}	3.39×10^{-3}	0.02
Al-Zn	-1226	0.79	35.24×10^{-3}	40.2×10^{-3}	0.0029
Elevated Temperature (250ºC)					
Ni-based	-624.2	14.68	13.6×10^{-3}	16.5×10^{-3}	0.0124
WC-Ni	-920	106	419.4×10^{-3}	95.9×10^{-3}	0.3927

CHAPTER 6. CONCLUSIONS

The effectiveness of using variety of the materials for protection of the carbon steel substrate have been experimented to perform at ambient and high temperature. Copper, Al-Cu-Bronze and Al-Zn were selected for the low temperature applications and Ni-base and WC-base were the candidates to perform at elevated temperature. The deposited coatings were subjected to several examination techniques such as electrochemical analysis, SEM, XRD, EDS, and hardness testing to evaluate and compare the effectiveness of the thermal sprayed coatings. Some notable conclusions have been drawn as follow:

Among thermal sprayed coatings deposited to protect carbon steel at ambient temperature, wire arc sprayed Al-Zn possessed the lowest corrosion rate due to formation of passive Al_2O_3 layer that hindered further diffusion of the deleterious elements such as Cl^- and Na^+ from corrosive medium. HVOF Cu-Al-Bronze coating had the highest porosity value that led by comparatively higher corrosion rate of the coating. However, this coating possessed the highest hardness value due to formation of $Ni_3ZnC_{0.7}$.

HVOF sprayed Inconel 718 performed much higher corrosion resistance compared to HVOF deposited WC-Ni at elevated temperature in NaCl solution. This attributed to galvanic corrosion between the WC and Ni constituents. This resulted in selectively separation of WC from the surface led to formation of small pits on the surface. HVOF deposited Inconel 718 coating performed a very high resistant against corrosive solution due to formation of passive layed made of chromium oxide. However, high solubility of chromium oxide at high temperature led to incomplete passivation on the surface and reduced the effectivity of corrosion protection.

CHAPTER 7. FUTURE WORKS

(1) Corrosion protection system was successfully developed as illustrated earlier. However, it has been observed that, having very high inflight particle speed, HVOF technique could damage the sensors and lower the accuracy of the measurement. Thus, wire arc spray technique was suggested as an alternative to this process. Effectivity of this method in reduction of the porosity level and improving the mechanical properties should be investigated.

(2) Developing the copper, and tungsten carbide coatings by HVOF also amalgamated considerable level of porosity and crack which makes the coating very susceptible to galvanic corrosion and rusting off the steel. Thus, some substitution methods for the coating technique or applying polymeric layer on the metallic coating should be investigated to reduce the corrosion rate.

(3) According the result, zinc and aluminum-based materials deposited with wire arc method led to better corrosion protection. However, more investigation is yet needed to elucidate the level of hydrogen embrittlement during the corrosion reaction.

CHAPTER 8. REFERENCES

[1] R.R. Fessler, Pipeline corrosion, Report, US Department of Transportation Pipeline and Hazardous Materials Safety Administration, Baker, Evanston, IL, (2008).

[2] R.W. Bonds, L.M. Barnard, A.M. Horton, G.L. Oliver, Corrosion and corrosion control of iron pipe: 75 years of research, Journal (American Water Works Association), 97 (2005) 88-98.

[3] N.G. Thompson, M. Yunovich, D. Dunmire, Cost of corrosion and corrosion maintenance strategies, Corrosion Reviews, 25 (2007) 247-262.

[4] R.W. Revie, H.H. Uhlig, Uhlig's corrosion handbook, John Wiley & Sons, 2011.

[5] A.W. Peabody, R. Bianchetti, Control of pipeline corrosion, National Association of Corrosion Engineers, 1967.

[6] M.H. GarcÁa, Sedimentation engineering: Processes, measurements, modeling, and practice, ASCE Publications, 2008.

[7] D.H. Kroon, O. Olabisi, L.G. Rankin, J.T. Carroll, D.D. Lindemuth, M.L. Miller, Improvements to the External Corrosion Direct Assessment Process-Part 2, Materials Performance, 50 (2011) 30-37.

[8] M. Handbook, ASM International, Vol. 13, Corrosion, (1987) 38.

[9] F. Mansfeld, Use of electrochemical impedance spectroscopy for the study of corrosion protection by polymer coatings, Journal of Applied Electrochemistry, 25 (1995) 187-202.

[10] A. Samimi, S. Zarinabadi, An Analysis of Polyethylene Coating Corrosion in Oil and Gas Pipelines, Journal of American science, USA, (2011).

[11] R. Tucker Jr, ASM Handbook, Volume 5A, Thermal Spray Technology, plastics industry, 335 (2013) 336.

[12] J.V. Heberlein, P. Fauchais, M.I. Boulos, Thermal Spray Fundamentals: From Powder to Part, 2014.

[13] P.L. Fuhr, D.R. Huston, Corrosion detection in reinforced concrete roadways and bridges via embedded fiber optic sensors, Smart Materials and Structures, 7 (1998) 217.

[14] I. Shitanda, A. Okumura, M. Itagaki, K. Watanabe, Y. Asano, Screen-printed atmospheric corrosion monitoring sensor based on electrochemical impedance spectroscopy, Sensors and Actuators B: Chemical, 139 (2009) 292-297.

[15] J. Liu, R. Ruedisueli, Development of an Intelligent Electromagnetic Sensor to Detect Ferrous Corrosion Products under Structural Coatings, in: AIP Conference Proceedings, 2003, pp. 1631-1636.

[16] M.V. Kulkarni, S.K. Apte, S.D. Naik, J.D. Ambekar, B.B. Kale, Ink-jet printed conducting polyaniline based flexible humidity sensor, Sensors and Actuators B: Chemical, 178 (2013) 140-143.

[17] X. Li, W. Chen, Z. Huang, S. Huang, K.D. Bennett, Fiber optic corrosion sensor fabricated by electrochemical method, in: 5th Annual International Symposium on Smart Structures and Materials, International Society for Optics and Photonics, 1998, pp. 126-133.

[18] M. Kouril, T. Prosek, B. Scheffel, F. Dubois, High sensitivity electrical resistance sensors for indoor corrosion monitoring, Corrosion Engineering, Science and Technology, 48 (2013) 282-287.

[19] A.S. Morris, R. Langari, Measurement and instrumentation: theory and application, Academic Press, 2012.

[20] S.A. Rahman, M. Ismail, N. Norhazilan, H. Bakhtiar, Embedded capacitor sensor for monitoring corrosion of reinforcement in concrete, Journal of Engineering Science and Technology, 7 (2012) 209-218.

[21] G. McAdam, P. Newman, I. McKenzie, C. Davis, B. Hinton, Fiber optic sensors for detection of corrosion within aircraft, Structural Health Monitoring, 4 (2005) 47-56.

[22] S. Wade, C. Wallbrink, G. McAdam, S. Galea, B. Hinton, R. Jones, A fibre optic corrosion fuse sensor using stressed metal-coated optical fibres, Sensors and Actuators B: Chemical, 131 (2008) 602-608.

[23] M.R.A. Hassan, M.H.A. Bakar, K. Dambul, F.R.M. Adikan, Optical-based sensors for monitoring corrosion of reinforcement rebar via an etched cladding Bragg grating, Sensors, 12 (2012) 15820-15826.

[24] K. Cooper, J. Elster, M. Jones, R. Kelly, Optical fiber-based corrosion sensor systems for health monitoring of aging aircraft, in: AUTOTESTCON Proceedings, 2001. IEEE Systems Readiness Technology Conference, IEEE, 2001, pp. 847-856.

[25] Y.-L. Lo, F.-Y. Xiao, Measurement of corrosion and temperature using a single-pitch Bragg grating fiber sensor, Journal of intelligent material systems and structures, 9 (1998) 800-807.

[26] M. Benounis, N. Jaffrezic-Renault, Elaboration of an optical fibre corrosion sensor for aircraft applications, Sensors and Actuators B: chemical, 100 (2004) 1-8.

[27] M. Shenoy, Development Of An Optical Fiber-based Corrosion Detection Sensor Based On Laser Light Reflection, (2010).

[28] P. Marcus, Corrosion mechanisms in theory and practice, CRC Press, 2011.

[29] D. Wortman, R. Fryxell, K. Luthra, P. Bergman, Mechanism of low temperature hot corrosion: Burner rig studies, Thin Solid Films, 64 (1979) 281-288.

[30] G.Y. Lai, High-temperature corrosion and materials applications, ASM International, 2007.

[31] J. Guilemany, N. Cinca, S. Dosta, A.V. Benedetti, Corrosion behaviour of thermal sprayed nitinol coatings, Corrosion Science, 51 (2009) 171-180.

[32] T. Sidhu, S. Prakash, R. Agrawal, Hot corrosion studies of HVOF NiCrBSi and Stellite-6 coatings on a Ni-based superalloy in an actual industrial environment of a coal fired boiler, Surface and Coatings Technology, 201 (2006) 1602-1612.

[33] T. Sidhu, S. Prakash, R. Agrawal, A comparative study of hot corrosion resistance of HVOF sprayed NiCrBSi and Stellite-6 coated Ni-based superalloy at 900 C, Materials Science and Engineering: A, 445 (2007) 210-218.

[34] E. Leivo, M. Vippola, P. Sorsa, P. Vuoristo, T. Mäntylä, Wear and corrosion properties of plasma sprayed AI2O3 and Cr2O3 coatings sealed by aluminum phosphates, Journal of Thermal spray technology, 6 (1997) 205-210.

[35] P. Suegama, C.S. Fugivara, A.V. Benedetti, J. Guilemany, J. Fernández, J. Delgado, The influence of gun transverse speed on electrochemical behaviour of thermally sprayed Cr 3 C 2–NiCr coatings in 0.5 MH 2 SO 4 solution, Electrochimica Acta, 49 (2004) 627-634.

[36] R.J. Wood, Tribology of thermal sprayed WC–Co coatings, International Journal of Refractory Metals and Hard Materials, 28 (2010) 82-94.

[37] C. Godoy, M. Lima, M. Castro, J. Avelar-Batista, Structural changes in high-velocity oxy-fuel thermally sprayed WC–Co coatings for improved corrosion resistance, Surface and Coatings Technology, 188 (2004) 1-6.

[38] G. Saha, T. Khan, G. Zhang, Erosion–corrosion resistance of microcrystalline and near-nanocrystalline WC–17Co high velocity oxy-fuel thermal spray coatings, Corrosion Science, 53 (2011) 2106-2114.

[39] H. Voorwald, R. Souza, W. Pigatin, M. Cioffi, Evaluation of WC–17Co and WC–10Co–4Cr thermal spray coatings by HVOF on the fatigue and corrosion strength of AISI 4340 steel, Surface and Coatings Technology, 190 (2005) 155-164.

[40] V. Souza, A. Neville, Mechanisms and kinetics of WC-Co− Cr high velocity oxy-fuel thermal spray coating degradation in corrosive environments, Journal of thermal spray technology, 15 (2006) 106-117.

[41] J. Cho, S. Hwang, K. Kim, Corrosion behavior of thermal sprayed WC cermet coatings having various metallic binders in strong acidic environment, surface and coatings technology, 200 (2006) 2653-2662.

[42] L. Ward, B. Hinton, D. Gerrard, K. Short, Corrosion Behaviour of Modified HVOF Sprayed WC Based Cermet Coatings on Stainless Steel, Journal of Minerals and Materials Characterization and Engineering, 10 (2011) 989.

[43] E.A. Esfahani, H. Salimijazi, M.A. Golozar, J. Mostaghimi, L. Pershin, Study of corrosion behavior of arc sprayed aluminum coating on mild steel, Journal of thermal spray technology, 21 (2012) 1195-1202.

[44] W. Gu, D. Shen, Y. Wang, G. Chen, W. Feng, G. Zhang, S. Fan, C. Liu, S. Yang, Deposition of duplex Al 2 O 3/Aluminum coatings on steel using a combined technique of arc spraying and plasma electrolytic oxidation, Applied surface science, 252 (2006) 2927-2932.

[45] H.-B. Choe, H.-S. Lee, J.-H. Shin, Experimental Study on the Electrochemical Anti-Corrosion Properties of Steel Structures Applying the Arc Thermal Metal Spraying Method, Materials, 7 (2014) 7722-7736.

[46] H. Yang, Z. Yao, D. Wei, W. Zhou, G. Yin, L. Feng, Anticorrosion of thermal sprayed Al–Zn–Si coating in simulated marine environments, Surface Engineering, 30 (2014) 801-805.

[47] A. Ctte, Corrosion Tests of Flame-Sprayed Coated Steel-19 Year Report, Amer Weld Soc, in, Miami, 1974.

[48] Q. Jiang, M. Qiang, T. Fei, X. Yi, B.-l. Ren, Z.-m. Liu, Z.-j. Yao, Electrochemical corrosion behavior of arc sprayed Al–Zn–Si–RE coatings on mild steel in 3.5% NaCl solution, Transactions of Nonferrous Metals Society of China, 24 (2014) 2713-2722.

[49] Q. Jiang, Q. Miao, W.-p. Liang, F. Ying, F. Tong, Y. Xu, B.-l. Ren, Z.-j. Yao, P.-z. Zhang, Corrosion behavior of arc sprayed Al–Zn–Si–RE coatings on mild steel in 3.5 wt% NaCl solution, Electrochimica Acta, 115 (2014) 644-656.

[50] K. Seong-Jong, L. Seung-Jun, K. In-Ju, K. Seong-Kweon, H. Min-Su, J. Seok-Ki, Cavitation and electrochemical characteristics of thermal spray coating with sealing material, Transactions of Nonferrous Metals Society of China, 23 (2013) 1002-1010.

[51] Y. Wang, W. Tian, T. Zhang, Y. Yang, Microstructure, spallation and corrosion of plasma sprayed Al 2 O 3–13% TiO 2 coatings, Corrosion Science, 51 (2009) 2924-2931.

[52] S. Liscano, L. Gil, M.H. Staia, Effect of sealing treatment on the corrosion resistance of thermal-sprayed ceramic coatings, Surface and Coatings Technology, 188 (2004) 135-139.

[53] Y. Xiao, X. Jiang, Y. Xiao, L. Ma, Research on Zn-Al15 thermal spray metal coating and its organic painting composite system protection performance, Procedia Engineering, 27 (2012) 1644-1653.

[54] O. Salas, O. Troconis de Rincón, D. Rojas, A. Tosaya, N. Romero, M. Sánchez, W. Campos, Six-year evaluation of thermal-sprayed coating of Zn/Al in tropical marine environments, International Journal of Corrosion, 2012 (2012).

[55] H. Katayama, S. Kuroda, Long-term atmospheric corrosion properties of thermally sprayed Zn, Al and Zn–Al coatings exposed in a coastal area, Corrosion Science, 76 (2013) 35-41.

[56] S. Schuerz, M. Fleischanderl, G. Luckeneder, K. Preis, T. Haunschmied, G. Mori, A. Kneissl, Corrosion behaviour of Zn–Al–Mg coated steel sheet in sodium chloride-containing environment, Corrosion Science, 51 (2009) 2355-2363.

[57] Y. Liu, B.-s. Xu, Z.-x. Zhu, Z.-x. Li, J. Ma, New pattern Zn-Al-Mg-RE coating technics for steel structure sustainable design, Journal of Central South University of Technology, 12 (2005) 211-214.

[58] L. Kuiren, M. Pengcheng, P. Nianwen, C. Jianshe, H. Qing, Influence of silicon coating on the corrosion resistance of Zn-Al-Mg-RE-Si alloy, Journal of rare earths, 28 (2010) 378-381.

[59] R.M.P. Rodriguez, R.S. Paredes, S.H. Wido, A. Calixto, Comparison of aluminum coatings deposited by flame spray and by electric arc spray, Surface and Coatings Technology, 202 (2007) 172-179.

[60] E. Irissou, B. Arsenault, Corrosion study of cold sprayed aluminum coatings onto Al-Lithium (Al 2195) and Al 7075 alloy substrates, (2007).

[61] H. Min-Su, W. Yong-Bin, K. Seok-Cheol, Y.-J. Jeong, J. Seok-Ki, K. Seong-Jong, Effects of thickness of Al thermal spray coating for STS 304, Transactions of Nonferrous Metals Society of China, 19 (2009) 925-929.

[62] E. Irissou, J.-G. Legoux, B. Arsenault, C. Moreau, Investigation of Al-Al2O3 cold spray coating formation and properties, Journal of Thermal Spray Technology, 16 (2007) 661-668.

[63] I. Park, S. Kim, Cavitation Damage Behavior in Seawater for Al-Mg Alloy Arc Thermal Spray Coating with Mg Content, Acta Physica Polonica A, 129 (2016) 572-577.

[64] Y. Takeyoshi, S. Takase, Y. Shimizu, M. Sueyoshi, Y. Uchida, Corrosion Protection of Steel by Al-Mg Plasma Spray Coating, in: Meeting Abstracts, The Electrochemical Society, 2010, pp. 910-910.

[65] K. Habib, J. Saura, C. Ferrer, M. Damra, E. Giménez, L. Cabedo, Comparison of flame sprayed Al 2 O 3/TiO 2 coatings: their microstructure, mechanical properties and tribology behavior, Surface and coatings technology, 201 (2006) 1436-1443.

[66] E. Celik, I. Ozdemir, E. Avci, Y. Tsunekawa, Corrosion behaviour of plasma sprayed coatings, Surface and Coatings Technology, 193 (2005) 297-302.

[67] H. Chen, Z. Liu, Y. Chuang, Degradation of plasma-sprayed alumina and zirconia coatings on stainless steel during thermal cycling and hot corrosion, Thin solid films, 223 (1993) 56-64.

[68] C. Amaya, W. Aperador, J. Caicedo, F. Espinoza-Beltrán, J. Muñoz-Saldaña, G. Zambrano, P. Prieto, Corrosion study of alumina/yttria-stabilized zirconia (Al 2 O 3/YSZ) nanostructured thermal barrier coatings (TBC) exposed to high temperature treatment, Corrosion Science, 51 (2009) 2994-2999.

[69] M. Campo, M. Carboneras, M. López, B. Torres, P. Rodrigo, E. Otero, J. Rams, Corrosion resistance of thermally sprayed Al and Al/SiC coatings on Mg, Surface and Coatings Technology, 203 (2009) 3224-3230.

[70] A. Gulec, O. Cevher, A. Turk, F. Ustel, F. Yilmaz, Accelerated corrosion behaviors of Zn, Al and Zn/15Al coatings on a steel surface, Materiali in tehnologije, 45 (2011) 477-482.

[71] S. Kuroda, J. Kawakita, M. Takemoto, Marine exposure tests of thermal sprayed coatings in Japan, Thermal spray, (2003) 343-352.

[72] S. Kuroda, J. Kawakita, M. Takemoto, An 18-year exposure test of thermal-sprayed Zn, Al, and Zn-Al coatings in marine environment, Corrosion, 62 (2006) 635-647.

[73] B.-R. Hou, J. Zhang, J.-Z. Duan, Y. Li, J.-L. Zhang, Corrosion of thermally sprayed zinc and aluminium coatings in simulated splash and tidal zone conditions, Corrosion engineering, science and technology, 38 (2003) 157-160.

[74] S. Matthews, B. James, Review of Thermal Spray Coating Applications in the Steel Industry: Part 1—Hardware in Steel Making to the Continuous Annealing Process, Journal of thermal spray technology, 19 (2010) 1267-1276.

[75] D. Varacelle, D. Zeek, V. Zanchuck, E. Sampson, K. Couch, D. Benson, G. Cox, Experimental studies of twin-wire electric arc sprayed zinc/aluminum alloy coatings, Journal of Thermal Spray Technology, 7 (1998) 513-520.

[76] M. Lou, Y.F. Lu, C.L. Ma, Y.L. Hu, M. Zhou, H. Yang, Study on Corrosion-Resisting Properties of High-Speed Arc Sprayed Zn-Al Alloy Coating in Caverns, in: Advanced Materials Research, Trans Tech Publ, 2012, pp. 2072-2078.

[77] B.A. Shaw, A.M. Leimkuhler, P.J. Moran, Corrosion Performance of Aluminum and Zinc-Aluminum Thermal Spray Coatings in Marine Environments, in: Testing of Metallic and Inorganic Coatings, ASTM International, 1987.

[78] S. Hong, Y. Wu, W. Gao, J. Zhang, Y. Qin, Corrosion Behavior of Arc-Sprayed Zn-Al Coating in the Presence of Sulfate-Reducing Bacteria in Seawater, Journal of Materials Engineering and Performance, 24 (2015) 4449-4455.

[79] B. Champagne, B. Arsenault, C. Gelinas, S. Dallaire, Novel zinc-based alloys, preparation and use thereof for producing thermal-sprayed coatings having improved corrosion resistance and adherence, in, Google Patents, 1990.

[80] K. Bobzin, M. Oete, T. Linke, C. Schulz, Corrosion of wire arc sprayed ZnMgAl, Materials and Corrosion, 66 (2015) 520-526.

[81] C. Commenda, J. Pühringer, Microstructural characterization and quantification of Zn–Al–Mg surface coatings, Materials Characterization, 61 (2010) 943-951.

[82] Y. Liu, B.-S. Xu, Z.-X. Zhu, X.-B. Liang, Y.-X. Chen, Microstructure and corrosion behaviour of arc sprayed Zn–Al–Mg–RE cathodic protection coatings on steel substrates, International Heat Treatment and Surface Engineering, (2013).

[83] T. Sidhu, S. Prakash, R. Agrawal, Characterisations of HVOF sprayed NiCrBSi coatings on Ni-and Fe-based superalloys and evaluation of cyclic oxidation behaviour of some Ni-based superalloys in molten salt environment, Thin Solid Films, 515 (2006) 95-105.

[84] T. Sidhu, S. Prakash, R. Agrawal, Evaluation of hot corrosion resistance of HVOF coatings on a Ni-based superalloy in molten salt environment, Materials Science and Engineering: A, 430 (2006) 64-78.

[85] T. Sidhu, S. Prakash, R. Agrawal, Hot corrosion behaviour of HVOF-sprayed NiCrBSi coatings on Ni-and Fe-based superalloys in Na 2 SO 4–60% V 2 O 5 environment at 900 C, Acta materialia, 54 (2006) 773-784.

[86] T. Sidhu, S. Prakash, R. Agrawal, Hot corrosion performance of a NiCr coated Ni-based alloy, Scripta materialia, 55 (2006) 179-182.

[87] T. Sidhu, A. Malik, S. Prakash, R. Agrawal, Oxidation and hot corrosion resistance of HVOF WC-NiCrFeSiB coating on Ni-and Fe-based superalloys at 800 C, Journal of Thermal Spray Technology, 16 (2007) 844-849.

[88] B.S. Sidhu, S. Prakash, Performance of NiCrAlY, Ni–Cr, Stellite-6 and Ni 3 Al coatings in Na 2 SO 4–60% V 2 O 5 environment at 900° C under cyclic conditions, Surface and Coatings Technology, 201 (2006) 1643-1654.

[89] i.S. Abualigaledar, M. Salimi Jazi, F. Azarmi, Y. Wang, High Temperature Corrosion and Electrochemical Behavior of HVOF Sprayed Inconel 718 Coating Using an Innovative Device: HTCMD, (2017).

[90] S. Hong, Y. Wu, G. Li, B. Wang, W. Gao, G. Ying, Microstructural characteristics of high-velocity oxygen-fuel (HVOF) sprayed nickel-based alloy coating, Journal of Alloys and Compounds, 581 (2013) 398-403.

[91] N. Bala, H. Singh, S. Prakash, Accelerated hot corrosion studies of cold spray Ni–50Cr coating on boiler steels, Materials & Design, 31 (2010) 244-253.

[92] K. Yamada, Y. Tomono, J. Morimoto, Y. Sasaki, A. Ohmori, Hot corrosion behavior of boiler tube materials in refuse incineration environment, Vacuum, 65 (2002) 533-540.

[93] Y. Longa-Nava, Y. Zhang, M. Takemoto, R. Rapp, Hot corrosion of nickel-chromium and nickel-chromium-aluminum thermal-spray coatings by sodium sulfate-sodium metavanadate salt, Corrosion, 52 (1996) 680-689.

[94] T. Sundararajan, S. Kuroda, T. Itagaki, F. Abe, Steam Oxidation Resistance of Ni-Cr Thermal Spray Coatings on 9Cr-1Mo Steel. Part 1: 80Ni-20Cr, ISIJ international, 43 (2003) 95-103.

[95] S. Abualigaledari, M. Salimi Jazi, F. Azarmi, Y. Wang, High Temperature Corrosion and Electrochemical Behavior of HVOF Sprayed Inconel 718 Coating Using an Innovative Device: HTCMD, (2017).

[96] W.-M. Zhao, Y. Wang, T. Han, K.-Y. Wu, J. Xue, Electrochemical evaluation of corrosion resistance of NiCrBSi coatings deposited by HVOF, Surface and Coatings Technology, 183 (2004) 118-125.

[97] W.-M. Zhao, Y. Wang, L.-X. Dong, K.-Y. Wu, J. Xue, Corrosion mechanism of NiCrBSi coatings deposited by HVOF, Surface and Coatings Technology, 190 (2005) 293-298.

[98] W.J.C. Jarosinski, L.B. Temples, Corrosion resistant powder and coating, in, Google Patents, 2003.

[99] K. Chiu, F. Cheng, H. Man, Cavitation erosion resistance of AISI 316L stainless steel laser surface-modified with NiTi, Materials Science and Engineering: A, 392 (2005) 348-358.

[100] F. Cheng, K. Lo, H. Man, A preliminary study of laser cladding of AISI 316 stainless steel using preplaced NiTi wire, Materials Science and Engineering: A, 380 (2004) 20-29.

[101] K. Chiu, F. Cheng, H. Man, Laser cladding of austenitic stainless steel using NiTi strips for resisting cavitation erosion, Materials Science and Engineering: A, 402 (2005) 126-134.

[102] K. Chiu, F. Cheng, H. Man, Corrosion behavior of AISI 316L stainless steel surface-modified with NiTi, Surface and Coatings Technology, 200 (2006) 6054-6061.

[103] K. Chiu, F. Cheng, H. Man, A preliminary study of cladding steel with NiTi by microwave-assisted brazing, Materials Science and Engineering: A, 407 (2005) 273-281.

[104] H. Ye, R. Liu, D. Li, R. Eadie, Development of a new wear-resistant material: TiC/TiNi composite, Scripta Materialia, 41 (1999) 1039-1045.

[105] F. Cheng, K. Lo, H. Man, NiTi cladding on stainless steel by TIG surfacing process: Part I. Cavitation erosion behavior, Surface and Coatings Technology, 172 (2003) 308-315.

[106] M. Verdian, K. Raeissi, M. Salehi, Corrosion performance of HVOF and APS thermally sprayed NiTi intermetallic coatings in 3.5% NaCl solution, Corrosion Science, 52 (2010) 1052-1059.

[107] M. Verdian, K. Raeissi, M. Salehi, Electrochemical impedance spectroscopy of HVOF-sprayed NiTi intermetallic coatings deposited on AISI 1045 steel, Journal of Alloys and Compounds, 507 (2010) 42-46.

[108] M. Bram, A. Ahmad-Khanlou, H. Buchkremer, D. Stöver, Vacuum plasma spraying of NiTi protection layers, Materials Letters, 57 (2002) 647-651.

[109] S. Siegmann, K. Halter, B. Wielage, Vacuum plasma sprayed coatings and freestanding parts of Ni-Ti shape memory alloy, in: International Thermal Spray Conference. Essen, Germany, 2002, pp. 1061.

[110] K. Halter, A. Sickinger, L. Zysset, S. Siegmann, Low pressure wire arc and vacuum plasma spraying of NiTi shape memory alloys, Thermal spray, (2003) 589-595.

[111] A. Sickinger, Thermal Spraying of NiTi alloys, in: SMST-2003: The International Conference on Shape Memory and Superelastic Technologies, 2004, pp. 153-162.

[112] A. Ashary, R. Tucker, Electrochemical and long-term corrosion studies of several alloys in bare condition and plasma sprayed with Cr 2 O 3, Surface and Coatings Technology, 43 (1990) 567-576.

[113] A. Ashary, R. Tucker, Corrosion characteristics of several thermal spray cermet-coating/alloy systems, Surface and Coatings Technology, 49 (1991) 78-82.

[114] J. Guilemany, N. Espallargas, P. Suegama, A.V. Benedetti, Comparative study of Cr 3 C 2–NiCr coatings obtained by HVOF and hard chromium coatings, Corrosion Science, 48 (2006) 2998-3013.

[115] B.Q. Wang, K. Luer, The erosion-oxidation behavior of HVOF Cr 3 C 2-NiCr cermet coating, Wear, 174 (1994) 177-185.

[116] N. Espallargas, J. Berget, J. Guilemany, A.V. Benedetti, P. Suegama, Cr 3 C 2–NiCr and WC–Ni thermal spray coatings as alternatives to hard chromium for erosion–corrosion resistance, Surface and Coatings Technology, 202 (2008) 1405-1417.

[117] L. Fedrizzi, S. Rossi, R. Cristel, P. Bonora, Corrosion and wear behaviour of HVOF cermet coatings used to replace hard chromium, electrochimica acta, 49 (2004) 2803-2814.

[118] J. Guilemany, J. Fernandez, J. Delgado, A.V. Benedetti, F. Climent, Effects of thickness coating on the electrochemical behaviour of thermal spray Cr 3 C 2–NiCr coatings, Surface and coatings technology, 153 (2002) 107-113.

[119] S. Kamal, R. Jayaganthan, S. Prakash, S. Kumar, Hot corrosion behavior of detonation gun sprayed Cr 3 C 2–NiCr coatings on Ni and Fe-based superalloys in Na 2 SO 4–60% V 2 O 5 environment at 900 C, Journal of alloys and compounds, 463 (2008) 358-372.

[120] S. Kamal, R. Jayaganthan, S. Prakash, Evaluation of cyclic hot corrosion behaviour of detonation gun sprayed Cr 3 C 2–25% NiCr coatings on nickel-and iron-based superalloys, Surface and coatings technology, 203 (2009) 1004-1013.

[121] Y. Liu, X.-M. Wang, S.-b. Cen, G.-Q. Gou, L.-J. Wang, H. Chen, M.-J. Tu, Y.-X. Li, Corrosion behavior of thermal-sprayed WC cermet coatings in SO4 2− environment, Rare Metals, 33 (2014) 318-323.

[122] M. Takeda, N. Morihiro, R. Ebara, Y. Harada, R. Wang, M. Kido, Corrosion Behavior of Thermally Sprayed WC Coating in Na2SO4 Aqueous Solution, Materials Transactions, 43 (2002) 2860-2865.

[123] M. Bjordal, E. Bardal, T. Rogne, T. Eggen, Erosion and corrosion properties of WC coatings and duplex stainless steel in sand-containing synthetic sea water, Wear, 186 (1995) 508-514.

[124] M. Bjordal, E. Bardal, T. Rogne, T.G. Eggen, Combined erosion and corrosion of thermal sprayed WC and CrC coatings, Surface and Coatings Technology, 70 (1995) 215-220.

[125] J.M. Perry, T. Hodgkiess, A. Neville, A comparison of the corrosion behavior of WC-Co-Cr and WC-Co HVOF thermally sprayed coatings by in situ atomic force microscopy (AFM), Journal of thermal spray technology, 11 (2002) 536-541.

[126] (!!! INVALID CITATION !!! {}).

[127] H. de Villiers Lovelock, Powder/processing/structure relationships in WC-Co thermal spray coatings: A review of the published literature, Journal of thermal spray technology, 7 (1998) 357-373.

[128] P. Shipway, L. Howell, Microscale abrasion–corrosion behaviour of WC–Co hardmetals and HVOF sprayed coatings, Wear, 258 (2005) 303-312.

[129] P.K. Aw, A.L.K. Tan, T.P. Tan, J. Qiu, Corrosion resistance of tungsten carbide based cermet coatings deposited by high velocity oxy-fuel spray process, Thin solid films, 516 (2008) 5710-5715.

[130] V. Souza, A. Neville, Corrosion and synergy in a WC Co Cr HVOF thermal spray coating—understanding their role in erosion–corrosion degradation, Wear, 259 (2005) 171-180.

[131] L.-J. Wang, P.-X. Qiu, L. Yan, W.-X. Zhou, G.-q. Gou, C. Hui, Corrosion behavior of thermal sprayed WC cermet coatings containing metallic binders in saline environment, Transactions of Nonferrous Metals Society of China, 23 (2013) 2611-2617.

[132] J. Berget, T. Rogne, E. Bardal, Erosion–corrosion properties of different WC–Co–Cr coatings deposited by the HVOF process—influence of metallic matrix composition and spray powder size distribution, Surface and coatings technology, 201 (2007) 7619-7625.

[133] J. Perry, A. Neville, V. Wilson, T. Hodgkiess, Assessment of the corrosion rates and mechanisms of a WC–Co–Cr HVOF coating in static and liquid–solid impingement saline environments, Surface and Coatings technology, 137 (2001) 43-51.

[134] B. Bozzini, B. Busson, G.P. De Gaudenzi, C. Humbert, C. Mele, S. Tedeschi, A. Tadjeddine, Corrosion of cemented carbide grades in petrochemical slurries. Part I-Electrochemical adsorption of CN^-, SCN^- and MBT: A study based on in situ SFG, International Journal of Refractory Metals and Hard Materials, 60 (2016) 37-51.

[135] M. Fargnoli, E. Rovida, R. Troisi, The morphological matrix: Tool for the development of innovative design solutions, in: Proc. ICAD, 2006, pp. 13-16.

[136] A.S. Kang, G. Singh, V. Chawla, Some problems associated with thermal sprayed ha coatings: a review, Int J Surf Eng Mater Surf Eng Mater Technol, 3 (2013) 10-20.

[137] S.L. Chawla, Materials selection for corrosion control, ASM international, 1993.

[138] M.F. Ashby, D. Cebon, Materials selection in mechanical design, Le Journal de Physique IV, 3 (1993) C7-1-C7-9.

[139] J.A. Beavers, N.G. Thompson, External corrosion of oil and natural gas pipelines, ASM handbook, 13 (2006) 1015-1025.

[140] M. Yunovich, S. Waters, External Corrosion Direct Assessment for Unique Threats to Underground Pipelines, Final Report of Pipeline and Hazardous Materials Safety Administration US Department of Transportation Washington, DC, (2007).

[141] R. Chattopadhyay, Surface wear: analysis, treatment, and prevention, ASM international, 2001.

[142] J.R. Davis, Handbook of thermal spray technology, ASM international, 2004.

[143] E. Rabald, Corrosion guide, Elsevier, 2012.

[144] X. Campaignolle, M. Meyer, F. Bernard, S. Gastaud, Organic coatings aging consequences on under cp buried pipelines corrosion protection-simulated defects, in: CORROSION 2004, NACE International, 2004.

[145] C. Manfredi, J. Otegui, Failures by SCC in buried pipelines, Engineering Failure Analysis, 9 (2002) 495-509.

[146] T. Kamimura, H. Kishikawa, Mechanism of cathodic disbonding of three-layer polyethylene-coated steel pipe, Corrosion, 54 (1998) 979-987.

[147] S.W. Guan, N. Gritis, A. Jackson, P. Singh, 2005 China International Oil & Gas Pipeline Technology (Integrity) Conference & Expo.

[148] C. Alliston, J. Banach, J. Dzatko, Extending pipe life, World pipelines, Nov/Dec, (2002).

[149] L. Raymond, Hydrogen embrittlement: prevention and control, ASTM International, 1988.

[150] G. Murray, Prevention of hydrogen embrittlement by surface films, in: Hydrogen Embrittlement: Prevention and Control, ASTM International, 1988.

[151] E.D. McCarty, D. Wetzel, B.S. Kloberdanz, Hydrogen embrittlement in automotive fastener applications, in, SAE Technical Paper, 1996.

[152] V. Sauvant-Moynot, S. Gonzalez, J. Kittel, Self-healing coatings: An alternative route for anticorrosion protection, Progress in Organic Coatings, 63 (2008) 307-315.

[153] K. GUJARATHI, Corrosion of aluminum alloy 2024 belonging to the 1930s in seawater environment, in, Texas A&M University, 2008.

[154] W.W. Nik, O. Sulaiman, A. Fadhli, R. Rosliza, Corrosion behaviour of aluminum alloy in seawater, in: Proceedings of MARTEC 2010. The International Conference on Marine Technology, 2010, pp. 175-180.

[155] F.M. Reinhart, J.F. Jenkins, Corrosion of materials in surface seawater after 12 and 18 months of exposure, in, DTIC Document, 1972.

[156] C. Ponton, R. Rawlings, Vickers indentation fracture toughness test Part 2 Application and critical evaluation of standardised indentation toughness equations, Materials Science and Technology, 5 (1989) 961-976.

[157] M.S. Jazi, S.A. Galedari, F. Azarmi, X. Tangpong, Y. Huang, Z. Lin, Evaluation of Mechanical Properties of Plasma Sprayed Mixture of Partially Stabilized Zirconia and Tungsten Carbide on Low Carbon Steel, in: ASME 2015 International Mechanical Engineering Congress and Exposition, American Society of Mechanical Engineers, 2015, pp. V014T011A017-V014T011A017.

[158] S. Siegmann, M. Dvorak, H. Gruetzner, K. Nassenstein, A. Walter, Shear testing for characterizing the adhesive and cohesive coating strength without the need of adhesives, in: Proc Int Therm Spray Conf, 2005, pp. 823-829.

[159] D.K. Shetty, I. Wright, P. Mincer, A. Clauer, Indentation fracture of WC-Co cermets, Journal of Materials Science, 20 (1985) 1873-1882.

[160] A.G. EVans, E.A. Charles, Fracture toughness determinations by indentation, Journal of the American Ceramic society, 59 (1976) 371-372.

[161] A. Committee, Standard test method for shear testing of calcium phosphate coatings and metallic coatings, in, April, 2005.

[162] A.M. Abyzov, M.J. Kruszewski, Ł. Ciupiński, M. Mazurkiewicz, A. Michalski, K.J. Kurzydłowski, Diamond–tungsten based coating–copper composites with high thermal conductivity produced by Pulse Plasma Sintering, Materials & Design, 76 (2015) 97-109.

[163] J. Guilemany, J. Nutting, J. Miguel, Z. Dong, Microstructure formation of HVOF sprayed WC-Ni coatings deposited on low alloy steel, Materials and manufacturing processes, 12 (1997) 901-909.

[164] R.L. Jones, High temperature vanadate corrosion of yttria-stabilized zirconia coatings on mild steel, Surface and Coatings Technology, 37 (1989) 271-284.

[165] S. Usmani, S. Sampath, D.L. Houck, D. Lee, Effect of carbide grain size on the sliding and abrasive wear behavior of thermally sprayed WC-Co coatings, Tribology transactions, 40 (1997) 470-478.

[166] P. Chivavibul, M. Watanabe, S. Kuroda, J. Kawakita, M. Komatsu, K. Sato, J. Kitamura, Effect of Powder Characteristics on Properties of Warm-Sprayed WC-Co Coatings, Journal of Thermal Spray Technology, 19 (2010) 81-88.

[167] R. Schwetzke, H. Kreye, Microstructure and properties of tungsten carbide coatings sprayed with various high-velocity oxygen fuel spray systems, Journal of thermal spray technology, 8 (1999) 433-439.

[168] J. Yuan, Q. Zhan, J. Huang, S. Ding, H. Li, Decarburization mechanisms of WC–Co during thermal spraying: Insights from controlled carbon loss and microstructure characterization, Materials Chemistry and Physics, 142 (2013) 165-171.

[169] M. Khan, T. Clyne, Microstructure and abrasion resistance of plasma sprayed cermet coatings, Thermal Spray: Practical Solutions for Engineering Problems, (1996) 113-122.

[170] M.J. Paterson, B. Ben-Nissan, Multilayer sol-gel zirconia coatings on 316 stainless steel, Surface and Coatings Technology, 86 (1996) 153-158.

[171] E. Celik, O. Culha, B. Uyulgan, N.A. Azem, I. Ozdemir, A. Turk, Assessment of microstructural and mechanical properties of HVOF sprayed WC-based cermet coatings for a roller cylinder, Surface and Coatings Technology, 200 (2006) 4320-4328.

[172] Q. Zhan, L. Yu, F. Ye, Q. Xue, H. Li, Quantitative evaluation of the decarburization and microstructure evolution of WC–Co during plasma spraying, Surface and Coatings Technology, 206 (2012) 4068-4074.

[173] B. Cullity, Elements of, X-ray! Jiffraction, (1978).

[174] H. Zhang, Y.-Z. He, Y. Pan, S. Guo, Thermally stable laser cladded CoCrCuFeNi high-entropy alloy coating with low stacking fault energy, Journal of Alloys and Compounds, 600 (2014) 210-214.

[175] S. Guo, C. Ng, Z. Wang, C. Liu, Solid solutioning in equiatomic alloys: limit set by topological instability, Journal of Alloys and Compounds, 583 (2014) 410-413.